Atlantic Meridional Overturning Circulation during the Last Glacial and Deglacial:

Inferences from the Atlantic Tropical Thermocline Temperature and Seawater Radiocarbon Activity

Dissertation zur Erlangung des
akademischen Grades eines Doktors
der Naturwissenschaften

Dr. rer. nat.

im Fachbereich 5 (Geowissenschaften)
der Universität Bremen

vorgelegt von:

Enqing Huang

Bremen, März 2013

PRÜFUNGSAUSSCHUSS

----- **Gutachter** -----

Herr Prof. Dr. Michael Schulz

Herr Prof. Dr. Michal Kucera

----- **Tag des öffentlichen Kolloquiums** -----

24 Mai 2013

----- **Mitglieder der Kommission** -----

Herr Prof. Dr. Michael Schulz

Herr Prof. Dr. Michal Kucera

Herr Prof. Dr. Heiko Pälike

Herr Dr. Stefan Mulitza

Frau Dr. Gema Martínez Méndez

Frau Martina Hollstein

Name : Enqing Huang Datum : 15-03-2013

Anschrift : App./Zi. 8-13, Leobenerstr. 4, D-28359 Bremen

E r k l ä r u n g

Hiermit versichere ich, dass ich

1. die Arbeit ohne unerlaubte fremde Hilfe angefertigt habe,

2. keine anderen als die von mir angegebenen Quellen und Hilfsmittel benutzt habe und

3. die den benutzten Werken wörtlich oder inhaltlich entnommenen Stellen als solche kenntlich gemacht habe.

_____, den .....

(Unterschrift)

Acknowledgements

First of all, I thank the almighty God who creates a wonderful and infinite universe. Meanwhile, he also generously gives us the wisdom and the ability to explore his mysteries. And to some extent, we can understand and appreciate his creation.

I genuinely thank Dr. Stefan Mulitza, Prof. Michael Schulz and Dr. André Paul for their supervision over the past three and a half years. Stefan designed lots of research contents and offered support and encouragement whenever I needed. Michael gave many constructive suggestions in developing projects and writing manuscripts. André's expertise in physical oceanography and climate modeling provided deeper insights to interpret sediment records.

I am grateful to Dr. Luke Skinner at the University of Cambridge for opening his radiocarbon laboratory and sharing his expertise in the radiocarbon method. I sincerely thank Dr. Stephan Steinke, Dr. Jeroen Groeneveld and Dr. Mahyar M. Hamadani for their assistance in the Mg/Ca analyses and data interpretation. I also appreciate Dr. Monika Segl and her team for measuring countless stable isotope samples and Dr. Jürgen Pätzold for his help to access to sediment materials in the MARUM core repository.

I thank all colleagues from the Bremen International Graduate School for Marine Sciences (GLOMAR). Particularly, I would like to thank Dr. Ulrike Holzwarth, Dr. Ines Hessler and Dr. Janna Just for organizing lots of interesting workshops; Dr. Uta Brathauer, Dr. Christina Klose, Carmen Murken as well as Jutta Bülten for their kind help in administrative affairs.

I shared an office and enjoyed a lot of fun with Dr. James Collins, Dr. Cyril Giry, Sebastian Hötzel, Dr. Julien Michel and Dr. Rodrigo Portilho-Ramos for years. I also would like to express my gratitude to colleagues from the GEOMOD group. They are Anna Kloss, Xiao Zhang, Dr. Heather Johnstone (who helped to refine the written English of chapter 1 and 5), Dr. Matthias Prange, Dr. Ute Merkel, Dr. Aline Govin, Dr. Takasumi Kurahashi, Dr. Andreas Manschke, Dr. Dian Handiani, Amanda Frigola, Dr. Vidya Varma, Rima Rachmayani, Thejna Tharammal, Huadong Liu, Nilima Natoo and many others.

Last but not the least, I thank my parents for their long-term unconditional love and support. Many thanks also go to sisters and brothers of Chinesische Christliche Gemeinde Bremen, with whom we carry burdens and share joy together.

Research works of this thesis were funded through the DFG Research Center/Excellence Cluster "The Ocean in the Earth System" and by the Helmholtz Climate Initiative "REKLIM." Enqing Huang is supported by the China Scholarship Council.

Abstract

The Atlantic Meridional Overturning Circulation (AMOC) is a key component of the global climate system, which facilitates the redistribution of heat, salinity, CO_2 and nutrients within oceans and between ocean-atmosphere reservoirs. Knowledge of past AMOC dynamics is important for understanding the correlation between the AMOC reorganization and global climate variability. The Last Glacial Maximum (LGM) is a particularly useful time period for testing the operation of the AMOC under extremely different climate conditions from the present. Although the geometry of the LGM AMOC has been relatively well reconstructed, the strength of the LGM AMOC is still controversial in different proxy records and climate model outputs. In addition, very little is known about the AMOC state prior to the LGM. This thesis aims to investigate variations of the glacial AMOC strength and the LGM Atlantic deepwater circulation rate through reconstructing glacial tropical thermocline temperatures and seawater $\Delta^{14}C$ values. Moreover, the role of the ocean circulation in redistributing ^{14}C between the atmosphere and the deep ocean for the pre-LGM time period was also explored.

Climate model simulations and modern observational data have suggested that thermocline temperatures in the tropical Atlantic show a sensitive response to changes in the AMOC strength. Therefore, tropical thermocline-temperature changes might be used as an indicator of variability in the AMOC strength. This possibility was tested through using benthic foraminiferal $\delta^{18}O$ and Mg/Ca results of a set of sediment cores retrieved from the eastern tropical Atlantic (9ºN, 15ºW; 300-670 m water depth) **(Chapter 2)**. We found that benthic Mg/Ca-based thermoline temperatures (200-570 m) during Heinrich Stadial 1 were indistinguishable from those of the LGM. Thermocline temperatures in the northeastern tropical Atlantic show no pronounced response to a significant reduction of the AMOC strength from the LGM to Heinrich Stadial 1. Therefore, using thermocline-temperature changes as an indicator for glacial variations of the AMOC strength is inapplicable in our research area. In contrast, thermocline salinities were found to have significantly increased during the LGM and Heinrich Stadial 1 with respect to the late Holocene. We inferred that glacial thermocline at our core locations were probably ventilated by saltier surface waters from the central North Atlantic rather than southern-sourced waters. This could indicate a

southward incursion of the glacial North Atlantic Central Water under glacial climate conditions.

Seawater $\Delta^{14}C$ is a proxy for deep ocean circulation ages. New paired planktonic and benthic foraminiferal ^{14}C ages from 28 sediment cores in combination with existing published results provided a first mapping of seawater $\Delta^{14}C$ distribution in the LGM Atlantic **(Chapter 3)**. The LGM B-P ages (^{14}C age differences between the paired planktonic and benthic foraminifera) and seawater $\Delta^{14}C$ values from the upper (< 1500 m) and the lower (> 1500 m) Atlantic show a strong vertical gradient. The mean B-P age and the mean seawater $\Delta^{14}C$ value of the lower Atlantic were 700 years larger and 105‰ less than those of the upper Atlantic, respectively. We took the LGM seawater $\delta^{13}C$ as a conservative water-mass tracer to calculate the relative contribution of different water masses at a given location. The mixing $\Delta^{14}C$ signals at core locations used in this study could therefore be estimated and further substracted from the reconstructed seawater $\Delta^{14}C$ values. The residual $\Delta^{14}C$ signal could ultimately be converted into water-mass circulation ages. Our results suggest that the LGM circulation ages at the vast majority of core locations from the lower Atlantic were less than 400 years, which were equal to or less than their pre-bomb values. Therefore, the LGM lower Atlantic (> 1500 m) was inferred to be well ventilated. Previously, the removal of the atmospheric CO_2 during glacial periods is hypothesized to be sequestrated in deep oceans partly through the mechanism of a slowdown of the deepwater ventilation. However, our results suggest that this mechanism did not play a major role in transferring the atmospheic CO_2 to the ocean interior during glacial periods.

The atmospheric $\Delta^{14}C$ between 40,000 and 25,000 yr BP was 580‰ higher than the preindustrial value. However, the relative contribution of a changed glacial carbon cycle to this elevated atmospheric $\Delta^{14}C$ is still unknown. New paired planktonic and benthic foraminiferal ^{14}C ages together with published results revealed that the abyssal Atlantic (below 2500 m) prior to the LGM was more depleted in $\Delta^{14}C$ values by 400‰ than the contemporary atmosphere **(Chapter 4)**. If our reconstructions are representative of the ocean volume below 3000 m, a simple mass-balance calculation suggests that the pre-LGM abyssal ocean carbon reservoir might have accounted for a 150‰ increase in the atmospheric $\Delta^{14}C$ level. Since the glacial deep ocean circulation was vigorous, the extremely depleted $\Delta^{14}C$ signature of the pre-LGM deep Atlantic Ocean was mostly likely caused by a decrease in the preformed $\Delta^{14}C$ values in the Southern Ocean source areas.

Contents

Chapter 1

Introduction

1.1 Atlantic Meridional Overturning Circulation and climate change

Ocean currents can be driven by winds, the density differences between water parcels and by tides (the gravitational pull of the Sun and the Moon). The density of a water parcel depends on its temperature and salinity. Therefore, the circulation driven by "fluxes of heat and freshwater across the sea surface and subsequent interior mixing of heat and salt" (Rahmstorf, 2003) are called thermohaline circulation. In reality, the thermohaline circulation is always tightly associated with the wind-driven circulation, and cannot be separated and measured in isolation. Therefore, another variable, Meridional Overturning Circulation, is more frequently used, which refers to the zonally-integrated volume transport in the ocean (Cunningham and Marsh, 2010). Although the thermohaline circulation is no more than a theoretical concept, it is a useful way to distinguish density-driven circulation from wind-driven circulation, because proxy records and climate model studies have confirmed that the thermohaline circulation is sensitive to external perturbations and might have undergone dramatic changes in the past (e.g., Sarnthein et al., 1994; Alley and Clark, 1999; Rahmstorf, 2002).

The Atlantic Meridional Overturning Circulation (AMOC) consists of the upper and the lower branch. Surface and intermediate waters enter into the South Atlantic through the Drake Passage and the passage off South Africa. Along their route towards to the north, surface waters increase in their salinities mainly in the northern subtropical gyre through net evaporation and decrease in their temperature in the mid-to-high latitude through air-sea exchange. At the northern end, surface waters become sufficiently dense to sink in the Nordic Seas and the Labrador Sea, forming the southward lower branch of the AMOC (extending down to 3000 m, Cunningham and Marsh, 2010). Below these northern-sourced waters, the abyssal Atlantic is filled with bottom waters formed in the Ross Sea and the Weddell Sea along the Antarctic slope through intensive evaporation and brine rejection (Killworth, 1983).

Today, the AMOC accounts for much of the total oceanic northward heat transport in the Atlantic, maintaining relatively mild climate conditions over Northern and Western Europe (Cunningham and Marsh, 2010). A slowdown or a collapse of the AMOC would give rise to a significant decrease in air temperatures over the northern North Atlantic (e.g., Manabe and Stouffer, 1995; Vellinga and Wood, 2001). Moreover, changes in the AMOC and the Northern Hemispheres high-latitude climate could be subsequently transmitted to the rest of the world through a series of atmospheric and oceanic teleconnections (e.g., Ganopolski and Rahmstorf, 2001; Flückiger et al., 2004).

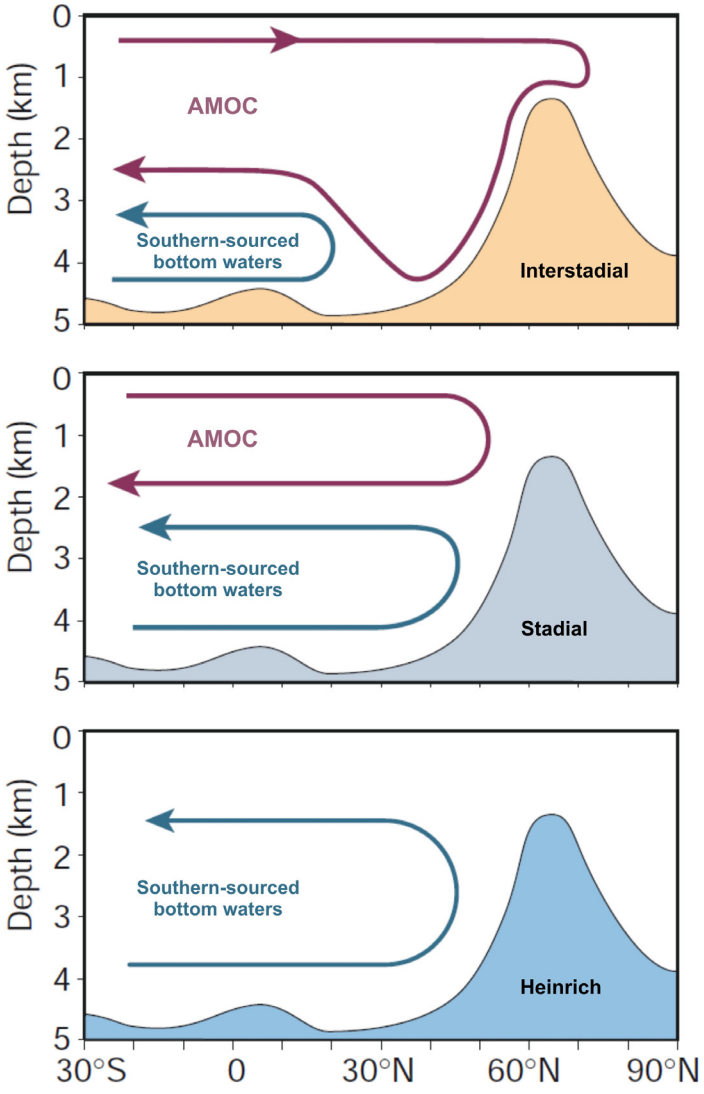

Figure 1.1 Schematic diagram of three different AMOC states prevailed during interstadial, stadial and Heinrich intervals respectively, modified from the original by Rahmstorf et al. (2002). Lines with arrows denote zonally-integrated volume transport across the Atlantic basin.

Previous studies indicate that the interstadial, stadial and Heinrich climate mode might correspond to different AMOC states (Sarnthein et al., 1994; Rahmstorf, 2002). As illustrated in Figure 1.1, the formation of North Atlantic Deep Water (NADW) is vigorous and occurs in the Nordic Seas during interstadials. The newly generated NADW subsequently flows over the sill between Greenland and Scotland to the south and dominantly influences deep and abyssal waters in the northern North Atlantic. During stadials, the NADW formation slows down and shifts to the subpolar open North Atlantic. The AMOC lower branch does not penetrate as deeply as during interstadial periods. During Heinrich intervals, deepwater convection in the North Atlantic halts, and the whole deep Atlantic is occupied by waters originated from the Southern Ocean. It is generally hypothesized that the freshwater flux to the northern North Atlantic from the surrounding ice sheets and sea ice could trigger the AMOC to switch between these three different states under certain climate background conditions (e.g., Broecker et al., 1985; Clark et al., 2002; Rahmstorf et al., 2002).

1.2 Reconstructions of changes in the past AMOC state

Since past AMOC variations are likely to be coupled with millennial-scale climate change, a variety of proxy records from a large number of sediment cores have been employed to reconstruct changes in past AMOC states and to test this linkage. These proxies can be classified into two types. (1) Based on the fact that northern- and southern-sourced deep waters have very different end-member values of $\delta^{13}C$, Cd/Ca, Zn/Ca, ε_{Nd} (neodymium isotopes), etc., these proxy records provide information on mixing ratios of different water masses at a given location and water depth. The geometry of past AMOC, namely the volume and the spatial distribution of different water masses, could be further mapped if enough reconstructions are available. (2) The second type of proxies, including sediment $^{231}Pa/^{230}Th$ ratio and grain size, the water-column density gradient across the pathway of the AMOC, etc., contain information about flow speed of deep ocean currents or ventilation ages of deep waters.

1.2.1 Reconstructions of changes in the geometry of past AMOC

Paleonutrient proxies ($\delta^{13}C$, Cd/Ca, Zn/Ca) are non-conservative water-mass tracers, as they are subject to the influence of nutrient cycling in the water column and other effects, while ε_{Nd} is a conservative tracer. Since $\delta^{13}C$ and Cd/Ca data have the best spatial coverage of any proxies in the Atlantic, it is still necessary to make use of these paleonutrient proxies to reconstruct past water-mass distribution, together with supplementary proof from ε_{Nd} results.

Reconstructions for the time period of Marine Isotope Stage 3 are relatively sparse. Nonetheless, several seawater $\delta^{13}C$ and ε_{Nd} records show coherent results. These indicate that the deep North and South Atlantic are influenced by nutrient-poor waters with negative ε_{Nd} values, likely sourced from the North Atlantic, during interstadials; and that they are influenced by nutrient-rich waters with less negative ε_{Nd} values, possibly originating from the Southern Ocean, during stadials and Heinrich intervals (e.g., Oppo and Lehman, 1995; Charles et al., 1996; Keigwin and Boyle, 1999; Shackleton et al., 2000; Piotrowski et al., 2005). This implies a shoaling of the glacial NADW (in some literatures this is also referred to as glacial North Atlantic Intermediate Water) and an upward expansion of the glacial Antarctic Bottom Water (AABW) during cold intervals of Marine Isotope Stage 3. More data are available for the last deglaciation. Likewise, the vertical extent of the northern-sourced deep waters expands during the warm Bølling-Allerød interval but shrinks during the cold Heinrich Stadial 1 and the Younger Dryas interval (e.g., Boyle and Keigwin, 1987; Keigwin et al., 1991; Sarnthein et al., 1994; Marchitto et al., 1998; Piotrowski et al., 2004).

So far, the only time period of the last glacial with relatively detailed mapping of water-mass distribution is the Last Glacial Maximum (LGM) (Figure 1.2B and 1.2C). According to different definitions, the time duration of the LGM is confined between 23.0-19.0 ka BP, 24.0-18.0 ka BP (Mix et al., 2001) or 26.5-19.0 ka (Clark et al., 2009). Strictly speaking, the LGM does not belong to interstadial, stadial or Heinrich climate modes. The millennial-scale climate variability is relatively stable within the LGM interval. However, the LGM is a special time interval when the global ice volume reaches its maximum and the atmospheric CO_2 concentration falls to its minimum for the past 130,000 years. Hence, the LGM time period has attracted lots of attention as it is an important benchmark for testing the operation of the AMOC under extreme climate conditions. The AMOC geometry during the LGM is inferred to be similar to that of the stadial climate mode (Sarnthein et al., 1994). As shown in Figure 1.2, the glacial NADW occupies the upper 2000 m of the North Atlantic. The glacial AABW dominates bottom waters below 3000 m of the central South Atlantic, and it progressively mixes with the glacial NADW along its pathway to the north. The glacial counterpart of the Antarctic Intermediate Water was also found at around 1000 m in the southwestern Atlantic (Figure 1.2B).

1.2.2 Reconstructions of changes in the strength of past AMOC

Currently, proxy records regarding the past AMOC strength concentrate on the LGM and the last deglaciation. Although in the literature there is a different viewpoint on the millennial variability of the deglacial AMOC strength (Gherardi et al., 2009), it seems that most of other

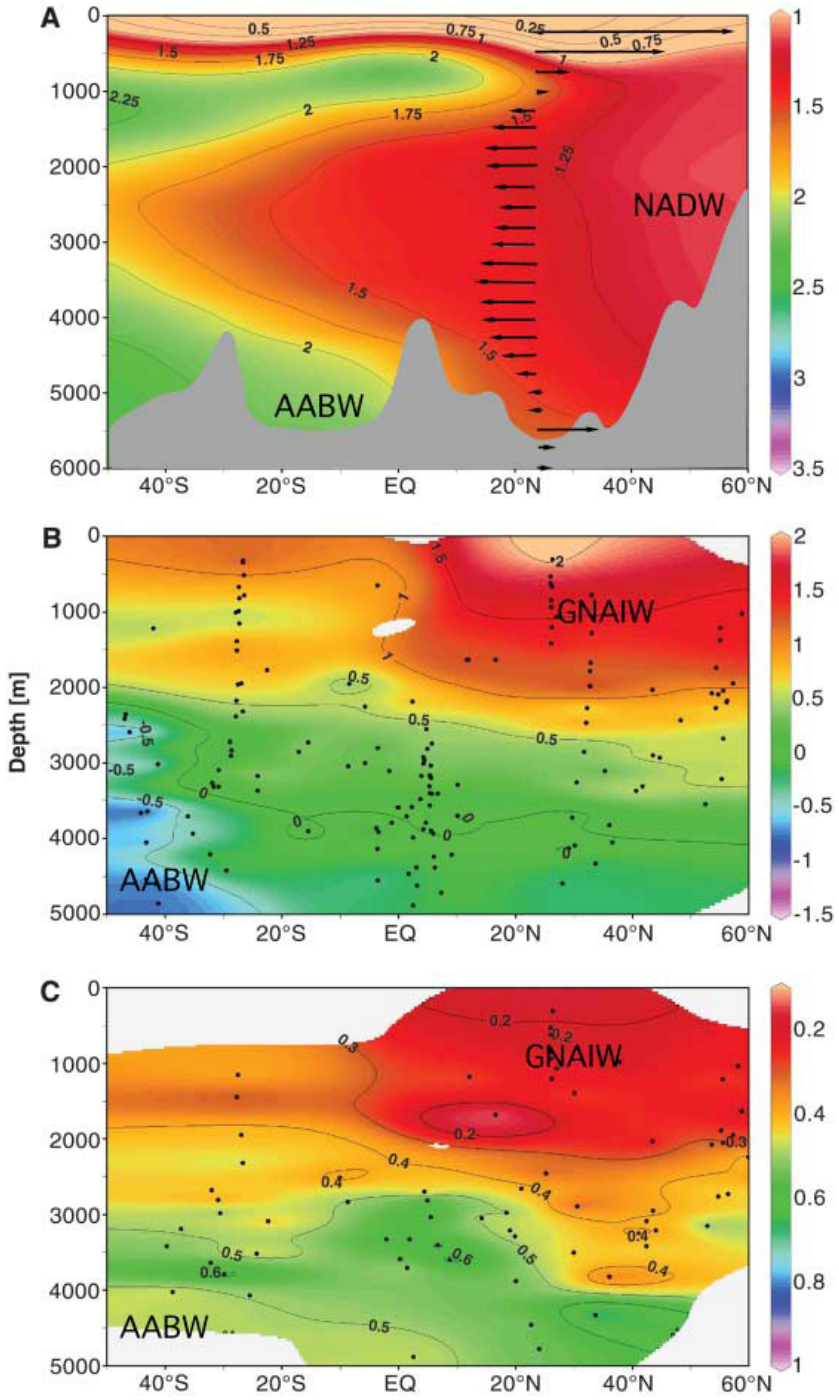

Figure 1.2 A comparison of the modern and the LGM water-mass distribution in the Atlantic, adopted from Lynch-Stieglitz et al. (2007). Figure 1.2A shows the distribution of dissolved phosphate (μmol/L) in the modern western Atlantic. Arrows indicate the direction of deepwater circulation. Figure 1.2B and 1.2C shows the distribution of benthic forminiferal $\delta^{13}C$ (‰, PDB) and seawater Cd (nmol/kg) in the LGM western and central Atlantic, respectively. GNAIW is the abbreviation of Glacial North Atlantic Intermediate Water. $\delta^{13}C$ data were compiled by Bickert and Mackensen (2004) and Curry and Oppo (2005), while Cd results were compiled by Marchitto and Broecker (2006).

researches reach a consistent conclusion. Reconstructions based on the $^{231}Pa/^{230}Th$ ratio (e.g., McManus et al., 2004), the sortable silt mean size (e.g., Manighetti and McCave, 1995; McCave and Hall, 2006; Praetorius et al., 2008) as well as the water-column density gradient across the Florida Straits (Lynch-Stieglitz et al., 2011), all indicate that the AMOC strength was significantly reduced during the Heinrich Stadial 1 and the Younger Dryas event relative to the present, but it recovers during the Bølling-Allerød warm interval in between the two cold episodes.

Opinion on the LGM AMOC strength is quite diverse in the literature. $^{231}Pa/^{230}Th$ (e.g., Yu et al., 1996; McManus et al., 2004; Lippold et al., 2012) and sediment grain-size records (e.g., Manighetti and McCave, 1995; McCave and Hall, 2006) suggest that the LGM AMOC strength is stronger than or comparable to the present. However, reconstructions based on the water-column density gradient across the Florida Straits or the upper South Atlantic basin indicate a weakened AMOC at the LGM (Lynch-Stieglitz et al., 1999; 2006). Climate models also present very different simulation results of LGM AMOC strength, which could be stronger, weaker or as strong as the present (Otto-Bliesner et al., 2007). In addition, the LGM deepwater circulation rate below the glacial NADW is also a matter of debate. Some studies have suggested that deepwater currents in the abyssal North Atlantic are as strong as at present (e.g., Manighetti and McCave, 1995; McCave and Hall, 2006); while others suggest that the speed of the deep northward flow is only half of that of the modern NADW (e.g., Negre et al., 2010).

Taken together, both the geological records and climate simulation studies confirm the coupling between millennial-scale climate change and the reorganization of the AMOC state. Stadials and Heinrich intervals are always associated with a shoaling of glacial NADW and a sluggish AMOC; while interstadials are accompanied with a deepened glacial NADW and a vigorous AMOC. The water-mass distribution in the LGM Atlantic has been quite well reconstructed, but the LGM AMOC strength is still a matter of discussion. Besides, deepwater circulation rates below the glacial NADW are also poorly known. It would, therefore, be useful if more reliable proxies for indicating past variations of the AMOC strength and deepwater circulation rates could be established.

1.3 Reconstructing past variations of the AMOC strength and deepwater ventilation rates using other approaches

1.3.1 Thermocline temperatures of the tropical Atlantic

Both instrumental data and climate model studies have revealed that changes in AMOC strength could result in a rapid adjust of ocean thermocline depths through the propagation of Rossby and Kelvin waves (e.g., Huang et al., 2000; Goodman, 2001; Zhang, 2007). A significant decrease in the NADW formation rate would give rise to a pronounced warming of thermocline waters in the tropical Atlantic (e.g., Zhang, 2007; Chang et al., 2008; Chiang et al., 2008; Figure 1.3). Therefore, thermocline temperature changes in the tropical Atlantic might be used as an indicator of variability in AMOC strength. However, the location and waters depth where thermocline temperatures show a high sensitivity to changes in the AMOC strength, are model-dependant (e.g., Zhang et al., 2007; Brady and Otto-Bliesner, 2011; Schmidt et al., 2012). Sediment records are thus required to validate this hypothesis and to constrain the location of thermocline waters for this target.

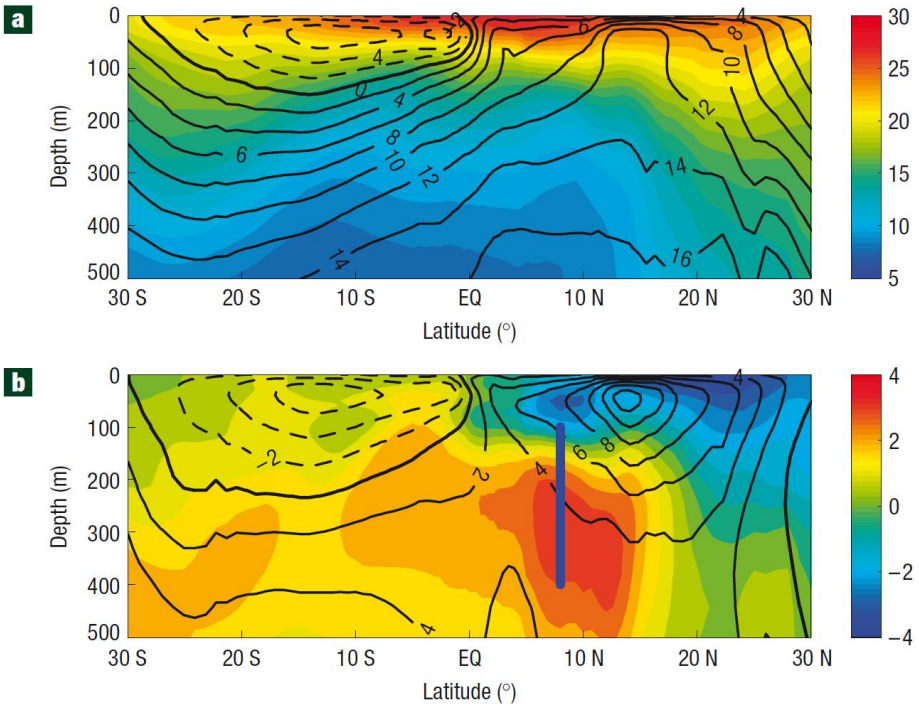

Figure 1.3 Modeled responses of Atlantic thermocline temperatures to a collapse of the AMOC, adopted from Chang et al. (2008). (a) The zonally-integrated AMOC streamfunction (contour) and seawater temperatures (color) in the upper 500 m of the Atlantic, results from a control simulation using modern boundary conditions. (b) Changes in the AMOC streamfunction and seawater temperatures in a water-hosing experiment with reference to the control simulation. The unit of the color bar is ºC.

A recent subsurface-dwelling planktonic foraminiferal Mg/Ca record from the western tropical Atlantic indicates that thermocline waters were indeed warmer during the Heinrich Stadial 1 and the Younger Dryas event than during the LGM (Schmidt et al., 2012). This provides the first evidence that a possible correlation between the AMOC strength and thermocline temperatures might exist. However, due to the possible shift of the average living depth of planktonic foraminifera in the past, planktonic foraminiferal Mg/Ca might not have faithfully recorded thermocline temperatures at a consistent water depth. This would increase the uncertainty when comparing Mg/Ca-temperature values of different time intervals. Therefore, the linkage between the past AMOC strength and thermocline temperatures needs to be tested by more reliable reconstructions.

1.3.2 Seawater ^{14}C

^{14}C atoms are primarily produced in the upper troposphere and stratosphere through the reaction between ^{14}N atoms and cosmic rays, which are further oxidized to $^{14}CO_2$. $^{14}CO_2$ is well mixed within the atmosphere and subsequently transferred into the ocean interior mainly through intermediate and deepwater formation. Once the newly formed deepwater is isolated from the atmosphere, without any other radiocarbon supply, the preformed ^{14}C of deepwater will decay at a known rate. Therefore, in principle, the ^{14}C-based ventilation age of a certain water parcel can be calculated. However, in practice, the estimate of past ventilation ages of deep oceans turns out to be much more complicated. Deep waters within the Atlantic are mixtures of waters sourced from the North Atlantic and the Southern Ocean. These two end members have significantly different $\Delta^{14}C$ values, with -68‰ for the modern NADW and -158‰ for the modern AABW (Broecker, 1991). Hence, ^{14}C signals of deep Atlantic waters mainly reflect the relative contribution of the northern- and the southern-sourced waters (mixing signal). A decrease in ^{14}C activity due to the radiocarbon decay within the ocean interior (ventilation signal) is of minor importance and difficult to detect (e.g., Broecker, 1991; Lynch-Stirglitz et al., 2007). The LGM ^{14}C age differences between the deep North Atlantic (> 3 km) and the surface Atlantic are greater than the Late Holocene values by more than one thousand years (e.g., Keigwin and Schlegel, 2002; Keigwin, 2004; Skinner and Shackleton, 2004). However, this is mostly likely induced by a northward incursion of ^{14}C-depleted southern-sourced waters rather than by a significant decrease in deep-ocean ventilation rates.

In order to extract the ventilation signal from the deepwater $\Delta^{14}C$ reconstruction, the $\Delta^{14}C$ end-member values of water masses from different sources must be known. The mixing ratio of different water masses at a given core location and water depth can be determined by an independent water-mass tracer. The mixing $\Delta^{14}C$ signal at a given core location can then be

calculated. The difference between the reconstructed $\Delta^{14}C$ value and the mixing $\Delta^{14}C$ signal can ultimately be converted into the water-mass ventilation age (e.g., Broecker, 1991; Matsumoto, 2007). So far, this calculation method has not been applied to estimate the ventilation age of the LGM Atlantic Ocean, because few seawater $\Delta^{14}C$ reconstructions are available and many important parameters are still lacking.

Not only can past variations of oceanic $\Delta^{14}C$ be used to estimate changes in deepwater ventilation ages, but also past variations of atmospheric $\Delta^{14}C$ can be employed to examine changes in the global mean formation rate of deep waters. For instance, at the onset of the Younger Dryas event, the atmospheric $\Delta^{14}C$ level increased by 70±10‰ in 200 years, while the contemporary ^{14}C production rate did not increase (e.g., Hughen et al., 1998, 2000). Therefore, the increase in the atmospheric $\Delta^{14}C$ is inferred to be caused by a decrease in the deepwater formation in the North Atlantic. A slowdown AMOC transfers less ^{14}C into the ocean interior and thus results in an extra accumulation of ^{14}C in the atmosphere (e.g., Hughen et al., 2000).

The atmospheric $\Delta^{14}C$ level between 40,000 and 25,000 yr BP was significantly higher than the pre-bomb value, being 580‰ greater (Reimer et al., 2009). An increase in the ^{14}C production rate due to the lowered geomagnetic field intensity is considered the main reason for the elevated atmospheric $\Delta^{14}C$ value during this time period (e.g., Beck et al., 2001; Hughen et al., 2004). However, if a sizable carbon reservoir sequestrated less ^{14}C from the atmosphere, this would also contribute to the ^{14}C accumulation in the atmosphere. This ^{14}C-depleted carbon reservoir was likely to be the deep ocean.. So far, this assumption, of reduced ^{14}C storage in the deep ocean prior to the LGM, has not been tested due to the lack of deepwater $\Delta^{14}C$ reconstructions.

1.4 Objectives

In this thesis, I aimed at reconstructing changes in the glacial AMOC strength and deepwater circulation rates through the use of thermocline temperatures and seawater radiocarbon activity. The following three working hypotheses will be evaluated in this study:

Working hypothesis 1: If thermocline temperatures in the eastern tropical Atlantic are sensitive to past changes in AMOC strength, then the significant reduction in AMOC strength from the LGM to Heinrich Stadial 1 would be recorded as a pronounced increase in thermocline temperatures.

We tested this hypothesis using benthic forminiferal Mg/Ca-temperature records from the eastern tropical Atlantic **(Chapter 2)**. Changes in thermocline temperatures could be induced by many other processes besides changes in the AMOC strength, such as changes in preformed seawater properties of the subduction areas, latitudinal shifts in isopycnal outcrops, etc. Therefore, we compared temperature results of the LGM interval with those of Heinrich Stadial 1. The AMOC strength during these two periods is significantly different but other climate background conditions are relatively similar. This would help to exclude the influences of other climatic processes.

Working hypothesis 2: If the deep Atlantic Ocean was poorly ventilated during the LGM, then deepwater $\Delta^{14}C$ reconstructions from the glacial deep Atlantic should contain a large fraction of ventilation signals.

The Mechanisms which drive glacial-interglacial variations in atmospheric CO_2 have long been fundamental research questions in plaeoceanography and paleoclimatology. A number of processes have been identified, yet the relative contributions of these processes and their interactions are still unknown (e.g., Sigman and Boyle, 2000; Sigman et al., 2010). The 80 ppm CO_2 removed from the atmosphere during the last glacial period is hypothesized to be sequestrated in deep oceans, in part through poorer ventilation of deep waters (e.g., Toggweiler, 1999; Toggweiler et al., 2006; Tschumi et al., 2011). However, the ventilation age of glacial deep waters has not been reconstructed by any robust methods. In **Chapter 3**, I give a first estimate of the radiocarbon-based circulation age of the LGM deep Atlantic Ocean. Based on these results, the working hypothesis 2 and the CO_2-sequestration hypothesis (Toggweiler, 1999; Toggweiler et al., 2006) were further tested.

Working hypothesis 3: If the deep ocean prior to the LGM was significantly depleted in ^{14}C with respect to the contemporary atmosphere, then the glacial marine carbon cycle should have contributed to the elevated atmospheric $\Delta^{14}C$ level considerably.

This can be tested by reconstructing changes in deepwater $\Delta^{14}C$ changes over the past 40,000 years **(Chapter 4)**. If a ^{14}C-depleted deep ocean did exist prior to the LGM, it could be caused by either a slow down of the global deepwater formation rate, or a decrease in preformed seawater $\Delta^{14}C$ values of source areas or a combination of both. Such deepwater $\Delta^{14}C$ records would provide valuable information about the ocean circulation state prior to the LGM.

1.5 Outline of the thesis

The thesis mainly comprises of three manuscripts, which are published in (Chapter 2), in preparation for (Chapter 3) or submitted to (Chapter 4) international peer-reviewed journals.

Chapter 2 (1st manuscript, published in *Paleoceanography*)
Response of eastern tropical Atlantic central waters to Atlantic meridional overturning circulation changes during the Last Glacial Maximum and Heinrich Stadial 1
by Enqing Huang, Stefan Mulitza, André Paul, Jeroen Groeneveld, Stephan Steinke, Michael Schulz

We developed a new Mg/Ca-temperature calibration for the epibenthic foraminifera *Planulina ariminensis* using new core-top samples from the eastern tropical Atlantic and previously published data. We applied this calibration to reconstruct thermocline temperatures in the eastern tropical Atlantic (9ºN, 15ºW; 300-670 m water depth) during the LGM, Heinrich Stadial 1 and the late Holocene. On this basis, the sensitivity of thermocline temperatures to past AMOC changes under glacial background conditions was discussed. Paired measurements of benthic foraminiferal $\delta^{18}O$ and Mg/Ca also allow reconstructions of thermocline salinities. We further used conservative temperature-salinity properties of water masses to trace possible source regions of the ventilated thermocline in the eastern tropical Atlantic during the LGM.

Chapter 3 (2nd manuscript, in preparation for *Quaternary Science Reviews*)
Radiocarbon distribution and radiocarbon-based circulation age of the Atlantic Ocean during the Last Glacial Maximum
by Enqing Huang, Luke C. Skinner, Stefan Mulitza, André Paul, Michael Schulz

New paired planktonic and benthic foraminiferal ^{14}C ages of 28 sediment cores from the tropical-subtropical Atlantic are presented. These data combined with previously existing ^{14}C results allowed us to map the spatial distribution of seawater $\Delta^{14}C$ in the LGM Atlantic. We assume that seawater $\delta^{13}C$ acted as a conservative water-mass tracer in the LGM Atlantic, which could be employed to calculate the relative contribution of different water masses at a given core location and water depth. By doing so, the radiocarbon-based circulation age of the deep Atlantic Ocean during the LGM was further estimated.

Chapter 4 (3rd manuscript, submitted to *Geophysical Research Letters*)
A ^{14}C-depleted abyssal Atlantic Ocean prior to the Last Glacial Maximum and its possible influence on the atmospheric $\Delta^{14}C$
by Enqing Huang, Luke C. Skinner, Stefan Mulitza, André Paul, Michael Schulz

Seawater $\Delta^{14}C$ variations at 2500 and 4000 m water depth of the southwestern Atlantic have been reconstructed for the past 40,000 years. Combined with existing results, we could determine seawater $\Delta^{14}C$ values of the abyssal Atlantic prior to the LGM. We further discussed the influence of a ^{14}C-depleted abyssal ocean carbon reservoir on the pre-LGM atmospheric $\Delta^{14}C$ level, and investigated changes in the volume of ^{14}C-depleted water masses over the LGM and the early deglacial.

Closing remarks and a research outlook are presented in **Chapter 5**.

All data presented in this thesis will be available through the PANGAEA database (http://www.pangaea.de).

1.6 References

Alley, R.B., Clark, P.U., 1999. The deglaciation of the northern hemisphere: a global perspective. Annual Review of Earth and Planetary Sciences 27, 149-182.

Beck, J.W., Richards, D.A., Edwards, R.L., Silverman, B.W., Smart, P.L., Donahue, D.J., Hererra-Osterheld, S., Burr, G.S., Calsoyas, L., Jull, A.J.T., Biddulph, D., 2001. Extremely large variations of atmospheric ^{14}C concentration during the last glacial period. Science 292, 2453-2458.

Bickert, T., Mackensen, A., 2004. Last Glacial to Holocene changes in South Atlantic deep water circulation. In: Wefer, G., Mulitza, S., Ratmeyer, V. (Eds.), The South Atlantic in the Late Quaternary: Reconstruction of Material Budgets and Current Systems. Springer-Verlag Berlin Heidelberg New York Tokyo, pp. 671-695.

Boyle, E.A., Keigwin L.D., 1987. North Atlantic thermohaline circulation during the last 20,000 years linked to high-latitude surface temperature. Nature 330, 35-40.

Brady, E.C., Otto-Bliesner, B.L., 2011. The role of meltwater-induced subsurface ocean warming in regulating the Atlantic meridional overturning in glacial climate simulations. Climate Dynamics 37, 1517-1532, doi:10.1007/s00382-010-0925-9.

Broecker, W.S., 1991. The great ocean conveyor. Oceanography 4(2), 79-89.

Broecker, W.S., Peteet, D.M., Rind, D., 1985. Does the ocean-atmosphere system have more than one stable mode of operation? Nature 315, 21-26.

Chang, P., Zhang, R., Hazeleger, W., Wen, C., Wan, X., Ji, L., Haarsma, R.J., Breugem, W.-P., Seidel, H., 2008. Oceanic link between abrupt changes in the North Atlantic Ocean and the African monsoon. Nature Geoscience 1, 444-448.

Charles, C.D., Lynch-Stieglitz, J., Ninnemann, U.S., Fairbanks, R.G., 1996. Climate connections between the hemispheres revealed by deep sea sediment core/ice core correlations. Earth and Planetary Science Letters 142, 19-27.

Chiang, J.C.H., Cheng, W., Bitz, C.M., 2008. Fast teleconnections to the tropical Atlantic sector from Atlantic thermohaline adjustment. Geophysical Research Letters 35, L07704, doi:10.1029/2008GL033292.

Clark, P.U., Dyke, A.S., Shakun, J.D., Carlson, A.E., Clark, J., Wohlfarth, B., Mitrovica, J.X., Hostetler, S.W., McCabe, A.M., 2009. The Last Glacial Maximum. Science 325, 710-714.

Clark, P.U., Pisias, N.G, Stocker, T.F., Weaver, A.J., 2002. The role of the thermohaline circulation in abrupt climate change. Nature 415, 863-869.

Cunningham, S.A., Marsh R., 2010. Observing and modeling changes in the Atlantic MOC. WIREs Climate Change 1, 180-191.

Curry, W.B., Oppo, D.W., 2005. Glacial water mass geometry and the distribution of $\delta^{13}C$ of ΣCO_2 in the western Atlantic Ocean. Paleoceanography 20, PA1017, doi:10.1029/2004PA001021.

Ganopolski, A., Rahmstrof, S., 2001. Rapid changes of glacial climate simulated in a coupled climate model. Nature 409, 153-158.

Gherardi, J.-M., Labeyrie, L., Nave, S., Francois, R., McManus, J.F., Cortijo, E., 2009. Glacial-interglacial circulation changes inferred from $^{231}Pa/^{230}Th$ sedimentary record in the North Atlantic region. Paleoceanography 24, PA2204, doi:10.1029/2008PA001696.

Goodman, P.J., 2001. Thermohaline adjustment and advection in an OGCM. Journal of Physical Oceanography 31, 1477-1497.

Huang, R.X., Cane, M.A., Naik, N., Goodman, P., 2000. Global adjustment of the thermocline in response to deepwater formation. Geophysical Research Letters 27(6), 759-762.

Hughen, K., Lehman, S., Southon, J., Overpeck, J., Marchal, O., Herring, C., Turnbull, J., 2004. ^{14}C activity and global carbon cycle changes over the past 50,000 years. Science 303, 202-207.

Hughen, K.A., Overpeck, J.T., Lehman, S.J., Kashgarian, M., Southon, J., Peterson, L.C., Alley, R., Sigman, D.M., 1998. Deglacial changes in ocean circulation from an extended radiocarbon calibration. Nature 391, 65-68.

Hughen, K.A., Southon, J.R., Lehman, S.J., Overpeck, J.T., 2000. Synchronous radiocarbon and climate shifts during the last deglaciation. Science 290, 1951-1954.

Keigwin, L.D., 2004. Radiocarbon and stable isotope constraints on last glacial maximum and younger Dryas ventilation in the western north Atlantic. Paleoceanography 19, PA4012, doi:10.1029/2004PA001029.

Keigwin, L.D., Boyle, E.A., 1999. Surface and deep ocean variability in the northern Sargasso Sea during marine isotope stage 3. Paleoceanography, 14(2), 164-170.

Keigwin, L.D., Jones, G.A., Lehman, S.J., Boyle, E.A., 1991. Deglacial meltwater discharge, North Atlantic deep circulation, and abrupt climate change. Journal of Geophysical Research 96(C9), 16811-16826.

Keigwin, L.D., Schlegel, M.A., 2002. Ocean ventilation and sedimentation since the glacial maximum at 3 km in the western North Atlantic, Geochemistry Geophysics Geosystems 3(6), 10.1029/2001GC000283.

Killworth, P.D., 1983. Deep convection in the World Ocean. Reviews of Geophysics 21(1), 1-26.

Knutti, R., Flückiger, J., Stocker, T.F., Timmermann, A., 2004. Strong hemispheric coupling of glacial climate through freshwater discharge and ocean circulation. Nature 430, 851-856.

Lippold, J., Luo, Y., Francois, R., Allen, S.E., Gherardi, J., Pichat, S., Hickey, B., Schulz, H., 2012. Strength and geometry of the glacial Atlantic Meridional Overturning Circulation. Nature Geoscience 5, 813-816.

Lynch-Stieglitz, J., Adkins, J.F., Curry, W.B., Dokken T., Hall, I.R., Herguera, J.C., Hirschi, J.J.-M., Ivanova, E.V., Kissel, C., Marchal, O., Marchitto, T.M., McCave, I.N., McManus, J.F., Mulitza, S., Ninnemann, U., Peeters, F., Yu, E.-F., Zahn, R., 2007. Atlantic meridional overturning circulation during the Last Glacial Maximum. Science 316, 66–69.

Lynch-Stieglitz, J., Curry, W.B., Oppo, D.W., Ninneman, U.S., Charles, C.D., Munson, J., 2006. Meridional overturning circulation in the South Atlantic at the last glacial maximum. Geochemistry, Geophysics, Geosystems 7, Q10N03, doi:10.1029/2005GC001226.

Lynch-Stieglitz, J., Curry, W.B., Slowey, N., 1999. Weaker Gulf Stream in the Florida Straits during the Last Glacial Maximum. Nature 402, 644-648.

Lynch-Stieglitz, J., Schmidt, M.W., Curry, W.B., 2011. Evidence from the Florida Straits for Younger Dryas ocean circulation changes. Paleoceanography 26, PA1205, doi:10.1029/2010PA002032.

Manabe, S, Stouffer, R.J., 1995. Simulation of abrupt climate change induced by freshwater input to the North Atlantic Ocean. Nature 378: 165-167.

Manighetti, B., McCave, I.N., 1995. Late glacial and Holocene palaeocurrents through South Rockall Gap, NE Atlantic Ocean. Paleoceanography 10(3), 611-626.

Marchitto, T.M., Broecker, W.S., 2006. Deep water mass geometry in the glacial Atlantic Ocean: A review of constraints from the paleonutrient proxy Cd/Ca. Geochemistry Geophysics Geosystems 7, Q12003, doi:10.1029/2006GC001323.

Marchitto, T.M., Curry, W.B., Oppo, D.W., 1998. Millennial-scale changes in North Atlantic circulation since the last glaciation. Nature 393, 557-561.

Matsumoto, K., 2007. Radiocarbon-based circulation age of the world oceans. Journal of Geophysical Research 112, C09004, doi:10.1029/2007JC004095.

McCave, I.N., Hall, I.R., 2006. Size sorting in marine muds: Processes, pitfalls, and prospects for paleoflow-speed proxies. Geochemistry, Geophysics, Geosystems 7, Q10N05, doi:10.1029/2006GC001284.

McManus, J.F., Francois, R., Gherardi, J.-M., Keigwin L. D., Brown-Leger, S., 2004. Collapse and rapid resumption of Atlantic meridional circulation linked to deglacial climate changes. Nature 428, 834-837.

Mix, A.C., Bard, E., Schneider, R., 2001. Environmental processes of the ice age: land, oceans, glaciers (EPILOG). Quaternary Science Reviews 20, 627-657.

Negre, C., Zahn, R., Thomas, A.L., Masqué, P., Henderson, G.M., Martínez-Méndez, G., Hall, I.R., Mas, J.L., 2010. Reversed flow of Atlantic deepwater during the Last Glacial Maximum. Nature 468, 84-88.

Oppo, D.W., Lehman, S.J., 1995. Suborbital timescale variability of North Atlantic deep water during the past 200,000 years. Paleoceanography 10, 901-910.

Otto-Bliesner, B.L., Hewitt, C.D., Marchitto, T.M., Brady, E., Abe-Ouchi, A., Crucifix, M., Murakami, S., Weber, S.L., 2007. Last Glacial Maximum ocean thermohaline circulation: PMIP2 model intercomparisons and data constraints. Geophysical Research Letters 34, L12706, doi:10.1029/2007GL029475.

Piotrowski, A.M., Goldstein, S.L., Hemming, S.R., Fairbanks, R.G., 2005. Temporal relationships of carbon cycling and ocean circulation at glacial boundaries. Science 307, 1933-1938.

Piotrowski, A.M., Goldstein, S.L., Hemming, S.R., Fairbanks, R.G., 2004. Intensification and variability of ocean thermohaline circulation through the last deglaciation. Earth and Planetary Science Letters 225, 205-220.

Praetorius, S.K., McManus, J.F., Oppo, D.W., Curry, W.B., 2008. Episodic reductions in bottom-water currents since the last ice age. Nature Geoscience 1(7), 449-452.

Rahmstorf, S., 2002. Ocean circulation and climate during the past 120000 years. Nature 419, 207-214.

Rahmstorf, S., 2003. The current climate. Nature 421, 699.

Reimer, P.J., Baillie, M.G.L., Bard, E., Bayliss, A., Beck, J.W., Blackwell, P.G., Bronk Ramsey, C., Buck, C.E., Burr, G.S., Edwards, R.L., Friedrich, M., Grootes, P.M., Guilderson, T.P., Hajdas, I., Heaton, T.J., Hogg, A.G., Hughen, K.A., Kaiser, K.F., Kromer, B., McCormac, F.G., Manning, S.W., Reimer, R.W., Richards, D.A., Southon, J.R., Talamo, S., Turney, C.S.M., van der Plicht, J., Weyhenmeyer, C.E., 2009. IntCal09

and Marine09 radiocarbon age calibration curves, 0-50,000 years cal BP. Radiocarbon 51(4), 1111-1150.

Sarnthein, M., Winn, K., Jung, S.J.A., Duplessy, J.-C., Labeyrie, L., Erlenkeuser, H., Ganssen, G., 1994. Changes in east Atlantic deep-water circulation over the last 30,000 years: Eight time slice reconstructions. Paleoceanography 9, 209-267.

Schmidt, M.W., Chang, P., Hertzberg, J.E., Them II, T.R., Link, J., Otto-Bliesner, B.L., 2012. Impact of abrupt deglacial climate change on tropical Atlantic subsurface temperatures. Proceedings of the National Academy of Sciences of the United States of America 109(36), 14348-14352.

Shackleton, N.J., Hall, M.A., Vincent, E., 2000. Phase relationships between millennial-scale events 64,000-24,000 years ago. Paleoceanography 15, 565-569.

Sigman, D., Hain, M.P., Haug, G.H., 2010. The polar ocean and glacial cycles in atmospheric CO2 concentration. Nature 446, 47-55.

Sigman, D.M., Boyle, E.A., 2000. Glacial/interglacial variations in atmospheric carbon dioxide. Nature 407, 859-869.

Skinner, L.C., Shackleton, N.J., 2004. Rapid transient changes in northeast Atlantic deep water ventilation age across Termination I. Paleoceanography 19, PA2005, doi:10.1029/2003PA000983.

Toggweiler, J.R., 1999. Variation of atmospheric CO_2 by ventilation of the ocean's deepest water. Paleoceanography 14(5), 571-588, doi:10.1029/1999PA900033.

Toggweiler, J.R., Russell, J.L., Carson, S.R., 2006. Midlatitude westerlies, atmospheric CO_2, and climate change during the ice ages. Paleoceanography 21, PA2005, doi:10.1029/2005PA001154.

Tschumi, T., Joos, F., Gehlen, M., Heinze, C., 2011. Deep ocean ventilation, carbon isotopes, marine sedimentation and the deglacial CO_2 rise. Climate of the Past 7, 771-800, doi:10.5194/cp-7-771-2011, 2011.

Vellinga, M., Wood, R.A., 2002. Global climatic impacts of a collapse of the Atlantic thermohaline circulation. Climate Change 54, 251-267.

Yu, E.-F., Francois, R., Bacon, M.P., 1996. Similar rates of modern and last-glacial ocean thermohaline circulation inferred from radiochemical data. Nature 379, 689-694.

Zhang, R., 2007. Anticorrelated multidecadal variations between surface and subsurface tropical North Atlantic. Geophysical Research Letters 34, L12713, doi:10.1029/2007GL030225.

Chapter 2

Response of eastern tropical Atlantic central waters to Atlantic meridional overturning circulation changes during the Last Glacial Maximum and Heinrich Stadial 1

Enqing Huang[1], Stefan Mulitza[1], André Paul[1,2], Jeroen Groeneveld[1,2], Stephan Steinke[1], Michael Schulz[1,2]

1. MARUM - Center for Marine Environmental Sciences, University of Bremen, Bremen, Germany.
2. Faculty of Geosciences, University of Bremen, Bremen, Germany.

(Published in *Paleoceanography 27, PA3229, doi:10.1029/2012PA002294*)

2.1 Abstract

Benthic foraminiferal $\delta^{18}O$ and Mg/Ca of sediment cores off tropical NW Africa are used to study the properties of Atlantic central waters during the Last Glacial Maximum (LGM) and Heinrich Stadial 1 (HS1). We combined our core top data with published results to develop a new Mg/Ca-temperature calibration for *Planulina ariminensis*, which shows a Mg/Ca-temperature sensitivity of 0.19 mmol/mol per °C. Estimates of the LGM and HS1 thermocline temperatures are comparable to the present-day values between 200 and 400 m water depth, but were 1.2-1.5°C warmer at 550-570 m depth. The HS1 thermocline waters (200-570 m depth) did not show any warming relative to the LGM. This is in contrast to previous climate model studies, which concluded that tropical Atlantic thermocline waters warmed significantly when Atlantic meridional overturning circulation was reduced. However, our results suggest that thermocline temperatures of the northeastern tropical Atlantic show no pronounced sensitivity to changes in the thermohaline circulation during glacial periods. In contrast, we find a significant increase in thermocline-water salinities during the LGM (200-

550 m depth) and HS1 (200-400 m depth) with respect to the present-day, which we relate to changes in the wind-driven circulation. We infer that the LGM thermocline (200-550 m depth) and the HS1 upper thermocline (200-400 m depth) in the northeastern tropical Atlantic was ventilated by surface waters from the North Atlantic rather than the southern-sourced waters. This suggests that the frontal zone between the modern South Atlantic and North Atlantic Central Waters was probably shifted southward during the LGM and HS1.

2.2 Introduction

The upper permanent thermocline waters of the tropical and subtropical Atlantic, usually termed central water masses, are a key component of the upper branch of the Atlantic meridional overturning circulation (AMOC). The renewal of thermocline waters is accomplished by the subduction of surface waters in the mid-to-high latitudes (e.g., Luyten et al., 1983). Driven by downward Ekman pumping and mixed-layer deepening during wintertime, surface waters are transformed into thermocline waters and subsequently move along isopycnal surfaces toward lower latitudes (Poole and Tomczak, 1999). By the same mechanism, surface waters from the subtropical gyre can also subduct and ventilate the shallower tropical thermocline, which are subsequently upwelled near the equator and return to the subduction areas forming a closed subtropical cell (e.g., Snowden and Molinari, 2003). The properties of the ventilated thermocline are therefore sensitive to changes in the atmospheric circulation and ocean surface conditions in the formation areas.

A variety of model simulations suggest that ocean thermocline depths could rapidly adjust to a change in the AMOC geometry and strength. For example, a signal of deep water formation changes in the northern North Atlantic can be rapidly transferred to the equatorial Atlantic in a few years or decades via the propagation of planetary waves (e.g., Huang et al., 2000; Goodman, 2001; Cessi et al., 2004). A reduction of the North Atlantic deep water (NADW) production can cause a deepening of the tropical Atlantic thermocline (e.g., Huang et al., 2000; Timmermann et al., 2005). This prediction has later been supported by modern observational data (Zhang, 2007) and paleoceanographic records (Lopes dos Santos et al., 2010). Thermocline temperatures of the northern tropical Atlantic have been found warmer, both on multidecadal (Zhang, 2007) and glacial-interglacial time scales (Lopes dos Santos et al., 2010) when NADW flux was reduced. Modeling studies also predict a pronounced warming of around 1-3°C at the thermocline depths of the tropical Atlantic when the AMOC strength and the NADW production are reduced by freshwater perturbations in the North Atlantic (Zhang, 2007; Chang et al., 2008; Chiang et al., 2008).

Associated with the thermocline adjustment, additional processes also contribute to the heat accumulation in the tropical Atlantic during the AMOC slowdown. First, stronger northeast trade winds over the tropical Atlantic could strengthen downward mixing of heat (Chiang et al., 2008). Second, because of the strong northward branch of the AMOC in the present upper ocean, the formation of the equatorward branch of the northern Atlantic subtropical cell is suppressed (e.g., Hazeleger and Drijfhout, 2006). However, weakened AMOC could invigorate the northern Atlantic subtropical cell leading to a transport of warm and salty subtropical-gyre water into the tropical thermocline (Chang et al., 2008; Wan et al., 2010). Third, a slowdown of the AMOC can trap heat in the tropics and the Southern Hemisphere (Chiang et al., 2008). Therefore, the tropical thermocline waters are heated up due to a reduction in the AMOC through the abovementioned processes. Because of its high sensitivity and rapid response, thermocline temperature changes in the northern tropical Atlantic are proposed as a possible indicator of the past and present AMOC variations (Zhang, 2007; Lopes dos Santos et al., 2010).

The interpretation of thermocline temperature changes in response to AMOC changes could be complicated by many other factors, such as changes in preformed seawater properties of the subduction regions and latitudinal shifts in the isopycnal outcrops. Thermocline waters of the western North Atlantic subtropical gyre were estimated to be 4°C cooler during the Last Glacial Maximum (LGM, 23-19 ka BP), which has been attributed to significantly cooler conditions in the subduction regions at that time (Slowey and Curry, 1995). A model study also predicts an equatorward shift of the outcrop regions of isopycnal surfaces in both hemispheres during the LGM, which led to a shoaling of the ventilated thermocline depths (Paul and Schäfer-Neth, 2003, 2004). Therefore, changes in glacial climate boundary conditions might have significantly influenced tropical thermocline temperatures, and could obscure effects associated with past changes in the AMOC. In order to assess the net result induced by different processes, and to test thermocline temperature changes as a proxy for past AMOC variations, it is crucial to obtain reliable temperature reconstructions for time periods when climate boundary condition were relatively similar whereas the AMOC strength experienced significant changes.

To this end, we utilized benthic foraminiferal $\delta^{18}O$ and Mg/Ca to study thermocline-water temperatures and salinities in the northeastern tropical Atlantic during the LGM and Heinrich Stadial 1 (HS1, 17.5-14.7 ka BP). We find that the HS1 thermocline temperatures (200-570 m water depth) did not show any significant warming relative to the LGM. A significant decline in the AMOC intensity from the LGM to HS1 (e.g., McManus et al., 2004; Gherardi et al., 2009) apparently did not leave its imprint in thermocline temperatures of the northeastern

tropical Atlantic. Moreover, we find a significant increase in thermocline-water $\delta^{18}O$ and salinity both during the LGM (200-550 m depth) and HS1 (200-400 m depth) relative to the late Holocene. Thermocline waters of the northeastern tropical Atlantic were probably influenced by the subducted salty surface waters from the North Atlantic during these two time periods rather than by surface waters from the Southern Hemisphere.

2.3 Material and oceanographic setting

Four gravity cores and their accompanying multi-cores from the continental slope off NW Africa were analyzed (Figure 2.1 and Table 2.1). They were recovered from water depths between 300-670 m during the Meteor-Cruise M65/1 in 2005 (Mulitza et al., 2006). Core material consists of sandy mud with abundant shells or shell fragments of various microfossils.

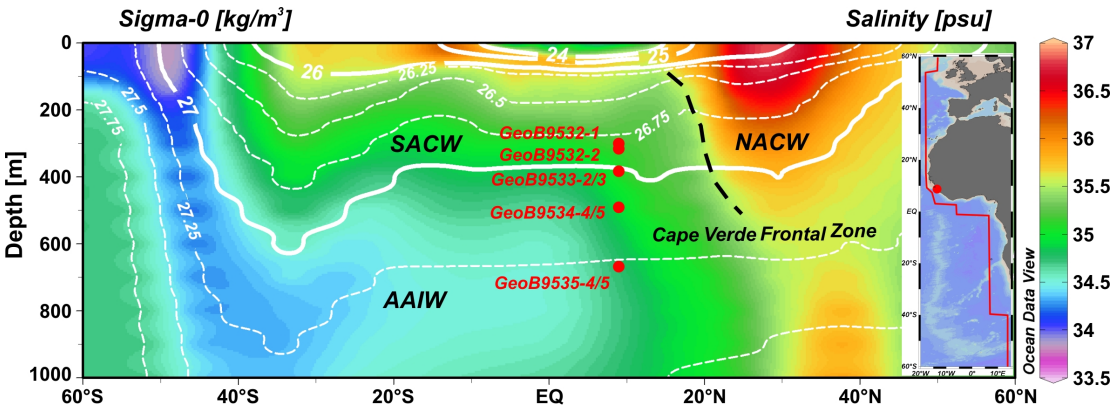

Figure 2.1 Meridional section of seawater salinity (colors) and potential density (contour lines) along the eastern Atlantic Ocean. The position of the section is indicated in the panel on the right. Data is from the World Ocean Atlas 2009 (WOA2009) (Antonov et al., 2009; Locarnini et al., 2009) and the figure was made by Ocean Data View 4 (R. Schlitzer, available at http://odv.awi.de). Dots denote core locations. The dashed line outlines the Cape Verde Frontal Zone, which represents the transition between the SACW and the NACW.

Modern bottom waters at the coring locations are influenced by the South Atlantic Central Water (SACW). The temperature-salinity properties of subsurface waters at our coring locations are consistent with that of the SACW (Figure 2.2). Within the isopycnal surfaces of σ_0=26.3 and σ_0=27.3, the in-situ measurements of seawater temperatures and salinity from four conductivity-temperature-depth (CTD) profiles fit well in a linear relationship (Figure

2.2), which is characteristic of the Atlantic central waters (Poole and Tomczak, 1999). The upper part of the SACW (roughly between 100-400 m in the tropics) is formed near the subtropical front in the southwestern Atlantic, while the lower part (>400 m) is derived from the Indian Central Water (Poole and Tomczak, 1999; Stramma and Schott, 1999). Bottom water over the deepest cores GeoB9535-4/5 is also partly influenced by the Antarctic Intermediate Water (Figures 2.1 and 2.2). North to our core locations, thermocline waters are influenced by the North Atlantic Central Water (NACW). The transition between these two central water masses is between 20°N and 25°N off the African coast, forming the so-called Cape Verde Frontal Zone in the eastern tropical Atlantic. The SACW is colder and fresher than the NACW within the same isopycnal surfaces, e.g., the SACW at our coring sites is 3.1-3.6ºC cooler and 0.7-0.9 psu fresher than the NACW at 30ºN within the isopycnal surfaces of σ_0=26.75 and σ_0=27.25 (Figures 2.1 and 2.2). Along the coast, the SACW penetrates further northward with increasing water depth (Figure 2.1) (Arhan et al., 1994; Poole and Tomczak, 1999).

Table 2.1 CTD stations and sediment cores used in this study.

Station	Type	Latitude(°N)	Longitude(°W)	Water Depth (m)	Core Section/Length (cm)
GeoB9532-4	CTD	8.94	14.90	9-287	
GeoB9533-4	CTD	8.92	14.92	9-365	
GeoB9534-1	CTD	8.90	14.94	9-432	
GeoB9535-1	CTD	8.87	14.96	10-628	
GeoB9532-1	Multi-core	8.95	14.89	301	17-23
GeoB9533-3	Multi-core	8.93	14.91	384	17-20
GeoB9534-4	Multi-core	8.90	14.94	493	14-15
GeoB9535-5	Multi-core	8.88	14.96	666	16-20
GeoB9532-2	gravity core	8.95	14.89	317	316
GeoB9533-2	gravity core	8.93	14.91	384	560
GeoB9534-5	gravity core	8.90	14.94	492	515
GeoB9535-4	gravity core	8.88	14.96	669	1008

2.4 Methods

2.4.1 X-ray fluorescence core scanning

The chemical element composition of the core material was measured by the X-Ray Fluorescence core scanner at MARUM, University of Bremen. The X-ray tube voltage and detector sensibility allows the analysis of elements from potassium through strontium (Röhl and Abrams, 2000). Split core sections were analyzed at a resolution of 1 or 2 cm. The

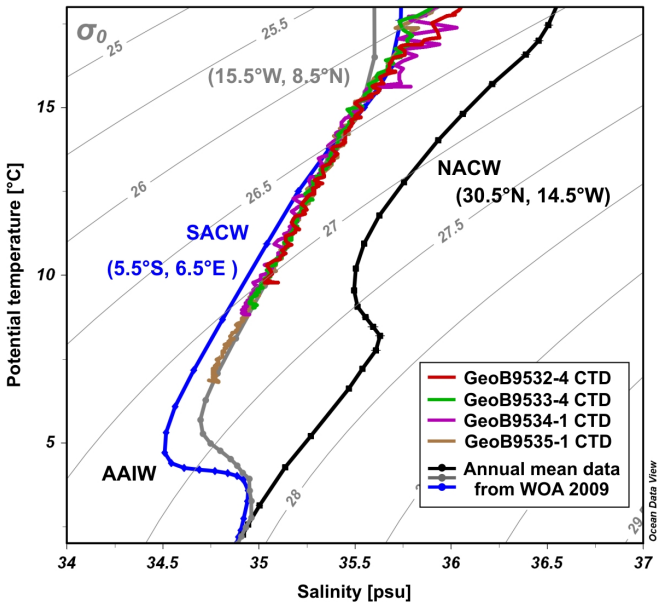

Figure 2.2 The temperature-salinity diagram of water masses at our core locations and several selected locations of the Atlantic Ocean. The CTD data well agree with the WOA2009 annual-mean data (shown in a thick grey curve) (Antonov et al., 2009; Locarnini et al., 2009) from the same locations. The potential density lines are also shown in thin grey curves.

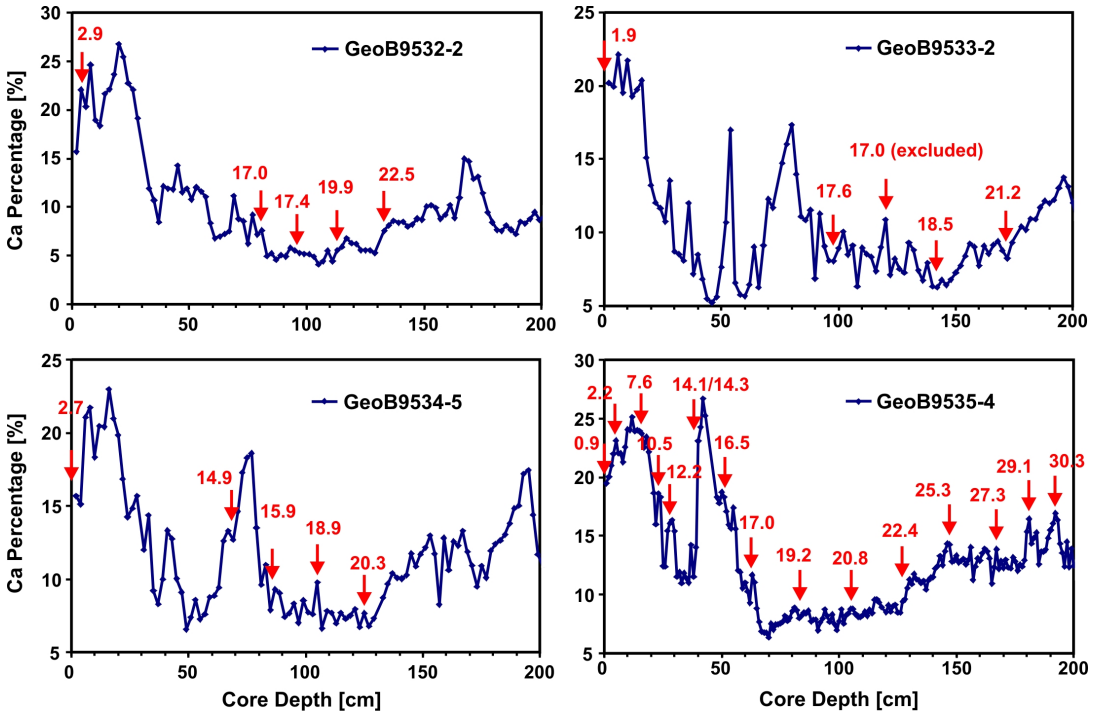

Figure 2.3 Downcore calcium percentage records from four gravity cores used in this study. Radiocarbon dates are denoted by arrows in each plot.

resulting data are element intensities in counts per second, which were further normalized as follows:

Percentage (element) = counts (element)/total counts (K, Ca, Ti, Mn, Fe, Cu, Sr)*100%. (1)

In this study we use the calcium-percentage records to correlate the stratigraphy in each core (Figure 2.3).

2.4.2 Radiocarbon dating

About 8-15 milligram of a mixture of shallow-dwelling planktonic foraminifera for each sample was picked for accelerator mass spectrometry (AMS) ^{14}C analyses performed at the Poznan Radiocarbon Laboratory (Table 2.2). Radiocarbon ages of core GeoB9535-4 were presented previously by Collins et al. (2011). AMS ^{14}C ages were converted to calendar ages using the "Fairbanks0107" calibration curve (Fairbanks et al., 2005), assuming a constant oceanic surface water reservoir age of 400 years.

Table 2.2 Radiocarbon dates of core GeoB9532-2, GeoB9533-2/3, and GeoB9534-5.

Lab NO.	Core	Sample Depth (cm)	Dating Species	^{14}C Age (yr, ±1σ uncertainty)	Calendar Age (yr BP, ±1σ uncertainty)
Poz-39025	GeoB9532-2	5	*G.ruber, G.sacculifer*	3245±35	2946±49
Poz-39027	GeoB9532-2	80	*G.ruber, G.sacculifer, O.universa*	14830±140	17020±266
Poz-32105	GeoB9532-2	95	*G.ruber, G.sacculifer, O.universa*	15060±110	17432±252
Poz-32106	GeoB9532-2	115	*G.ruber, G.sacculifer, O.universa*	17170±120	19919±158
Poz-39024	GeoB9532-2	135	*G.ruber, G.sacculifer*	19270±110	22450±118
Poz-32107	GeoB9533-3	0	*G.ruber, G.sacculifer, O.universa*	605±30	221±83
Poz-39028	GeoB9533-2	0	*G.ruber, G.sacculifer*	2375±30	1917±33
Poz-39029	GeoB9533-2	100	*G.ruber, G.sacculifer*	15160±80	17622±215
Poz-32134	GeoB9533-2	120	*G.ruber, G.sacculifer, O.universa*	14850±80	17046±184
Poz-32135	GeoB9533-2	140	*G.ruber, G.sacculifer, O.universa*	15630±90	18473±127
Poz-39031	GeoB9533-2	170	*G.ruber, G.sacculifer*	18250±100	21153±166
Poz-39034	GeoB9534-5	0	*G.ruber, G.sacculifer*	3015±35	2742±16
Poz-39038	GeoB9534-5	70	*G.ruber, G.sacculifer*	13160±110	14865±157
Poz-39041	GeoB9534-5	85	*G.ruber, G.sacculifer*	14060±80	15900±142
Poz-32136	GeoB9534-5	105	*G.ruber, G.sacculifer, O.universa*	16070±100	18862±107
Poz-32137	GeoB9534-5	125	*G.ruber, G.sacculifer, O.universa*	17550±120	20328±122

We dated one multi-core core-top sample (GeoB9533-3), which gives an age of 221±83 yr BP (Table 2.2). For each gravity core, the core-top age is determined by radiocarbon dating, while the LGM and HS1 intervals are basically constrained by two radiocarbon ages, respectively (Figure 2.3). The sedimentation rate in each core varies between 2 and 3 cm/kyr during the Holocene. However, the sedimentation rates are much higher during the LGM and HS1 (approximately 8-36 cm/kyr). The age of core-top samples of gravity core GeoB9533-2 and GeoB9535-4 (Collins et al. 2011) is younger than 2000 yr BP. For gravity core GeoB9532-2, we dated the sediment at core depth of 5 cm, which gives an age of 2946±19 yr BP. Based on the Holocene sedimentation rate along this core, the age of the core-top sample should also be younger than 2000 yr BP. In core GeoB9533-2, a ^{14}C age reversal occurs at 120 cm core depth. Based on the visual correlation of four downcore calcium-percentage records (Figure 2.3), we consider that the younger radiocarbon age at 120 cm is unreliable and therefore rejected.

Table 2.3 lists all multi-core core-top samples and gravity-core core-top samples younger than 2000 yr BP. The estimated calcification temperatures of benthic foraminifera derived from benthic $\delta^{18}O$ agree with modern bottom-water temperatures at each core location. This might suggest that the mean hydrographic conditions at our coring locations over the past two thousand years are similar to the present day. Therefore, core-top data of all multi-cores and several gravity cores (core-top samples are younger than 2000 yr BP from cores GeoB9532-2, 9533-2 and 9535-4) were used for Mg/Ca-temperature and calcite $\delta^{18}O$ calibrations in this study.

2.4.3 Foraminiferal $\delta^{18}O$ and Mg/Ca analyses

Benthic foraminifera *Planulina ariminensis* were picked for stable isotope (4-8 specimens, >400 μm) and Mg/Ca (25-40 specimens, >400 μm) analyses at MARUM, University of Bremen. *P. ariminensis* is an epifaunal species with an elevated microhabitat (Lutze and Thiel, 1989). Oxygen isotopes were measured using a Finnigan MAT 252 mass spectrometer equipped with an automatic carbonate preparation device. The isotopic results were converted into international Pee Dee Belemnite (PDB) scale by using the National Bureau of Standards (NBS) 18 and 19 standards. Internal precision for $\delta^{18}O$ analysis, based on replicates of an internal limestone standard, was better than ±0.07%.

For Mg/Ca analyses, foraminiferal tests were crushed using two glass plates in order to open the test chambers and then were cleaned following the cleaning protocol of Barker et al. (2003). Foraminiferal test fragments were rinsed with deionized water and methanol for a few

Table 2.3 *P. ariminensis* $\delta^{18}O$ and Mg/Ca, the predicted $\delta^{18}O$ of calcite and the calcification temperature of core-top samples, as well as temperature, salinity, $\Delta[CO_3^{2-}]_{calcite}$ of bottom waters.

Core	Water Depth (m)	Sample Depth (cm)	*P. ariminensis* Mg/Ca (mmol/mol)	*P. ariminensis* $\delta^{18}O$ (PDB, ‰)	Temperature (°C)	Salinity (psu)	$\Delta[CO_3^{2-}]_{calcite}$ (µmol/kg) [c]	Predicted $\delta^{18}O$ (PDB, ‰)	$\Delta\delta^{18}O$(Predicted - Measurement) [d]	Calcification Temperature (°C) [e]	ΔT (°C) [f]
GeoB9532-1	301	0-1	2.11	1.24	10.7 [a]	35.1 [a]	53	1.58	0.34	11.13	0.41
GeoB9532-1	301	0-1	2.1	1.37	10.7 [a]	35.1 [a]	53	1.58	0.22	10.62	-0.1
GeoB9532-1	301	0-1	2.17	1.31	10.7 [a]	35.1 [a]	53	1.58	0.27	10.83	0.11
GeoB9532-2	317	0	1.92		10.3 [a]	35.1 [a]	51	1.67			
GeoB9532-2	317	0	2.07	1.38	10.3 [a]	35.1 [a]	51	1.67	0.28	10.51	0.18
GeoB9533-3	384	0-1	1.77	1.64	9.2 [a]	35.0 [a]	43	1.88	0.24	9.22	0
GeoB9533-3	384	0-1	1.81	1.6	9.2 [a]	35.0 [a]	43	1.88	0.28	9.38	0.16
GeoB9533-3	384	0-1	1.75	1.71	9.2 [a]	35.0 [a]	43	1.88	0.18	8.97	-0.26
GeoB9533-2	384	0	1.84		9.2 [a]	35.0 [a]	43	1.88			
GeoB9533-2	384	0	1.86		9.2 [a]	35.0 [a]	43	1.88			
GeoB9533-2	384	0	1.83	1.74	9.2 [a]	35.0 [a]	43	1.88	0.14	8.83	-0.4
GeoB9534-4	493	0-1	1.62	1.85	7.9 [a]	34.8 [a]	35	2.16	0.31	8.17	0.28
GeoB9534-4	493	0-1	1.59	2	7.9 [a]	34.8 [a]	35	2.16	0.16	7.54	-0.34
GeoB9534-4	493	0-1	1.52	2.16	7.9 [a]	34.8 [a]	35	2.16	0	6.92	-0.96
GeoB9535-5	666	0-1		1.96	6.6 [b]	34.7 [b]	31	2.44	0.48	7.56	0.96
GeoB9535-4	669	2		2.42	6.6 [b]	34.7 [b]	31	2.44	0.02	5.69	-0.89
Mean Value									0.22		-0.06
Standard Deviation (±1σ)									0.13		0.52

a. Mean values of CTD stations GeoB9532-4, 9533-4, 9534-1, 9535-1;
b. Data from the WOA2009 (Antonov et al., 2009; Locarnini et al., 2009);
c. $\Delta[CO_3^{2-}]$ was calculated by the CO2sys_xls_program (Lewis and Wallace, 2006);
d. $\Delta\delta^{18}O$(Predicted - Measurement) is the difference between the predicted $\delta^{18}O$ of calcite and the *P. ariminensis* $\delta^{18}O$;
e. The calcification temperature is calculated after equation (5);
f. ΔT is the difference between the calcification temperature and the bottom-water temperature.

times to remove clays. Between each rinse, samples were ultrasonicated for one minute. After adding an oxidizing reagent (100 µl 30% H_2O_2 buffered with 10 ml 0.1 M NaOH), samples were put in a sub-boiling water bath for 10 minutes to remove organic matter. Sample vials were removed from the water bath every 2.5 minutes in order to release any gaseous build-up by rapping on the vials. The oxidizing step was repeated after replacement of the oxidizing reagent. Thereafter, samples were transferred to new clean vials. After a weak acid leach (0.001 M QD HNO_3), samples were dissolved in 0.075 M QD HNO_3. The solution was further centrifuged (10 min., 6000 rpm) to remove any insoluble remains and then diluted with deionized water. Finally, the solution was analyzed on a Perkin-Elmer Optima 3300RL ICP-OES equipped with autosampler and ultrasonic nebulizer.

Instrumental precision of the ICP-OES was determined by analyzing an in-house standard solution with a Mg/Ca value of 2.93 mmol/mol and an international limestone standard of ECRM 752-1 with a reported Mg/Ca value of 3.75 mmol/mol (Greaves et al., 2008). Both standards are matrix-matched with the samples. The in-house standard was run after every five samples showing a long term standard deviation of ±0.04 mmol/mol. The ECRM 752-1 standard was run twice before analyzing each batch of 50 samples showing a long-term mean value of 3.81 mmol/mol and a standard deviation of ±0.04 mmol/mol. The analytical precision, based on three replicate measurements per analysis, was 0.07% for Mg/Ca (n = 136), while mean reproducibility of the samples (n = 14; separately cleaned and analyzed during different ICP-OES sessions) was ± 0.05 mmol/mol (±1 standard deviation). Al/Ca was used to monitor contamination of clays, and Fe/Ca and Mn/Ca to monitor contamination by Fe/Mn oxides and Fe/Mn-rich carbonate coatings. The results show that our Mg/Ca data are not contaminated as the concentrations of Al, Fe and Mn were all below detection limits.

2.4.4 Planktonic foraminifera fragmentation index

Foraminiferal samples were split into an aliquot containing >250 specimens. Numbers of fragments and complete tests of planktonic foraminifera were counted. The fragmentation index was calculated after (Le and Shackleton, 1992):

$$\text{Fragmentation index} = (Fr/8)/(Fr/8 + CT)*100\%, \quad (2)$$

where Fr is number of test fragments of planktonic foraminifera, and CT is number of complete tests of planktonic foraminifera.

2.4.5 Estimate of oxygen isotopic equilibrium

The predicted $\delta^{18}O$ of calcite (Table 2.3) was calculated from the equation by Shackleton (1974) (the quadratic term in the original equation has only a small effect and was therefore ignored in this study):

$$\delta^{18}O_{calcite} = (16.9 - Temperature)/4 + \delta^{18}O_{seawater} - 0.27, \quad (3)$$

where temperature is the mean value of four CTD stations GeoB9532-4, 9533-4, 9534-1 and 9535-1. As we do not have any $\delta^{18}O_{seawater}$ measurements of in-situ seawater samples, we converted the mean salinity data from four CTD stations into $\delta^{18}O_{seawater}$ based on the modern $\delta^{18}O_{seawater}$-salinity relationship of the Atlantic central waters (Figure 2.4):

$$\delta^{18}O_{seawater} = (0.46\pm0.03)\ Salinity - (15.85\pm1.02). \quad (4)$$

The uncertainty in the coefficients of equation (4) is the standard error. The CTD data extend to a maximum water depth of 628 m. For water below this depth, we extracted annual-mean temperature and salinity data from the WOA2009 database for our calculation (Antonov et al., 2009; Locarnini et al., 2009).

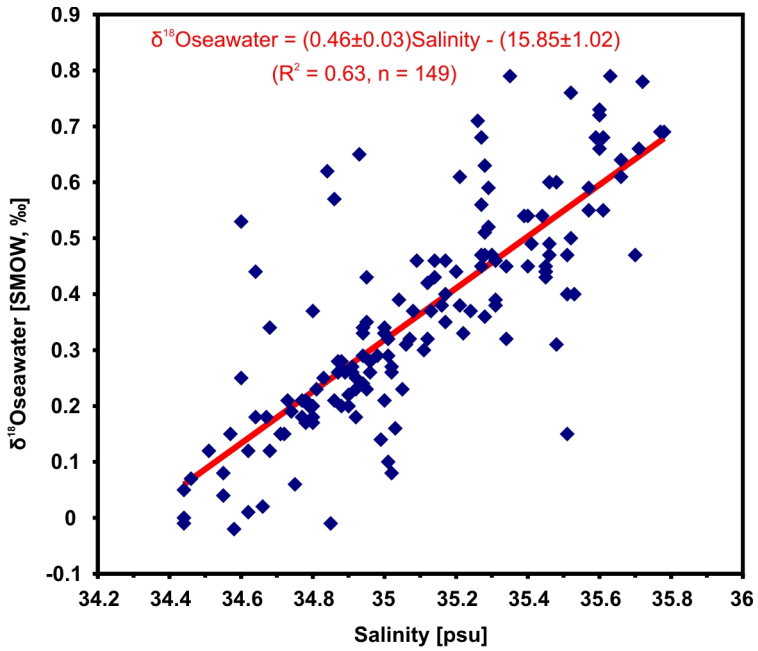

Figure 2.4 Modern $\delta^{18}O_{seawater}$-salinity relationship of Atlantic central water masses. Data was selected from a global database of seawater $\delta^{18}O$ (Schmidt, 1999b; Bigg and Rohling, 2000; an online global seawater oxygen-18 database is available at http://data.giss.nasa.gov/o18data/, edited by G. A. Schmidt, G. R. Bigg and E. J. Rohling.) using the interval [5.9ºC; 16.2ºC] for temperature and [34.4 psu; 35.8 psu] for salinity (Poole and Tomczak, 1999).

2.4.6 Seawater $\delta^{18}O$ and paleo-salinity estimates

We used the equation after Shackleton (1974):

$$\delta^{18}O_{seawater} = \delta^{18}O_{calcite} + (Temperature - 16.9)/4 + 0.27 + 0.22, \quad (5)$$

to estimate past changes in seawater $\delta^{18}O$. The constant 0.22±0.13‰ is the average offset between our core-top *P. ariminensis* $\delta^{18}O$ and the predicted $\delta^{18}O$ of calcite (Table 2.3). Paleo-salinity estimates were calculated using the equation suggested by Schäfer-Neth and Paul (2004),

$$Salinity = \Delta Salinity_{glacial} + A*(\delta^{18}O_{seawater} - \delta^{18}O_{glacial}) + B, \quad (6)$$

where A = 2.17, B = 34.46 were adopted from equation (4), assuming that the modern $\delta^{18}O_{seawater}$-salinity is also applicable for the last glacial period. $\delta^{18}O_{glacial}$ is the glacial increase in global mean seawater $\delta^{18}O$ due to the buildup of continental ice sheets. $\delta^{18}O_{glacial}$ equals to 1.0±0.1‰ during the LGM (Schrag et al., 2002) when the sea-level was 120 m lower than the present (Peltier and Fairbanks, 2006). If we applied the proportion of 120 m/1.0‰ to HS1 when the sea-level was 100 m lower relative to the present day (Peltier and Fairbanks, 2006), then $\delta^{18}O_{glacial}$ is estimated to be roughly 0.83‰ during HS1. $\Delta Salinity_{glacial}$ is the glacial increase in the global mean seawater salinity due to the sea-level lowering and a decrease in the ocean volume. It can be calculated as

$$\Delta Salinity_{glacial} = 34.7*\Delta/(3800 - \Delta), \quad (7)$$

where Δ is the mean sea-level change in m (Schmidt, 1999a). ΔSalinity is thus approximately 1.1 psu during the LGM and 0.9 psu during HS1. We followed the method described in Schmidt (1999a) to calculate the uncertainty of seawater $\delta^{18}O$ and salinity estimates. The following error sources are taken into account: the duplicated measurements of *P. ariminensis* $\delta^{18}O$ show a standard error of ±0.1‰; the core-top *P. ariminensis* $\delta^{18}O$ shows a nearly constant offset towards lower values from the predicted $\delta^{18}O$ of calcite by 0.22±0.13‰ (Table 2.3), ±0.13‰ was therefore taken into account; the Mg/Ca-temperature estimate has a standard error of ±0.6°C (see section 2.5.2). For glacial seawater $\delta^{18}O$ estimate, we still need to include the error of $\delta^{18}O_{glacial}$, which is ±0.1‰ for the LGM (Schrag et al., 2002) but is unknown for the HS1 period. Therefore, the standard error of the LGM and the core-top seawater $\delta^{18}O$ estimate is ±0.32‰ and ±0.30‰, respectively.

The standard error of equation (4) is ±0.12‰, and the error for the LGM ΔSalinity estimate is ±0.05 psu (the LGM sea-level is estimated to be 120±5 m lowering relative to the present day (Peltier and Fairbanks, 2006)). Therefore, the standard error of the core-top and the LGM salinity estimate is ±0.70 psu and ±0.74 psu, respectively. It is practically impossible to calculate the errors of the HS1 seawater $\delta^{18}O$ and salinity estimates. We simply assume that they are equal to the errors of the LGM estimates. However, since the glacial and the deglacial $\delta^{18}O_{seawater}$-salinity relationships were possibly different from the present day, the standard errors of the LGM and HS1 seawater $\delta^{18}O$ and salinity estimates could be even larger (Schmidt, 1999a).

2.4.7 Estimates of thermocline-water $\Delta[CO_3^{2-}]$ values

Thermocline-water $\Delta[CO_3^{2-}]$ values are calculated using the CO2sys_xls_program (Lewis and Wallace, 2006). Input parameters of temperature, salinity, pressure, total silicate and total phosphorous were taken from the WOA2009 (Antonov et al., 2009; Garcia et al., 2009; Locarnini et al., 2009), total alkalinity and total CO_2 are from the GLODAP database (Key et al., 2004). When calculating thermocline-water $\Delta[CO_3^{2-}]$ of the northeastern tropical Atlantic, temperature and salinity of the in-situ CTD data (Figure 2.2) are used instead of those from the World Ocean Atlas 2009 (Antonov et al., 2009; Locarnini et al., 2009). The equilibrium constants of K_1 and K_2 were taken from Mehrbach et al. (1973) refitted later by Dickson and Millero (1987). The dissociation constant for K_{HSO4} is from Dickson (1990). $[CO_3^{2-}]_{saturation}$ at a given location and water depth is calculated by $[CO_3^{2-}]/\Omega$, where Ω is the solubility ratio of calcite. $\Delta[CO_3^{2-}]$ is further obtained by calculating $[CO_3^{2-}] - [CO_3^{2-}]_{saturation}$.

2.5 *P. ariminensis* Mg/Ca-temperature calibration

2.5.1 Evaluating *P. ariminensis* Mg/Ca as a proxy for thermocline-water temperature

Benthic foraminiferal Mg/Ca allows for reconstruction of bottom-water temperatures. Earlier studies have established an exponential relationship between *Cibicidoides* spp. Mg/Ca and temperatures (Rosenthal et al., 1997; Lear et al., 2002; Martin et al., 2002). However, a later study suggested a strong linear dependence of *Cibicidoides pachyderma* Mg/Ca on temperature within the temperature range from 6 to 19ºC (Marchitto et al., 2007). The earlier exponential fit between *Cibicidoides* Mg/Ca and temperatures was probably biased by warm water samples from the Little Bahamas Bank, where foraminiferal tests were contaminated by secondary high-Mg calcite overgrowth (Marchitto et al., 2007; Curry and Marchitto, 2008). Recent studies reveal that a linear regression between Mg/Ca and temperatures fits for a variety of benthic foraminiferal species (e.g., Rosenthal et al., 2006, 2011; Bryan and

Marchitto, 2008; Elderfield et al., 2010). Moreover, the published exponential relationship of benthic Mg/Ca-temperature (e.g., Rathmann et al., 2004; Healey et al., 2008) could actually be replaced by linear ones. Large inter-genus and inter-species differences in Mg/Ca have also been observed (e.g., Elderfield et al., 2006). The Mg/Ca-temperature sensitivity varies from 0.03 mmol/mol per °C for *Hoeglundina elegans* (Bryan and Marchitto, 2008) to 0.40 mmol/mol per °C for *Hyalinea balthica* (Rosenthal et al., 2011). Therefore, it is essential to use a species-specific Mg/Ca-temperature calibration rather than a multi-species approach.

An increasing number of studies suggested that the Mg/Ca of benthic foraminifera is not only a function of bottom-water temperature but also can be affected by the carbonate-ion saturation state ($\Delta[CO_3^{2-}]$). At the low temperature end (<3°C), the slope of the Mg/Ca-temperature calibration is steeper than that at the high temperature end (Martin et al., 2002; Elderfield et al., 2006; Healey et al., 2008). This was attributed to a considerable influence of $\Delta[CO_3^{2-}]$ on the Mg uptake of benthic foraminifera (Elderfield et al., 2006; Yu and Elderfield, 2008). A global ocean data compilation reveals that the Mg/Ca of the epibenthic species *Cibicidoides wuellerstorfi* from water depths with $\Delta[CO_3^{2-}]$ values below 25 µmol/kg, is positively correlated with ambient sea water $\Delta[CO_3^{2-}]$, showing a sensitivity of 0.008-0.010 mmol/mol per µmol/kg (Elderfield et al., 2006; Healey et al., 2008; Raitzsch et al., 2008, Yu and Elderfield, 2008). The influence of $\Delta[CO_3^{2-}]$ on the benthic Mg/Ca, therefore, limits the application of the benthic Mg/Ca for reconstruction of temperatures <3ºC.

A few studies suggest that there might exist a $\Delta[CO_3^{2-}]$ threshold for changes in benthic foraminiferal Mg/Ca. The current dataset indicates that only when $\Delta[CO_3^{2-}]_{calcite}$ is <25 µmol/kg and $\Delta[CO_3^{2-}]_{aragonite}$ is <15 µmol/kg, the carbonate-ion effect plays an important role on the Mg/Ca values of calcareous species *Cibicidoides wuellerstorfi* (Yu and Elderfield, 2008) and aragonitic species *Hoeglundina elegans* (Rosenthal et al., 2006), respectively. Yet it is unknown whether such a threshold also exists for the calcareous species *P. ariminensis* and if so, how large the threshold is. Thermocline waters in the North Atlantic are usually supersaturated or near-saturated with carbonate, e.g., bottom-water $\Delta[CO_3^{2-}]$ ranges between 31 and 53 µmol/kg at our coring locations (Table 2.3). The benthic Mg/Ca from thermocline waters might not be complicated by changes in seawater $\Delta[CO_3^{2-}]$ and therefore a promising proxy for reconstruction of thermocline temperatures (e.g., Bamberg et al., 2010). Nevertheless, an estimate of a possible influence of the carbonate-ion effect on the benthic Mg/Ca samples from thermocline waters is still necessary.

At thermocline water depths, bottom-water temperature and $\Delta[CO_3^{2-}]$ are usually well correlated. It is thus difficult to disentangle the effects of temperature and $\Delta[CO_3^{2-}]$ on Mg/Ca

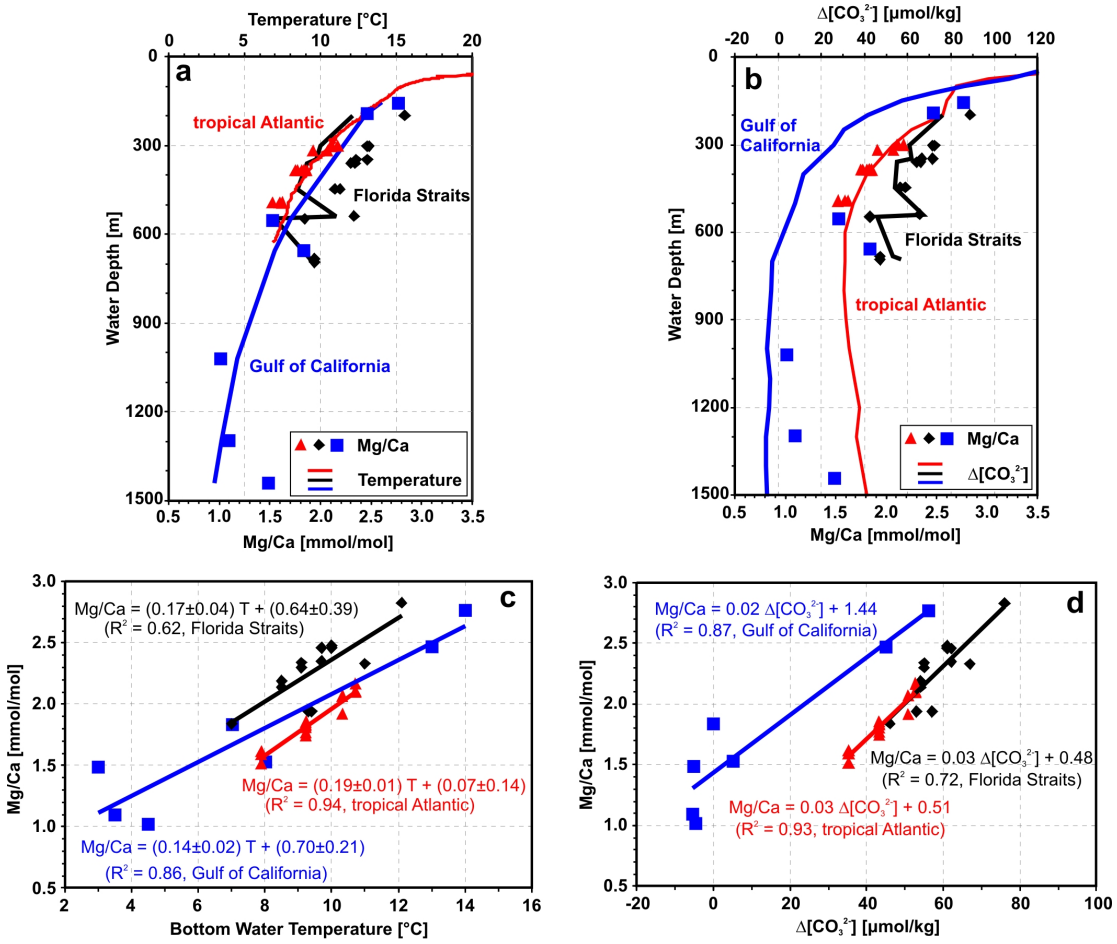

Figure 2.5 Comparison of *P. ariminensis* Mg/Ca, bottom-water temperatures and $\Delta[CO_3^{2-}]$ from the Florida Straits, the Gulf of California, and the northeastern tropical Atlantic. (a) Changes of water temperatures and the benthic Mg/Ca with water depth in the three research areas. (b) Changes of seawater $\Delta[CO_3^{2-}]$ and the benthic Mg/Ca with water depth. (c) *P. ariminensis* Mg/Ca plotted versus bottom-water temperatures. (d) *P. ariminensis* Mg/Ca plotted versus bottom-water $\Delta[CO_3^{2-}]$. The best fit linear regressions of two variables were also presented in (c) and (d). In each plot, diamond dots are samples from the Florida Straits (Bryan and Marchitto, 2008), rectangle dots from the Gulf of California (Lear et al., 2002) and triangle dots from the northeastern tropical Atlantic (this study). *P. ariminensis* Mg/Ca of the Florida Straits and the Gulf of California were corrected by +0.1 mmol/mol. Bottom-water $\Delta[CO_3^{2-}]$ values and temperatures of the Florida Straits are in-situ measurements (Bryan and Marchitto, 2008). Seawater temperature profiles of the tropical Atlantic and the Gulf of California are from the CTD and the WOA2009 data (Locarnini et al., 2009), respectively. Bottom-water $\Delta[CO_3^{2-}]$ values of the Gulf of California and the tropical Atlantic were calculated using the CO2sys_xls_program (Lewis and Wallace, 2006).

(Marchitto et al., 2007). One solution is to collect samples of benthic foraminifera from areas with different bottom-water $\Delta[CO_3^{2-}]$ values but same temperatures. We compare published *P. ariminensis* Mg/Ca data from the Florida Straits (Bryan and Marchitto, 2008) and the Gulf of California (Lear et al., 2002) with our new data from the northeastern tropical Atlantic. Modern thermocline waters of the Florida Straits, the Gulf of California and the northeastern tropical Atlantic between 200-700 m have a similar thermal structure (Figure 2.5a) but very different $\Delta[CO_3^{2-}]$ values (Figure 2.5b). Therefore, not only do core-top samples of these three areas allow to test the influence of temperature and $\Delta[CO_3^{2-}]$ on the benthic Mg/Ca, but also they allow an intercomparison of regional Mg/Ca-temperature calibrations. Our new data (Table 2.3) cover a temperature range from 7.9 to 10.7ºC. Except five samples of the Gulf of California that are from water depths below 500 m with relatively low $\Delta[CO_3^{2-}]$ values of -6 to +5 μmol/kg, all other samples are located in thermocline waters with $\Delta[CO_3^{2-}]$ values higher than the possible threshold of 25 μmol/kg for calcareous species (Yu and Elderfield, 2008) (Figure 2.5b).

It should be noted that the samples of Lear et al. (2002) and Bryan and Marchitto (2008) were cleaned using oxidative and reductive steps (Boyle and Keigwin, 1985), while our samples were cleaned using only an oxidative step (Barker et al., 2003). Mg/Ca ratios in samples cleaned by oxidative and reductive steps are 0.10±0.09 mmol/mol lower than those only cleaned by an oxidative step (Elderfield et al., 2006; Yu and Elderfield, 2008). Therefore, the Mg/Ca data of Lear et al. (2002) (Table 2.4) and Bryan and Marchitto (2008) are corrected by 0.10 mmol/mol in order to be comparable to our data.

As shown in Figure 2.5a and 2.5c, *P. ariminensis* Mg/Ca of all the three areas follow thermocline temperature changes along water depths. In each area, benthic Mg/Ca and bottom-water temperatures can be fit in a linear relationship. The slopes of the three linear regressions range between 0.14 and 0.19 mmol/mol per ºC, which are close to each other given their uncertainties. This might indicate a dominant control of temperature on the benthic Mg/Ca. However, absolute Mg/Ca values of the Florida Straits samples are about 0.40 mmol/mol higher than those of the tropical Atlantic samples within the temperature range from 8 to 11ºC. In contrast, in a Mg/Ca vs. $\Delta[CO_3^{2-}]$ plot, samples of the tropical Atlantic and the Florida Straits fit in a same linear relationship (Figure 2.5d). In this sense, the benthic Mg/Ca ratios from thermocline waters seemingly are also impacted by the carbonate-ion effect. Several other lines of evidence, however, argue that $\Delta[CO_3^{2-}]$ does not exert an obvious control on the benthic Mg/Ca:

First, the averaged seawater $\Delta[CO_3^{2-}]$ value between 150-700 m of the Gulf of California is significantly lower than that of the tropical Atlantic and that of the Florida Straits by 25 and 40 μmol/kg, respectively (Figure 2.5b). If the 0.4 mmol/mol offset between the Florida Straits and our data was caused by the carbonate-ion effect, then the Mg/Ca data of the Gulf of California should be significantly lower than those of the other two areas. However, within the temperature range from 7 to 14ºC, the four Mg/Ca data point of the Gulf of California are still close to either our data or those of the Florida Straits (Figure 2.5a and 2.5c).

Second, if the $\Delta[CO_3^{2-}]$ had a profound effect on the benthic Mg/Ca from thermocline waters, the slope of the Mg/Ca-temperature calibration would become steeper towards the low temperature end (e.g., Rosenthal et al., 2006). However, at least for *P. ariminensis* data within the temperature range from 7 to 14ºC, we cannot find such a trend (Figure 2.5a and 2.5c). Marchitto et al. (2007) reported another contrary phenomenon that the Mg uptake of *C. pachyderma* from the Florida Straits is possibly suppressed at high levels of carbonate supersaturation. The slope of the *C. pachyderma* Mg/Ca-temperature calibration therefore flattens at temperatures of 12 to 18.6ºC (Marchitto et al., 2007). We do not observe this trend for the available data of *P. ariminensis* either (Figure 2.5c).

Third, if indeed the carbonate-ion effect could influence the Mg uptake of benthic foraminifera from thermocline depths, then to what extent might $\Delta[CO_3^{2-}]$ alter the benthic Mg/Ca signal? The current *P. ariminensis* Mg/Ca dataset is still limited. Although all the Mg/Ca samples of the Florida Straits and the northeastern tropical Atlantic are concentrated in the temperature range from 7 to 12ºC (Figure 2.5c), the significant offset between these two

Table 2.4 Estimated bottom-water $\Delta[CO_3^{2-}]$ values at sediment core locations in the Gulf of California (Lear et al., 2002).

Core	latitude	longitude	Water Depth (m)	Temperature (ºC)	*P. ariminensis* Mg/Ca (mmol/mol) [a]	$\Delta[CO_3^{2-}]$ (μmol/kg) [b]
GGC73	30.57ºN	114.10ºW	154	14.0	2.77	56
GGC71	30.68ºN	114.12ºW	190	13.0	2.47	45
GGC47	27.93ºN	111.80ºW	552	8.0	1.53	5
BC43	27.90ºN	111.65ºW	655	7.0	1.84	0
GGC24	26.08ºN	110.83ºW	1020	4.5	1.02	-5
GGC16	26.00ºN	110.67ºW	1295	3.5	1.10	-6
GGC53	27.62ºN	111.93ºW	1442	3.0	1.49	-5

a. Mg/Ca data was corrected by 0.1 mmol/mol;

b. $\Delta[CO_3^{2-}]$ was calculated by the CO2sys_xls_program (Lewis and Wallace, 2006).

data sets might be caused by other reasons rather than the carbonate-ion effect (discussed below). For samples from the Gulf of California, only two Mg/Ca data are available for the temperature range from 7 to 12ºC. Therefore, we cannot estimate the Mg/Ca-$\Delta[CO_3^{2-}]$ sensitivity of *P. ariminensis* by comparing data from thermocline waters with different $\Delta[CO_3^{2-}]$ values. In previous studies, the Mg/Ca-$\Delta[CO_3^{2-}]$ sensitivity of benthic foraminifera was also assessed by using samples from waters undersaturated or slightly saturated with respect to carbonate (e.g., Elderfield et al., 2006; Rosenthal et al., 2006). Unfortunately, we do not have enough data from less saturated waters either (Figure 2.5c). This also prohibits the attempt to estimate the sensitivity of *P. ariminensis* Mg/Ca to $\Delta[CO_3^{2-}]$.

Therefore, we assume that a $\Delta(Mg/Ca/\Delta[CO_3^{2-}])$ sensitivity of 0.009 mmol/mol per µmol/kg of *C. wuellerstorfi* (Elderfield et al., 2006) is also applicable to *P. ariminensis*, although this possibly overestimates the Mg/Ca-$\Delta[CO_3^{2-}]$ sensitivity of *P. ariminensis*. As discussed above, the slope of Mg/Ca-temperature calibration is not found to be flattened or steepened at high or low $\Delta[CO_3^{2-}]$ values, respectively (Figure 2.5). In our study area, the bottom-water $\Delta[CO_3^{2-}]$ difference between the shallowest core GeoB9532-1 (301 m) and a deeper core GeoB9534-4 (493 m) is 18 µmol/kg (Table 2.3), which is presumed to be able to cause a 0.16 mmol/mol change in the Mg/Ca signal. However, 0.16 mmol/mol can only account for 30% of a total of 0.55 mmol/mol changes in the Mg/Ca between core GeoB9532-1 and GeoB9534-4 (Table 2.3). This is also the case for samples from the Florida Straits (Figure 2.5). Therefore, a possible carbonate-ion effect would not be fully able to explain the benthic Mg/Ca changes between different cores in each area.

If the entire dataset of *P. ariminensis* Mg/Ca was determined by both temperature and $\Delta[CO_3^{2-}]$, we can also try to disentangle the contributions caused by these two factors as follows: In a Mg/Ca vs. temperature plot, the global core-top Mg/Ca data and temperatures can be fit by a straight line with a slope of 0.15 mmol/mol per ºC (Figure 2.S1). We thus arbitrarily adopted this value as the Mg/Ca-temperature sensitivity of *P. ariminensis*. The Mg/Ca variations caused by the temperature effect can therefore be subtracted from the measured Mg/Ca. The residual Mg/Ca values, however, do not show any correlation with thermocline-water $\Delta[CO_3^{2-}]$ (auxiliary material and Figure 2.S2). This indicates that the offsets between Mg/Ca data from different areas are actually not related to the carbonate-ion effect. Taken together, although we still cannot completely exclude a possible influence of the carbonate-ion effect on *P. ariminensis* Mg/Ca ratios from thermocline waters, the above estimates suggest that it should be very minor. Temperature seems to be the primary control of changes in Mg/Ca. But one question still remains: why are *P. ariminensis* Mg/Ca data of the Florida Straits higher than our data by 0.4 mmol/mol (Figure 2.5c)?

C. pachyderma from the same subset of samples of the Florida Straits were analyzed both by ICP-MS (Marchitto et al. 2007) and secondary ionization mass spectrometry (Curry and Marchitto, 2008). *C. pachyderma* Mg/Ca results obtained using ICP-MS are found systematically higher than those of secondary ionization mass spectrometry data by 0.5-0.7 mmol/mol within the temperature range from 9 to 12ºC (Curry and Marchitto, 2008). The elevated ICP-MS values were suspected to be caused by contamination or diagenetic alteration of secondary high-Mg calcite, which is hard to be removed by chemical cleaning methods. However, because no convincing evidence was found to support such an inference, the reasons for the data offset are still unknown (Marchitto et al. 2007; Curry and Marchitto, 2008). The *P. ariminensis* Mg/Ca of the Florida Straits were also analyzed by ICP-MS (Bryan and Marchitto, 2008) and show higher values than our data over nearly the same temperature range from 8 to 11ºC. The good correlation between the Mg/Ca and temperatures (Figure 2.5c) suggests that the core-top *P. ariminensis* tests from the Florida Straits are not contaminated by secondary high-Mg calcite, although this might be the case for *P. ariminensis* tests from the LGM samples in this area (Bryan and Marchitto, 2008). The 0.4 mmol/mol offset is also too high to be explained by a potential inter-laboratory offset (Rosenthal et al., 2004). Our above discussion also excludes the possibility of the carbonate-ion effect. Therefore, at the moment we do not really understand the exact reason for the offset between the Florida Strait and our data, but it is likely due to some local reasons. This would call for further studies by reanalyzing samples of the Florida Straits and the eastern tropical Atlantic using different methods, or by comparing core-top *P. ariminensis* samples from more geographic locations.

2.5.2 Core-top *P. ariminensis* Mg/Ca-temperature calibration

In an attempt to establish a new *P. ariminensis* Mg/Ca-temperature calibration, we exclude the Florida Straits data as they show a significant offset from our data due to unknown reasons. We combine our core-top data only with the data of Lear et al. (2002) in order to cover a broader temperature range. Mg/Ca data from the Gulf of California is relatively scattered at the low temperature end (Figure 2.5). However, the slope of the Mg/Ca-temperature calibration is not steepened at the low temperature end, which indicates that the scattered data is not likely induced by the carbonate-ion effect. Nevertheless, because previous studies suggest that the Mg/Ca of calcareous benthic foraminifera is very likely biased by the carbonate-ion effect when bottom-water $\Delta[CO_3^{2-}]$ values are below 25 μmol/kg, and we are more interested in the Mg/Ca-temperature calibration at the high temperature end in this study, we included only samples from sites with $\Delta[CO_3^{2-}]$ values above this possible threshold. Hence, only two samples from Lear et al. (2002) were used. These data show a linear relationship (Figure 2.6):

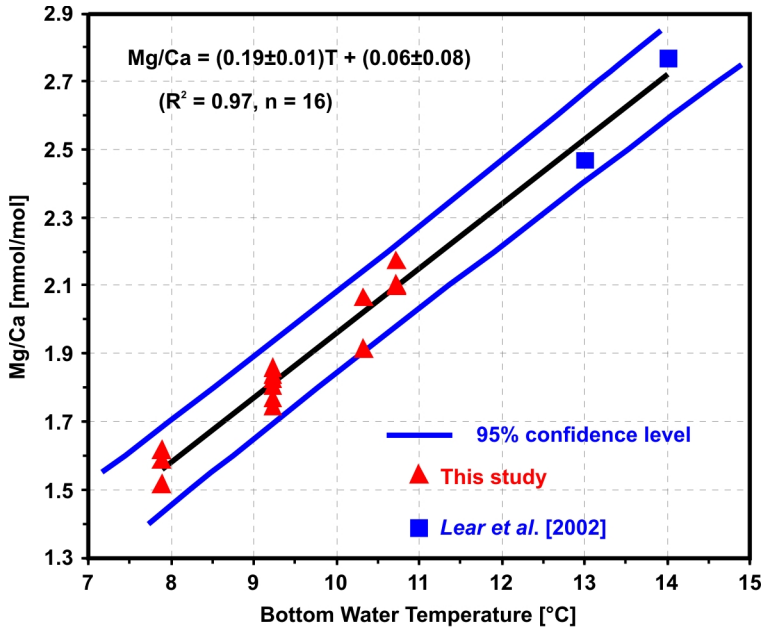

Figure 2.6 Mg/Ca-bottom water temperature calibration of *P. ariminensis*, based on core-top data from the northeastern tropical Atlantic (this study) and the Gulf of California (Lear et al., 2002). P. *ariminensis* Mg/Ca of the Gulf of California was corrected by +0.1 mmol/mol. The linear regression and 95% confidence intervals for the linear regression are shown in black and blue curves, respectively.

$$\text{Mg/Ca} = (0.19\pm0.01)\ \text{Temperature} + (0.06\pm0.08). \quad (8)$$

This new calibration covers a temperature range from 8.0 to 14.0°C. The Mg/Ca-temperature sensitivity of 0.19 mmol/mol per ºC is slightly higher than 0.12 mmol/mol per ºC for *C. pachyderma* (Marchitto et al. 2007). The uncertainty in the coefficients of equation (8) is the standard error. The linear relationship between the Mg/Ca and temperatures also suggests that the carbonate-ion effect on the benthic Mg/Ca is very limited over the temperature range of 8.0 to 14.0°C. Otherwise, the calibration slope might become steeper at the low temperature end (e.g., Rosenthal et al., 2006) or flattened at the high temperature end (Marchitto et al. 2007). The standard error of this regression is ±0.05 mmol/mol: this equals to an uncertainty of the temperature estimate of ±0.3°C. At the 95% confidence level, the prediction uncertainty is ±0.7°C within the temperature range from 7.0 to 14.0°C. However, if we considered the propagated error from reproducibility of Mg/Ca samples (±0.05 mmol/mol) and the uncertainty caused by combining data from different chemical cleaning methods (±0.09 mmol/mol) (Yu and Elderfield, 2008), the total standard error of the Mg/Ca estimate would reach up to ±0.11 mmol/mol. This equals to an uncertainty of the temperature estimate

of ±0.6°C. This uncertainty could be even larger if a minor carbonate-ion effect existed. However, as we do not know the exact Mg/Ca-$\Delta[CO_3^{2-}]$ sensitivity of *P. ariminensis*, it is practically impossible to exclude the carbonate-ion effect on Mg/Ca variations and to estimate the associated uncertainty.

2.5.3 Fragmentation index and past changes in seawater $\Delta[CO_3^{2-}]$ values

Although a possible carbonate-ion effect on core-top samples was estimated to be minor, we further tested whether there were significant changes in past thermocline-water $\Delta[CO_3^{2-}]$ and whether changes in $\Delta[CO_3^{2-}]$ might have biased our Mg/Ca-temperature estimates during the LGM and HS1. As we lack proxy records such as foraminiferal B/Ca (e.g., Yu and Elderfield, 2007) to quantify past changes in bottom-water $\Delta[CO_3^{2-}]$, we use the fragmentation index of planktonic foraminifera as a proxy. A recent study revealed that the non-fragmented foraminiferal shell content (equals to the grain size fraction >63 μm) in pelagic sediments from the equatorial Atlantic is well correlated with seawater $\Delta[CO_3^{2-}]$ within the $\Delta[CO_3^{2-}]$ range from -10 to +40 μmol/kg (Raitzsch et al., 2011). The fragmentation index is different from but a more precise proxy than the non-fragmented foraminiferal shell content for indicating carbonate-dissolution changes. The results of Raitzsch et al. (2011) imply that the fragmentation index should also be able to indicate past changes in seawater $\Delta[CO_3^{2-}]$. The fragmentation index could also be impacted by the sedimentation processes such as reworking of sediment and subsequently downslope transport. Foraminiferal tests are often poorly preserved in reworked sediment. However, except the core-top sample of core GeoB9535-5, the fragmentation index is generally low (< 23%) in all samples (Figure 2.7), suggesting that these samples are not originating from re-deposition processes.

The core-top fragmentation index increases with water depth (Figure 2.7). In the upper three cores, the indices remain at a relatively low level of below 23%. In contrast, the core-top fragmentation index reaches up to 45% in the deepest core GeoB9535-5. We suggest that this is because the modern bottom water over this core location is partly influenced by the corrosive Antarctic Intermediate Water (Figure 2.1 and 2.2). The core-top fragmentation indices and modern bottom-water $\Delta[CO_3^{2-}]$ values fit well in a exponential relationship (Figure 2.7):

$$\text{Fragmentation index} = 1233.3\exp(-0.1109\Delta[CO_3^{2-}]). \quad (9)$$

The fragmentation index is strongly sensitive to $\Delta[CO_3^{2-}]$ changes within the $\Delta[CO_3^{2-}]$ range from 30 to 43 μmol/kg, but is much less sensitive when $\Delta[CO_3^{2-}] > 43$ μmol/kg. This result is

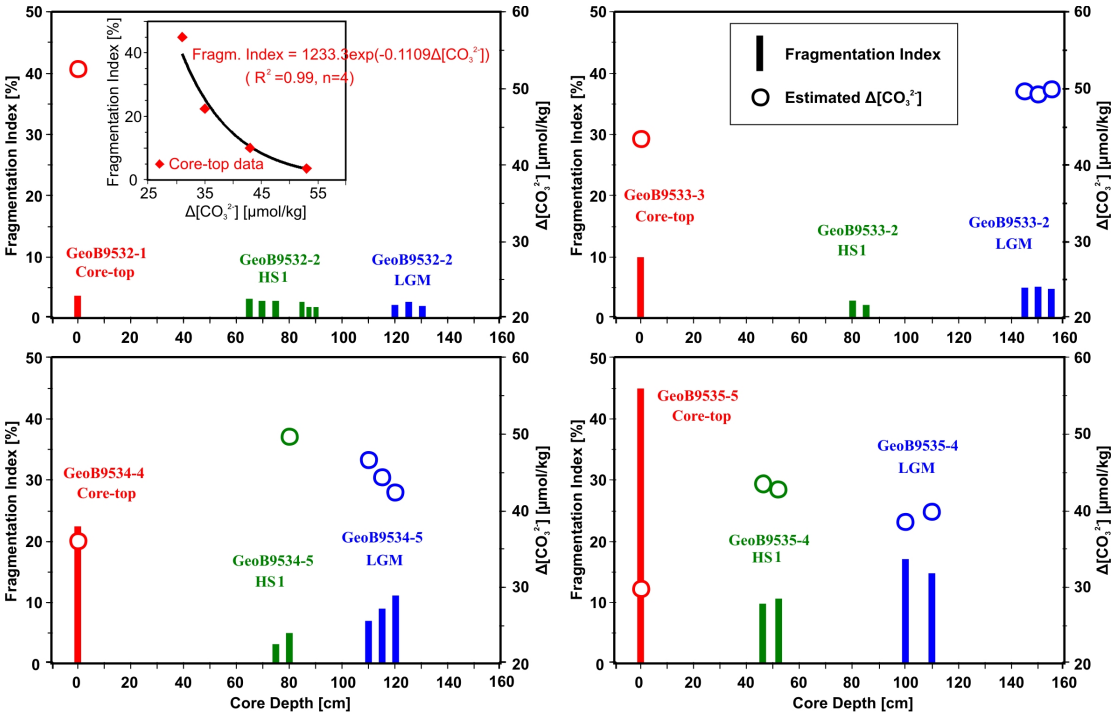

Figure 2.7 Planktonic foraminiferal fragmentation indices and the estimated bottom-water $\Delta[CO_3^{2-}]$ values for selected time slices. The core-top fragmentation indices and modern bottom-water $\Delta[CO_3^{2-}]$ values are well fit in a exponential relationship.

in line with that of Raitzsch et al. (2011), in that the dissolution index becomes insensitive in highly carbonate oversaturated waters as the carbonate dissolution is negligible there. We use equation (9) to convert the downcore fragmentation indices into $\Delta[CO_3^{2-}]$ values.

During the LGM and HS1, the fragmentation indices remain the same as for the core-top in GeoB9532-2 (Figure 2.7). In all the three deeper cores, the glacial fragmentation indices decreased relative to their core-top values. Especially in core GeoB9535-4, the fragmentation indices decreased to 15% during the LGM and to 10% during HS1, respectively. This indicates a better preservation and elevated bottom-water $\Delta[CO_3^{2-}]$ levels. We suggest that core GeoB9535-4 was not influenced by the glacial Antarctic Intermediate Water when the sea-level was 120 m and 100 m lower during the LGM and HS1, respectively (Peltier and Fairbanks, 2006). Glacial bottom waters over this core location were presumed to be glacial Atlantic central water masses, which should be more supersaturated with $\Delta[CO_3^{2-}]$.

We only present the estimated $\Delta[CO_3^{2-}]$ values within the calibration range (Figure 2.7) and make use of them for the following calculation. We notice that most of the glacial

fragmentation indices are below 10%, that is, in a range, in which the fragmentation index-$\Delta[CO_3^{2-}]$ sensitivity is small. Therefore, there might be a large uncertainty associated with the glacial bottom-water $\Delta[CO_3^{2-}]$ estimate. The averaged LGM seawater $\Delta[CO_3^{2-}]$ values are 6.6, 9.5 and 8.2 µmol/kg higher than their core-top values in core GeoB9533-2/3, 9534-4/5 and 9535-4/5, respectively. If we again adopted a $\Delta(Mg/Ca/\Delta[CO_3^{2-}])$ sensitivity of 0.009 mmol/mol per µmol/kg (Elderfield et al., 2006) for *P. ariminensis* (although possibly it is an overestimate), then increases in the LGM bottom-water $\Delta[CO_3^{2-}]$ might result in a Mg/Ca overestimate of 0.06, 0.09 and 0.07 mmol/mol, and a temperature overestimate of 0.3°C, 0.5°C and 0.4°C (based on equation (8)) in samples from core GeoB9533-2/3, 9534-4/5 and 9535-4/5, respectively.

The difference between core-top and the HS1 fragmentation indices is even larger (Figure 2.7). Therefore, the HS1 temperature estimate at core GeoB9534-5 and GeoB9535-4 might be possibly biased by the carbonate-ion effect by up to 0.7°C and 0.6°C, respectively. The HS1 fragmentation indices of core GeoB9533-2 and all the glacial fragmentation indices of the shallowest core GeoB9532-2 are beyond the calibration range, and therefore not reliable for a glacial $\Delta[CO_3^{2-}]$ estimate. Modern seawater $\Delta[CO_3^{2-}]$ values show a nearly linear relationship with water depths between 200-400 meters at our coring locations. We thus assume that a possible Mg/Ca overestimate of 0.06 mmol/mol and a possible temperature overestimate of 0.3ºC caused by the carbonate-ion effect for glacial samples of core GeoB9533-2 also apply to the glacial samples of core GeoB9532-2. However, the averaged Mg/Ca difference between glacial and core top samples is 0.40, 0.38, 0.24 mmol/mol in core GeoB9532-2, 9533-2/3, 9534-4/5, respectively (Table 2.3 and 2.5), which apparently cannot be fully explained by changes in bottom-water $\Delta[CO_3^{2-}]$ and the carbonate-ion effect at these core locations.

Taken together, the above estimate, although not in a strictly quantitative way, suggests that there were no significant changes in thermocline-water $\Delta[CO_3^{2-}]$ during the LGM and HS1 relative to the late Holocene. If the carbonate-ion effect had an influence on the *P. ariminensis* Mg/Ca, it would bias past Mg/Ca-temperature estimates only at a limited level. Overall, changes in the benthic Mg/Ca should be dominantly caused by temperature rather than $\Delta[CO_3^{2-}]$ at our coring sites during the LGM, HS1 and the present day.

2.6 Downcore results

2.6.1 *P. ariminensis* Mg/Ca-temperatures of the LGM and HS1

We used the newly developed *P. ariminensis* Mg/Ca-temperature calibration to estimate

Table 2.5 LGM and HS1 *P. ariminensis* Mg/Ca and $\delta^{18}O$ results of four gravity cores.

Core	Sample Depth (cm)	*P. ariminensis* Mg/Ca (mmol/mol)	*P. ariminensis* $\delta^{18}O$ (PDB, ‰)	Remarks	Core	Sample Depth (cm)	*P. ariminensis* Mg/Ca (mmol/mol)	*P. ariminensis* $\delta^{18}O$ (PDB, ‰)	Remarks
GeoB9532-2	70	2.40	2.64	HS1	GeoB9534-5	105	1.73	3.28	LGM
GeoB9532-2	75	2.55	2.62	HS1	GeoB9534-5	110	1.90	3.05	LGM
GeoB9532-2	80	2.07	2.37	HS1	GeoB9534-5	115	1.80	3.31	LGM
GeoB9532-2	85	2.08	2.36	HS1	GeoB9534-5	120	1.89	3.16	LGM
GeoB9532-2	87	2.12	2.73	HS1	GeoB9534-5	125	1.79	3.32	LGM
GeoB9532-2	90	2.30	2.61	HS1	GeoB9534-5	130	1.73	3.45	LGM
GeoB9532-2	95	2.38	2.75	HS1	GeoB9534-5	135		3.30	LGM
GeoB9532-2	110	2.65	2.74	LGM					
GeoB9532-2	115	2.40	2.68	LGM	GeoB9535-4	44	1.71	2.73	HS1
GeoB9532-2	120	2.69	2.69	LGM	GeoB9535-4	46	1.75		HS1
GeoB9532-2	125	2.40	2.68	LGM	GeoB9535-4	48	1.78		HS1
GeoB9532-2	130	2.46	2.88	LGM	GeoB9535-4	50		2.88	HS1
GeoB9532-2	135		2.57	LGM	GeoB9535-4	51	1.79		HS1
GeoB9532-2	140	2.50	2.75	LGM	GeoB9535-4	54		3.09	HS1
					GeoB9535-4	58		3.60	HS1
GeoB9533-2	75	2.42	2.46	HS1	GeoB9535-4	60		2.85	HS1
GeoB9533-2	80	2.38	2.83	HS1	GeoB9535-4	62	1.63	2.62	HS1
GeoB9533-2	85	2.19	2.12	HS1	GeoB9535-4	64	1.77		HS1
GeoB9533-2	90	2.09	2.86	HS1	GeoB9535-4	66		2.46	HS1
GeoB9533-2	95	2.15	2.94	HS1	GeoB9535-4	84		3.04	LGM
GeoB9533-2	145	2.01	3.01	LGM	GeoB9535-4	92		3.15	LGM
GeoB9533-2	150	2.21	3.07	LGM	GeoB9535-4	98		3.50	LGM
GeoB9533-2	155	2.03	3.10	LGM	GeoB9535-4	105		3.46	LGM
GeoB9533-2	160	2.28	2.97	LGM	GeoB9535-4	109		3.59	LGM
GeoB9533-2	165	2.19	2.93	LGM	GeoB9535-4	110.5	1.68		LGM
GeoB9533-2	170	2.03	2.98	LGM	GeoB9535-4	115.5	1.79		LGM
					GeoB9535-4	116		3.28	LGM
GeoB9534-5	70		2.79	HS1	GeoB9535-4	124		3.43	LGM
GeoB9534-5	75	1.80	3.00	HS1	GeoB9535-4	128		3.56	LGM
GeoB9534-5	80	1.80	3.22	HS1					
GeoB9534-5	81	1.76	2.34	HS1					
GeoB9534-5	83	1.87	3.35	HS1					
GeoB9534-5	85	1.93	2.63	HS1					
GeoB9534-5	90	1.82	3.32	HS1					
GeoB9534-5	95		3.21	HS1					

bottom-water temperature changes at our coring sites for the selected time slices. After correction for changes in sea-level, the LGM thermocline temperatures are comparable to the present day between 200-372 m water depths (Figure 2.8). In contrast, the LGM thermocline temperatures are approximately 1.2°C warmer at intermediate depth (550 m) compared to modern values. The thermal gradient of the LGM water column between 400-570 m depth was therefore reduced with respect to the present day. Thermocline temperature estimates for HS1 are close to those of the LGM. Relative to the present day, the HS1 thermocline temperatures are about 0.6°C cooler at 217 m depth, 0.8°C warmer at 284 m depth, nearly unchanged at 392 m depth and 1.5°C warmer at 570 m depth (Figure 2.8). Given the

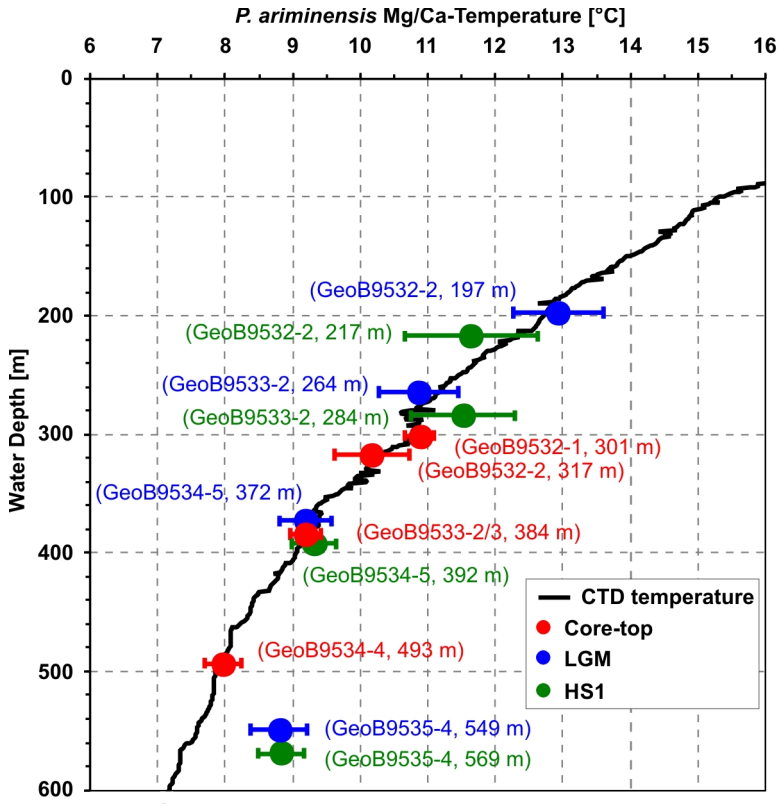

Figure 2.8 Estimated bottom-water temperature changes with water depth. Dots are mean values from each core for a specific time interval. Error bars represent one standard deviation (±1σ) of a few individual measurements. Mean temperature data of four CTD stations is shown in black curve. The HS1 and the LGM core water depths are adjusted by -100 m and -120 m, respectively, to account for sea-level lowering (Peltier and Fairbanks, 2006). We did not find enough benthic foraminifera for Mg/Ca analyses from core-top samples of cores GeoB9535-4/5.

uncertainty of Mg/Ca-temperature estimate, temperature variations at 217 m and 284 m depths during HS1 are not significant with respect to the present day. The LGM and HS1 warming signal of 1.2-1.5°C at intermediate depths (550-570 m) is larger than the uncertainty of the temperature estimate, and it is reproduced by a couple of individual samples. We therefore consider this warming signal to be robust.

2.6.2 $\delta^{18}O$ of *P. ariminensis* and reconstruction of seawater $\delta^{18}O$ and paleo-salinity

The core-top benthic foraminiferal $\delta^{18}O$ values show an offset of -0.22±0.13‰ from the predicted $\delta^{18}O$ of calcite (Figure 2.9 and Table 2.3). LGM and HS1 foraminiferal $\delta^{18}O$ values are enriched in ^{18}O mainly due to the preferential storage of ^{16}O in ice sheets during the last

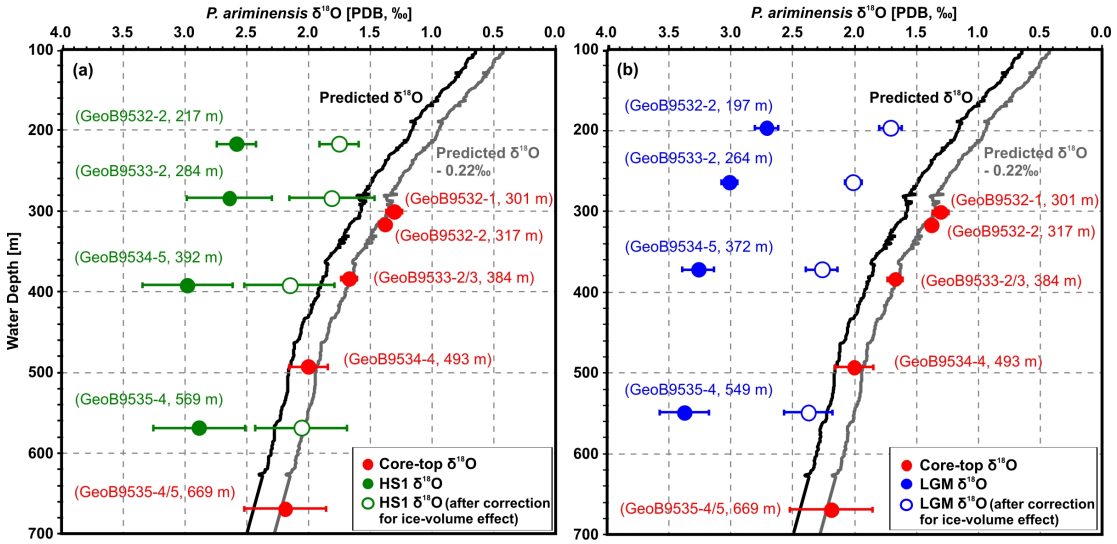

Figure 2.9 Benthic foraminiferal $\delta^{18}O$ changes with water depth. Dots are mean values from each core for a specific time interval. Error bars represent one standard deviation (±1σ) of a few individual measurements. The modern predicted $\delta^{18}O$ of calcite at our coring locations are shown in a black curve. In order to compare with our core-top *P. ariminensis* $\delta^{18}O$, the predicted $\delta^{18}O$ of calcite adjusted by -0.22‰ is also shown in a grey curve. The HS1 and the LGM core water depths are adjusted by -100 m and -120 m, respectively (Peltier and Fairbanks, 2006). The open dots are forminiferal $\delta^{18}O$ values after corrections for ice-volume effects, 0.83‰ for HS1 and 1.0‰ for the LGM (Schrag et al., 2002), respectively.

glacial period. After correction for the ice-volume effect, however, the LGM and HS1 foraminiferal $\delta^{18}O$ values are still 0.44‰ to 0.77‰ heavier than the modern predicted $\delta^{18}O$ values between 200-400 m depth (we mean the predicted $\delta^{18}O$ after correction by -0.22‰, grey line in Figure 2.9). As there are very limited temperature changes within this depth interval during the LGM and HS1 relative to the present day (Figure 2.8), the deviations in $\delta^{18}O$ indicate a significant change in local seawater $\delta^{18}O$ and salinity. At 550-570 m depth, after correction for the ice-volume effect, the LGM foraminiferal $\delta^{18}O$ is 0.36‰ heavier than while the HS1 $\delta^{18}O$ equals to the modern predicted $\delta^{18}O$ (after correction by -0.22‰).

We further estimated the LGM and HS1 seawater $\delta^{18}O$ and salinity changes. In temperature-$\delta^{18}O_{seawater}$ and temperature-salinity diagrams (Figure 2.10), the core-top estimates are consistent with the characteristics of the modern SACW. The average $\delta^{18}O_{seawater}$ value of the LGM and HS1 thermocline water is 1.7‰ and 1.3‰ higher than at present, respectively. Based on our calculation (see equation (5) and Figure 2.10c), the ice-volume effect could

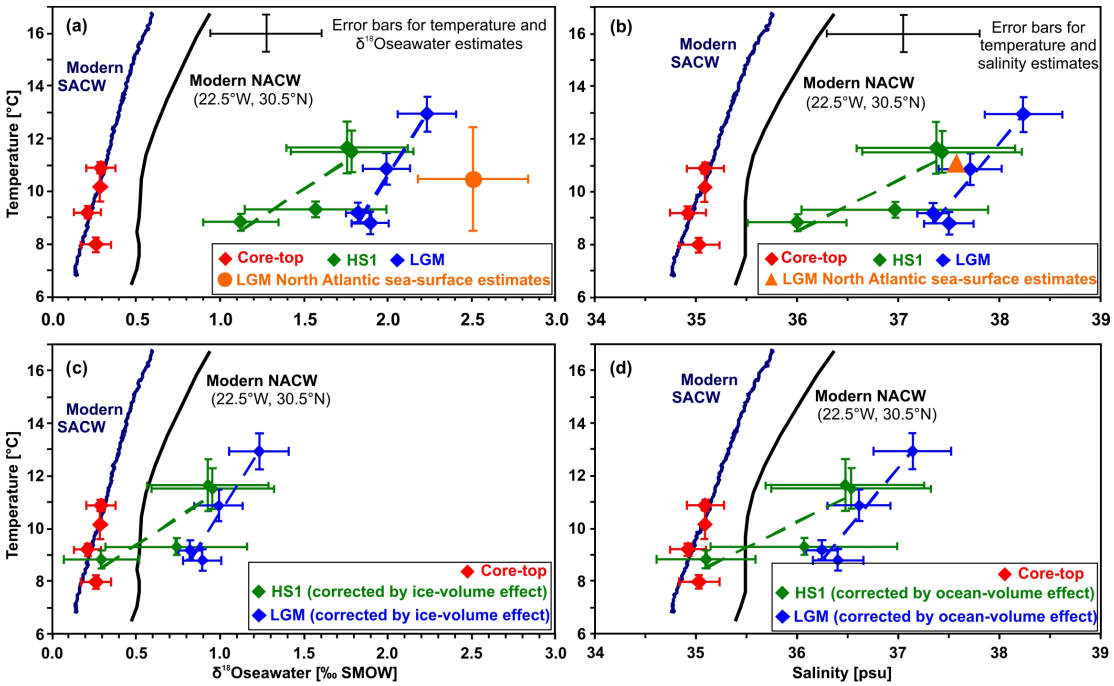

Figure 2.10 Temperature-$\delta^{18}O_{seawater}$ and temperature-salinity diagrams of the tropical central waters at our core locations (diamonds) and the North Atlantic surface waters (circles and triangles). Diamond dots are mean values of each core for a specific time interval. The circle in (a) is the mean value of winter sea-surface temperatures and summer $\delta^{18}O_{seawater}$ estimated from a few North Alantic sediment cores (core S8-79-04, SU81-18, SU81-14, M15672, Duplessy et al., 1991; Schäfer-Neth and Paul, 2004). The triangle in (b) is the surface ocean mean value from a range of the North Atlantic (32.5-41.5°N, indicated in Figure 2.11a. Data is from a gridded LGM database, Schäfer-Neth and Paul, 2004). The $\delta^{18}O_{seawater}$ results after correction by the ice-volume effect (-0.83‰ for HS1 and -1.0‰ for the LGM, respectively) is shown in (c). The salinity results after correction by the ocean-volume effect (-0.9 psu for HS1 and -1.1 psu for the LGM, respectively) are shown in (d). Error bars associated with each dot represent one standard deviation (±1σ) of a few individual estimates. Error bars for an individual temperature, salinity and $\delta^{18}O_{seawater}$ estimate in our study are also presented on the upper right of plots. Solid lines denote the modern SACW (The mean value of four CTD stations. The seawater $\delta^{18}O$ is calculated using equation (4) and CTD salinity data) and NACW (data is from LeGrande and Schmidt, 2006). Dashed lines indicate the trend of changes in the LGM and HS1 data.

partly contribute to this increase in glacial $\delta^{18}O_{seawater}$ by about 1.0‰ during the LGM (Schrag et al., 2002) and 0.83‰ during HS1. The average thermocline-water salinity increased by 2.6 psu during the LGM and 1.9 psu during HS1 compared to the late Holocene. This is also

partly due to a glacial decrease in global ocean volume, which could result in 1.1 psu increase in global mean seawater salinity during the LGM and 0.9 psu increase during HS1 (see equation (6) and Figure 2.10d). We note that the HS1 thermocline waters show a clear freshening at 570 m depth (water depth after correction for glacial sea-level changes) with respect to the LGM. The whole HS1 central water column shows a strong gradient between 400-570 m depth in terms of seawater $\delta^{18}O$ and salinity changes (Figure 2.10).

2.7 Discussion

2.7.1 The structure of the glacial thermocline

In LGM modeling experiments without freshwater perturbations, the ventilated thermocline waters in the tropical Atlantic was predicted to be 2-5°C cooler on average relative to the present day. These experiments also predicted a shoaling of the thermocline depth (e.g., Paul and Schäfer-Neth, 2003, 2004; Rühlemann et al., 2004). Foraminiferal $\delta^{18}O$ records confirmed that the LGM thermocline (400-900 m depth) of the western North Atlantic subtropical gyre was 4°C cooler than the late Holocene and the base of the main thermocline was estimated to be 100 m shallower (Slowey and Curry, 1995). However, our reconstructions do not support a significant cooling scenario for the glacial northeastern tropical Atlantic thermocline (Figure 2.8). At our coring locations, a general LGM cooling of the tropical Atlantic thermocline might be offset by changes in the location of the subduction areas (discussed below in section 2.6.3) and/or in surface water properties over source regions.

2.7.2 Insensitivity of thermocline temperatures of the northeastern tropical Atlantic to thermohaline circulation variations under glacial boundary conditions

Climate boundary conditions during the LGM and HS1 were relatively similar. Therefore, it is plausible to compare the LGM thermocline temperatures with those of HS1 and further assess the effect of changing thermohaline circulation on tropical thermocline temperatures. Proxy data suggest that during HS1, the volume transport by the overturning circulation reduced at all water depths in the North Atlantic relative to the LGM (e.g., McManus et al., 2004; Gherardi et al., 2009). However, the similar thermocline temperature estimates between 200-570 m depth during the LGM and HS1 seemingly indicate that the northeastern tropical Atlantic thermocline temperatures did not respond to this significant decline in glacial thermohaline circulation strength.

Several freshwater-hosing experiments using the LGM boundary conditions predict that thermocline waters in the southern subtropical and equatorial Atlantic warmed, whereas

thermocline waters in the northern subtropical Atlantic cooled during a slowdown of AMOC (Rühlemann et al., 2004; Cheng et al., 2007; Brady and Otto-Bliesner, 2011). The region between the equatorial Atlantic and the northern subtropical gyre is located in a transition area where thermocline temperatures are relatively insensitive to AMOC changes (Rühlemann et al., 2004; Brady and Otto-Bliesner, 2011). The geographic location of this transition is model-dependent. For the upper water column between 200-600 m depth, the transition area can shift from 5-15ºN in one model (Rühlemann et al., 2004) to 15-20ºN in another (Brady and Otto-Bliesner, 2011). Our sediment cores (~9ºN) are located in this transition area. Therefore, we speculate that the response of thermocline temperatures to glacial thermohaline circulation changes in this area might be too small to be reflected in our Mg/Ca-temperature reconstructions.

Another question is to what extent our data from the ocean margin are representative of the zonal mean conditions of the tropical Atlantic thermocline. Freshwater-hosing experiments using either modern (Zhang, 2007; Chiang et al., 2008; Lopes dos Santos et al., 2010; Heslop and Paul, 2012) or LGM boundary conditions (Brady and Otto-Bliesner, 2011; Schmidt et al., 2012) all confirm that the northeastern and the northwestern tropical Atlantic thermocline temperatures show the same sign of response but different sensitivity to reduced AMOC strength. Therefore, we can not assume that our temperature reconstructions from the eastern ocean margin represent zonal mean conditions. However, taking modeling results and proxy data together, it is reasonable that at least the northeastern tropical Atlantic thermocline temperatures were rather insensitive to AMOC changes under glacial boundary conditions.

2.7.3 Possible southward penetration of the NACW during the LGM and HS1

Significant increases in glacial central water $\delta^{18}O$ and salinity (Figure 2.10) suggest that there might be pronounced changes in the source regions of thermocline waters during the LGM and HS1. As seawater temperature, seawater $\delta^{18}O$ and salinity are conservative properties, we can use these three parameters to trace the possible source regions of the central water mass at our coring sites during the last glacial. The subduction of surface waters into thermocline occurs mostly during wintertime in the mid-to-high latitudes of both hemispheres (Poole and Tomczak, 1999). Therefore, we mapped the regions in the Atlantic in which winter sea-surface temperature and salinity data from a reconstruction of LGM sea-surface conditions (Schäfer-Neth and Paul, 2004, Paul and Schäfer-Neth, 2003) correspond to our data for the LGM thermocline (Figure 2.11). In this dataset, the seasonal sea-surface temperature is based on the GLAMAP reconstruction, which in turn is derived from planktonic foraminiferal assemblages (Sarnthein et al., 2003 and references therein). Summer sea-surface salinity in

the North Atlantic is estimated from the reconstructed sea-surface temperatures and planktonic foraminiferal test $\delta^{18}O$. With the reconstructed glacial summer salinity and modern ocean data, the glacial-to-modern salinity anomaly in the summer North Atlantic is known. This anomaly is added to the modern monthly salinity data, and the glacial North Atlantic sea-surface salinity field data with a full seasonal cycle are obtained. In the South Atlantic, the LGM salinity is obtained by adding the global glacial-to-modern salinity anomaly of 1.07 psu to the modern monthly salinity data (Schäfer-Neth and Paul, 2004, Paul and Schäfer-Neth, 2003, 2004).

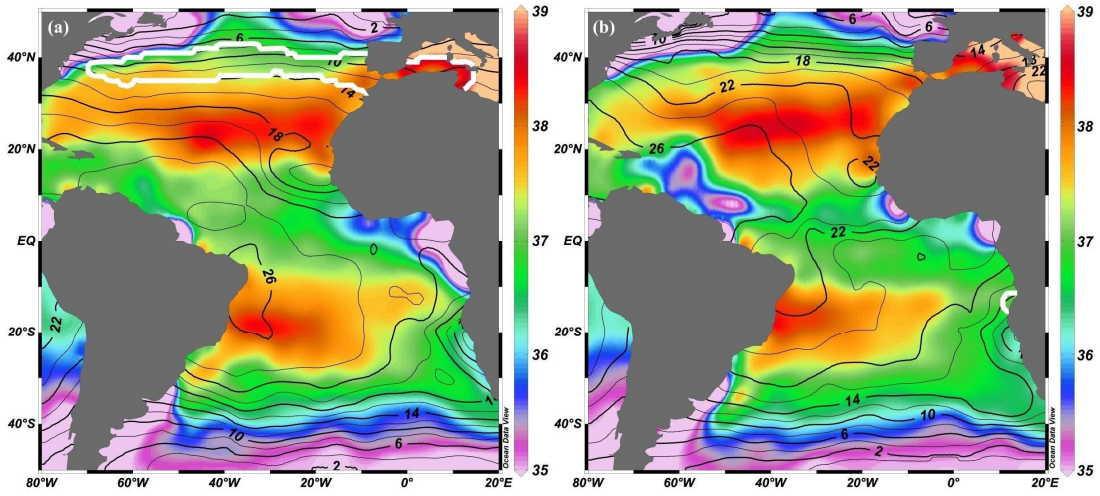

Figure 2.11 Potential source regions of central waters at our coring sites during the LGM. Sea-surface temperature (contour lines) and salinity (colors) data are from a reconstruction of sea-surface conditions during the LGM February (a) and August (b) (Sarnthein et al., 2003 and references therein; Schäfer-Neth and Paul, 2004; Paul and Schäfer-Neth, 2003, 2004). Areas enclosed by white lines were selected from this dataset using the interval [8.5°C; 13°C] for temperature and [37 psu; 38.5 psu] for salinity. The figure was made by Ocean Data View 4 (R. Schlitzer, available at http://odv.awi.de).

We found that only the characteristics of the wintertime North Atlantic surface water from a range of 32.5-41.5°N match the properties of the tropical central water mass at the LGM (Figure 2.10b and Figure 2.11a). However, surface ocean data from the wintertime South Atlantic do not match the properties of the central water mass (Figure 2.11b). Despite of the rough glacial sea-surface salinity estimates in the South Atlantic and large uncertainties associated with paleo-salinity estimates (Figure 2.10b), the results at least indicate that central waters in the northeastern tropical Atlantic probably originated from surface waters of the

North Atlantic during the LGM. In that way the LGM Cape Verde Frontal Zone off the African coast was possibly shifted to the south with respect to the present.

We further collected available LGM sea-surface temperature and $\delta^{18}O_{seawater}$ reconstructions from the North Atlantic between 32.5 and 41.5°N and compared them with the properties of the central waters. These data were published by Duplessy et al. (1991) and were later re-calculated by Schäfer-Neth and Paul (2004) using results obtained from newly available planktonic foraminifera transfer functions. We find that $\delta^{18}O_{seawater}$ values derived from the planktonic foraminifer *G. bulloides* are heavier than that of central waters at our core locations by about 0.5‰ during the LGM (Figure 2.10a). This is because the calcification temperature of *G. bulloides* in the North Atlantic is considered to be close to summer sea-surface temperatures (Duplessy et al., 1991). Reconstructed surface-water $\delta^{18}O$ results (Figure 2.10a) are representative of glacial summer seasons. During glacial wintertime, surface waters of the central part of the North Atlantic should be fresher than in summer seasons due to a southward shift of the North Atlantic polar front (e.g., Eynaud et al., 2009). With respect to the surface waters south of the polar front, surface waters to the north of it were estimated to be 0-0.5‰ more depleted in $\delta^{18}O$ during the LGM summer (Duplessy et al., 1991). Therefore, an increased influx of surface waters from the north to the central part of the North Atlantic might have decreased $\delta^{18}O$ values of surface waters during the glacial winter. In that case $\delta^{18}O$ values of surface waters in the possible subduction area (32.5-41.5°N) of the wintertime North Atlantic would be in better agreement with those of the tropical central waters.

Evidence of benthic foraminiferal $\delta^{13}C$ and Cd/Ca from the western Atlantic support a further penetration of the glacial North Atlantic Intermediate Water to the south during the LGM relative to the present day (e.g., Curry and Oppo, 2005; Marchitto and Broecker, 2006). Glacial thermocline waters in the western tropical Atlantic were also significantly influenced by the relatively well-ventilated water mass from the North Atlantic (e.g., Came et al., 2003; Curry and Oppo, 2005). Here from a different approach, our data suggest that thermocline waters of the northeastern tropical Atlantic were also flushed by the northern-sourced surface waters during the LGM.

The salinity of the HS1 central waters between 200-400 m depth seems lower than but statistically indistinguishable from the LGM reconstructions (Figure 2.10b and 2.10d), suggesting that the HS1 central waters between 200-400 m depth were still mainly influenced by the North Atlantic surface waters. However, a significant freshening of central waters at 570 m depth (Figure 2.10b and 2.10d) suggests that the water mass at intermediate depth might have originated from a different surface source during HS1. After correction for the

glacial ice-volume effects and ocean volume changes, the properties of the HS1 central waters at 570 m depth coincide with those of the modern SACW (Figure 2.10c and 2.10d). This may indicate that the HS1 central waters at intermediate depth were mainly influenced by the southern-sourced surface waters, although the seasonal temperature-salinity properties of the Southern Ocean surface waters for HS1 time period are still not resolved. Our speculation is supported by a biogenic silicon sedimentary record north to our core location: the LGM interval was associated with moderate silicate accumulations off NW Africa possibly due to upwelling of the silica-poor NACW. The HS1 interval, on the other hand, was characterized by an extraordinary increase in silicate accumulations possibly induced by upwelling of the silica-rich SACW (Romero et al., 2008). Hence, both our data and this previous study suggest a northward intrusion of glacial equivalent of the SACW during HS1, although the influence of the glacial SACW was probably limited in the lower thermocline.

2.8 Conclusions

We evaluate and confirm the reliability of benthic foraminiferal Mg/Ca of *P. ariminensis* as a thermocline-water temperature proxy in the northeastern tropical Atlantic both for the late Holocene and the last glacial period. Although a possible influence of the carbonate-ion effect on the benthic Mg/Ca can not be excluded based on the current data set, it is estimated to be minor.

We find that both the LGM and HS1 thermocline-water temperatures in the northeastern tropical Atlantic were similar to the present day between 200-400 m water depth, but were warmer by 1.2-1.5°C at 550-570 m depth. We do not observe warmer thermocline temperatures during HS1 relative to the LGM. This indicates that the northeastern tropical Atlantic thermocline temperatures were insensitive to changes in thermohaline circulation strength under glacial boundary conditions. However, it appears that the glacial thermocline-water properties were significantly different from the present day by changes in the wind-driven circulation. We find that the $\delta^{18}O$ and salinity of the northeastern tropical Atlantic central waters were significantly increased during the LGM (200-550 m depth) and HS1 (200-400 m depth) with respect to the late Holocene. We also observed the HS1 central waters at intermediate depth (570 m depth) were significant fresher relative to the upper central waters. The temperature-salinity characteristics of the LGM central waters (200-550 m depth) were similar to those of the LGM surface waters from the central part of the North Atlantic. Therefore, we infer that the LGM thermocline in the eastern equatorial Atlantic was possibly ventilated by the northern-sourced surface waters. During HS1, the upper central waters (200-400 m depth) might remain influenced by the northern-sourced surface waters, while the

lower thermocline (570 m depth) was possibly ventilated by the southern-sourced surface waters.

2.9 Acknowledgements

We thank the crew and scientific party of Meteor Cruise M65/1. Thanks also go to Monika Segl and her team for stable isotope analyses and to U. Röhl and V. Lukies for technical support while using the XRF Core Scanner at MARUM. Matthias Prange, Ute Merkel and Heather Johnstone are thanked for their discussions and suggestions. Three anonymous reviewers' comments have greatly improved an earlier version of this manuscript. This work was funded through the DFG Research Center/Excellence Cluster "The Ocean in the Earth System." EH is supported by the China Scholarship Council (CSC No. 2009626073).

2.10 References

Antonov, J.I., Seidov, D., Boyer, T.P., Locarnini, R.A., Mishonov, A.V., Garcia, H.E., Baranova, O.K., Zweng, M.M., Johnson, D.R., 2010. World Ocean Atlas 2009, Volume 2: Salinity. In: Levitus, S. (Ed), NOAA Atlas NESDIS 69. U.S. Government Printing Office, Washington, D.C., 184 pp.

Arhan, M., Colin De Verdière, A., Mémery, L., 1994. The eastern boundary of the Subtropical North Atlantic. Journal of Physical Oceanography 24, 1295-1316.

Bamberg, A., Rosenthal, Y., Paul, A., Heslop, D., Mulitza, S., Rühlemann, C., Schulz, M., 2010. Reduced North Atlantic Central Water formation in response to early Holocene ice-sheet melting. Geophysical Research Letters 37, L17705, doi:10.1029/2010GL043878.

Barker, S., Greaves, M., Elderfield, H., 2003. A study of cleaning procedures used for foraminiferal Mg/Ca paleothermometry. Geochemistry, Geophysics, Geosystems 4(9), 8407, doi:10.1029/2003GC000559.

Bigg, G.R., Rohling, E.J., 2000. An oxygen isotope data set for marine water. Journal of Geophysical Research 105, 8527-8535.

Boyle, E.A., Keigwin, L.D., 1985. Comparison of Atlantic and Pacific Paleochemical records for the last 215,000 years: Changes in deep ocean circulation and chemical inventories. Earth and Planetary Science Letters 76, 135-150.

Brady, E.C., Otto-Bliesner, B.L., 2011. The role of meltwater-induced subsurface ocean warming in regulating the Atlantic meridional overturning in glacial climate simulations. Climate Dynamics 37, 1517-1532, doi:10.1007/s00382-010-0925-9.

Bryan, S.P., Marchitto, T.M., 2008. Mg/Ca-temperature proxy in benthic foraminifera: New calibrations from the Florida Straits and a hypothesis regarding Mg/Li. Paleoceanography 23, PA2220, doi:10.1029/2007PA001553.

Came, R.E., Oppo, D.W., Curry, W.B., 2003. Atlantic Ocean circulation during the Younger Dryas: Insights from a new Cd/Ca record from the western subtropical South Atlantic. Paleoceanography 18(4), 1086, doi:10.1029/2003PA000888.

Cessi, P., Bryan, K., Zhang, R., 2004. Global seiching of thermocline waters between the Atlantic and the Indian-Pacific Ocean Basins. Geophysical Research Letters 31, L04302, doi:10.1029/2003GL019091.

Chang, P., Zhang, R., Hazeleger, W., Wen, C., Wan, X., Ji, L., Haarsma, R.J., Breugem, W.-P., Seidel, H., 2008. Oceanic link between abrupt changes in the North Atlantic Ocean and the African monsoon, Nature Geoscience 1, 444-448.

Cheng, W., Bitz, C.M., Chiang, J.C.H., 2007. Adjustment of the global climate to an abrupt slowdown of the Atlantic meridional overturning circulation. In: Schmittner, A., Chiang, J.C.H., Hemming, S.R. (Eds), Ocean Circulation: Mechanisms and Impacts-Past and Future Changes of Meridional Overturning. Geophysical Monograph Series, volume 173, AGU, Washington, D.C., pp. 295-313,

Chiang, J.C.H., Cheng, W., Bitz, C.M., 2008. Fast teleconnections to the tropical Atlantic sector from Atlantic thermohaline adjustment. Geophysical Research Letters 35, L07704, doi:10.1029/2008GL033292.

Collins, J.A., Schefuß, E., Heslop, D., Mulitza, S., Prange, M., Zabel, M., Tjallingii, R., Dokken, T.M., Huang, E., Mackensen, A., Schulz, M., Tian, J., Zarriess, M., Wefer, G., 2011. Interhemispheric symmetry of the tropical African rainbelt over the past 23,000 years. Nature Geoscience 4, 42-45.

Curry, W.B., Marchitto, T.M., 2008. A secondary ionization mass spectrometry calibration of Cibicidoides pachyderma Mg/Ca with temperature. Geochemistry, Geophysics, Geosystems 9, Q04009, doi:10.1029/2007GC001620.

Curry, W.B., Oppo, D.W., 2005. Glacial water mass geometry and the distribution of $\delta^{13}C$ of $\sum CO_2$ in the western Atlantic Ocean. Paleoceanography 20, PA1017, doi:10.1029/2004PA001021.

Dickson, A.G., 1990. Standard potential of the reaction: $AgCl(s) + 1/2H_2(g) = Ag(s) + HCl(aq)$, and the standard acidity constant of the ion HSO_4^- in synthetic seawater from 273.15 to 318.15 K. The Journal of Chemical Thermodynamics 22, 113-127.

Dickson, A.G., Millero, F.J., 1987. A comparison of the equilibrium constants for the dissociation of carbonic acid in seawater media. Deep-Sea Research 34(10), 1733-1743.

Duplessy, J.-C., Labeyrie, L., Juillet-Leclerc, A., Maitre, F., Duprat, J., Sarnthein, M., 1991. Surface salinity reconstruction of the North Atlantic Ocean during the last glacial maximum. Oceanologica Acta 14(4), 311-324.

Elderfield, H., Greaves, M., Barker, S., Hall, I.R., Tripati, A., Ferretti, P., Crowhurst, S., Booth, L., Daunt, C., 2010. A record of bottom water temperature and seawater $\delta^{18}O$ for the Southern Ocean over the past 440 kyr based on Mg/Ca of benthic foraminiferal *Uvigerina* spp. Quaternary Science Reviews 29, 160-169.

Elderfield, H., Yu, J., Anand, P., Kiefer, T., Nyland, B., 2006. Calibrations for benthic foraminiferal Mg/Ca paleothermometry and the carbonate ion hypothesis. Earth and Planetary Science Letters 250, 633-649.

Eynaud, F., Abreu, L., Voelker, A., Schönfeld, J., Salgueiro, E., Turon, J.-L., Penaud, A., Toucanne, S., Naughton, F., Goñi, M.F.S., Malaizé, B., Cacho, I., 2009. Position of the Polar Front along the western Iberian margin during key cold episodes of the last 45 ka. Geochemistry, Geophysics, Geosystems 10, Q07U05, doi:10.1029/2009GC002398.

Fairbanks, R.G., Mortlock, R.A., Chiu, T.-C., Cao, L., Kaplan, A., Guilderson, T.P., Fairbanks, T.W., Bloom, A.L., Grootes, P.M., Nadeau, M.-J., 2005. Radiocarbon calibration curve spanning 0 to 50,000 years BP based on paired $^{230}Th/^{234}U/^{238}U$ and ^{14}C dates on pristine corals. Quaternary Science Reviews 24, 1781-1796.

Garcia, H.E., Locarnini, R.A., Boyer, T.P., Antonov, J.I., Zweng, M.M., Baranova, O.K., Johnson, D.R., 2010. World Ocean Atlas 2009, Volume 4: Nutrients (phosphate, nitrate, silicate). In: Levitus, S. (Ed), NOAA Atlas NESDIS 71. U.S. Government Printing Office, Washington, D.C., 184 pp.

Gherardi, J.-M., Labeyrie, L., Nave, S., Francois, R., McManus, J.F., Cortijo, E., 2009. Glacial-interglacial circulation changes inferred from $^{231}Pa/^{230}Th$ sedimentary record in the North Atlantic region. Paleoceanography 24, PA2204, doi:10.1029/2008PA001696.

Goodman, P.J., 2001. Thermohaline adjustment and advection in an OGCM. Journal of Physical Oceanography 31, 1477-1497.

Greaves, M., Caillon, N., Rebaubier, H., Bartoli, G., Bohaty, S., Cacho, I., Clarke, L., Cooper, M., Daunt, C., Delaney, M., deMenocal, P., Dutton, A., Eggins, S., Elderfield, H., Garbe-Schönberg, D., Goddard, E., Green, D., Groeneveld, J., Hastings, D., Hathorne, E., Kimoto, K., Klinkhammer, G., Labeyrie, L., Lea, D.W., Marchitto, T., Martínez-Botí, M.A., Mortyn, P.G., Ni, Y., Nürnberg, D., Paradis, G., Pena, L., Quinn, T., Rosenthal, Y., Russell, A., Sagawa, T., Sosdian, S., Stott, L., Tachikawa, K., Tappa, E., Thunell, R., Wilson, P.A., 2008. Interlaboratory comparison study of calibration standards for foraminiferal Mg/Ca thermometry. Geochemistry Geophysics Geosystems 9, Q08010, doi:10.1029/2008GC001974.

Hazeleger, W., Drijfhout, S., 2006. Subtropical cells and meridional overturning circulation pathways in the tropical Atlantic. Journal of Geophysical Research 111, C03013, doi:10.1029/2005JC002942.

Healey, S.L., Thunell, R.C., Corliss, B.H., 2008. The Mg/Ca-temperature relationship of benthic foraminiferal calcite: New core-top calibrations in the <4 °C temperature range. Earth and Planetary Science Letters 272: 523-530.

Heslop, D., Paul, A., 2012. Fingerprinting of the Atlantic meridional overturning circulation in climate models to aid in the design of proxy investigations. Climate Dynamics doi:10.1007/s00382-011-1042-0.

Huang, R.X., Cane, M.A., Naik, N., Goodman, P., 2000. Global adjustment of the thermocline in response to deepwater formation. Geophysical Research Letters 27(6), 759-762.

Key, R.M., Kozyr, A., Sabine, C.L., Lee, K., Wanninkhof, R., Bullister, J.L., Feely, R.A., Millero, F.J., Mordy, C., Peng, T.-H., 2004. A global ocean carbon climatology: Results from Global Data Analysis Project (GLODAP). Global Biogeochemical Cycles 18, GB4031, doi:10.1029/2004GB002247.

Le, J., Shackleton, N.J., 1992. Carbonate dissolution fluctuations in the western equatorial Pacific during the late Quaternary. Paleoceanography 7, 21-42.

Lear, C.H., Rosenthal, Y., Slowey, N., 2002. Benthic foraminiferal Mg/Ca paleothermometry: A revised core-top calibration. Geochimica et Cosmochimica Acta 66(19), 3375-3387.

LeGrande, A.N., Schmidt G.A., 2006. Global gridded data set of the oxygen isotopic composition in seawater. Geophysical Research Letters 33, L12604, doi:10.1029/2006GL026011.

Lewis, P.D.E., Wallace, D.W.R. 2006. MS Excel program developed for CO2 system calculations. Report ORNL/CDIAC-105a. Carbon Dioxide Information Analysis Center, Oak Ridge National Laboratory, Oak Ridge, Tennessee.

Locarnini, R.A., Mishonov, A.V., Antonov, J.I., Boyer, T.P., Garcia, H.E., Baranova, O.K., Zweng, M.M., Johnson, D.R., 2010. World Ocean Atlas 2009, Volume 1: Temperature. In: Levitus, S. (Ed), NOAA Atlas NESDIS 68. U.S. Government Printing Office, Washington, D.C., 184 pp.

Lopes dos Santos, R.A., Prange, M., Castañeda, I.S., Schefuß, E., Mulitza, S., Schulz, M., Niedermeyer, E.M., Damsté, J.S.S., Schouten, S., 2010. Glacial-interglacial variability in Atlantic meridional overturning circulation and thermocline adjustments in the tropical North Atlantic. Earth and Planetary Science Letters 300, 407-414.

Lutze G.F., Thiel H., 1989. Epibenthic foraminifera from elevated microhabitats: *Cibicidoides wuellerstorfi* and *Planulina ariminensis*. Journal of Foraminiferal Research 19(2): 153-158.

Luyten, J.R., Pedlosky, J., Stommel H., 1983. The ventilated thermocline. Journal of Physical Oceanography 13, 192-309.

Marchitto, T.M., Broecker, W.S., 2006. Deep water mass geometry in the glacial Atlantic Ocean: A review of constraints from the paleonutrient proxy Cd/Ca. Geochemistry, Geophysics, Geosystems 7, Q12003, doi:10.1029/2006GC001323.

Marchitto, T.M., Bryan, S.P., Curry, W.B., McCorkle, D.C., 2007. Mg/Ca temperature calibration for the benthic foraminifer *Cibicidoides pachyderma*. Paleoceanography 22, PA1203, doi:10.1029/2006PA001287.

Martin, P.A., Lea, D.W., Rosenthal, Y., Shackleton, N.J., Sarnthein, M., Papenfuss, T., 2002. Quaternary deep sea temperature histories derived from benthic foraminiferal Mg/Ca. Earth and Planetary Science Letters 198, 193-209.

McManus, J.F., Francois, R., Gherardi, J.-M., Keigwin L. D., Brown-Leger, S., 2004. Collapse and rapid resumption of Atlantic meridional circulation linked to deglacial climate changes. Nature 428, 834-837.

Mehrbach, C., Culberson, C.H., Hawley, J.E., Pytkowicz, R.M., 1973. Measurement of the apparent dissociation constants of carbonic acid in seawater at atmospheric pressure. Limnology and Oceanography 18(6), 897-907.

Mulitza, S., Bouimetarhan, I., Brüning, M., Freesemann, A., Gussone, N., Filipsson, H., Heil, G., Hessler, S., Jaeschke, A., Johnstone, H., Klann, M., Klein, F., Küster, K., März, C., McGregor, H., Minning, M., Müller, H., Ochsenhirt, W.-T., Paul, A., Schewe, F., Schulz, M., Steinlöchner, J., Stuut, J.-B., Tjallingii, R., Dobeneck, T.v., Wiesmaier, S., Zabel, M., Zonneveld, K., 2006. Report and preliminary results of Meteor-Cruise M65/1. Berichte No. 252, Fachbereich Geowissenschaften, Universität Bremen, Bremen.

Paul, A., Schäfer-Neth, C., 2003. Modeling the water masses of the Atlantic Ocean at the Last Glacial Maximum. Paleoceanography 18(3), 1058, doi:10.1029/2002PA000783.

Paul, A., Schäfer-Neth, C., 2004. The Atlantic Ocean at the Last Glacial Maximum: 2. Reconstructing the current systems with a global ocean model. In: Wefer, G., Mulitza, S., Ratmeyer, V. (Eds.), The South Atlantic in the Late Quaternary: Reconstruction of Material Budgets and Current Systems. Springer-Verlag Berlin Heidelberg New York Tokyo, pp. 553-587.

Peltier, W.R., Fairbanks R.G., 2006. Global glacial ice volume and Last Glacial Maximum duration from an extended Barbados sea level record. Quaternary Science Reviews 25, 3322-3337.

Poole, R., Tomczak, M., 1999. Optimum multiparameter analysis of the water mass structure in the Atlantic Ocean thermocline. Deep Sea Research Part I 46, 1895-1921.

Raitzsch, M., Hathorne, E.C., Kuhnert, H., Groeneveld, J., Bickert, T., 2011. Modern and late Pleistocene B/Ca ratios of the benthic foraminifer *Planulina wuellerstorfi* determined with laser ablation ICP-MS. Geology 39(11), 1039-1042.

Raitzsch, M., Kuhnert, H., Groeneveld, J., Bickert, T., 2008. Benthic foraminifer Mg/Ca anomalies in South Atlantic core top sediments and their implications for paleothermometry. Geochemistry, Geophysics, Geosystems 9, Q05010, doi:10.1029/2007GC001788.

Rathmann, S., Hess, S., Kuhnert, H., Mulitza, S., 2004. Mg/Ca ratios of the benthic foraminifera *Oridorsalis umbonatus* obtained by laser ablation from core top sediments: Relationship to bottom water temperature. Geochemistry, Geophysics, Geosystems 5, Q12013, doi:10.1029/2004GC000808.

Röhl, U., Abrams, L.J., 2000. High-resolution, downhole and non-destructive core measurements from Sites 999 and 1001 in the Caribbean Sea: Application to the late Paleocene thermal maximum. In: Leckie, R.M., Sigurdsson, H., Acton, G.D., Draper, G., (Eds.), Proceeding of the Ocean Drilling Program, Scientific Results 165. College Station, TX, pp. 191-203.

Romero, O.E., Kim, J.-H., Donner, B., 2008. Submillennial-to-millennial variability of diatom production off Mauritania, NW Africa, during the last glacial cycle. Paleoceanography 23, PA3218, doi:10.1029/2008PA001601.

Rosenthal, Y., Boyle, E.A., Slowey, N., 1997. Temperature control on the incorporation of magnesium, strontium, fluorine, and cadmium into benthic foraminiferal shells from Little Bahama Bank: Prospects for thermocline paleoceanography. Geochimica et Cosmochimica Acta 61(17), 3633-3643.

Rosenthal, Y., Lear, C.H., Oppo, D.W., Linsley B.K., 2006. Temperature and carbonate ion effects on Mg/Ca and Sr/Ca ratios in benthic foraminifera: Aragonitic species *Hoeglundina elegans*. Paleoceanography 21, PA1007, doi:10.1029/2005PA001158.

Rosenthal, Y., Morley, A., Barras, C., Katz, M.E., Jorissen, F., Reichart, G.-J., Oppo, D.W., Linsley, B.K., 2011. Temperature calibration of Mg/Ca ratios in the intermediate water benthic foraminifer *Hyalinea balthica*. Geochemistry, Geophysics, Geosystems 12, Q04003, doi:10.1029/2010GC003333.

Rosenthal, Y., Perron-Cashman, S., Lear, C.H., Bard, E., Barker, S., Billups, K., Bryan, M., Delaney, M.L., deMenocal, P.B., Dwyer, G.S., Elderfield, H., German, C.R., Greaves, M., Lea, D.W., Marchitto, T.M., Pak, D.K., Paradis, G.L., Russell, A.D., Schneider, R.R., Scheiderich, K., Stott, L., Tachikawa, K., Tappa, E., Thunell, R., Wara, M., Weldeab, S., Wilson, P.A., 2004. Interlaboratory comparison study of Mg/Ca and Sr/Ca measurements in planktonic foraminifera for paleoceanographic research. Geochemistry, Geophysics, Geosystems 5, Q04D09, doi:10.1029/2003GC000650.

Rühlemann, C., Mulitza, S., Lohmann, G., Paul, A., Prange, M., Wefer, G., 2004. Intermediate depth warming in the tropical Atlantic related to weakened thermohaline circulation: Combining paleoclimate data and modeling results for the last deglaciation. Paleoceanography 19, PA1025, doi:10.1029/2003PA000948.

Sarnthein, M., Gersonde, R., Niebler, S., Pflaumann, U., Spielhagen, R., Thiede, J., Wefer, G., Weinelt, M., 2003. Overview of Glacial Atlantic Ocean Mapping (GLAMAP 2000). Paleoceanography 18(2), 1030, doi:10.1029/2002PA000769.

Schäfer-Neth, C., Paul, A., 2004. The Atlantic Ocean at the Last Glacial Maximum: 1. Objective Mapping of the GLAMAP Sea-Surface Conditions. In: Wefer, G., Mulitza, S., Ratmeyer, V. (Eds.), The South Atlantic in the Late Quaternary: Reconstruction of Material Budgets and Current Systems. Springer-Verlag Berlin Heidelberg New York Tokyo, pp. 531-548.

Schmidt, G.A., 1999a. Error analysis of paleosalinity calculations. Paleoceanography 14(3), 422-429.

Schmidt, G.A., 1999b. Forward modeling of carbonate proxy data from planktonic foraminifera using oxygen isotope tracers in a global ocean model. Paleoceanography 14, 482-497.

Schmidt, M.W., Chang, P., Hertzberg, J.E., Them II, T.R., Link, J., Otto-Bliesner, B.L., 2012. Impact of abrupt deglacial climate change on tropical Atlantic subsurface temperatures. Proceedings of the National Academy of Sciences of the United States of America 109(36), 14348-14352.

Schrag, D.P., Adkins, J.F., McIntyre, K., Alexander, J.L., Hodell, D.A., Charles, C.D., McManus, J.F., 2002. The oxygen isotopic composition of seawater during the Last Glacial Maximum. Quaternary Science Reviews 21, 331-342.

Shackleton, N.J., 1974. Attainment of isotopic equilibrium between ocean water and the benthonic foraminifera genus *Uvigerina*: Isotopic changes in the ocean during the last glacial. CNRS, Colloques Internationals 219, 203-209.

Slowey, N.C., Curry, W.B., 1995. Glacial-interglacial differences in circulation and carbon cycling within the upper western North Atlantic. Paleoceanography 10(4), 715-732, doi:10.1029/95PA01166.

Snowden, D.P., Molinari, R.L., 2003. Subtropical cells in the Atlantic Ocean: An observational summary. In: Goni, G.J., Malanotte-Rizzoli, P. (Eds), Interhemispheric Water Exchange in the Atlantic Ocean. Elsevier Oceanography Series, volume 68, Elsevier, New York, pp. 287- 312.

Stramma, L., Schott, F., 1999. The mean flow field of the tropical Atlantic Ocean. Deep Sea Research Part II 46, 279-303.

Timmermann, A., An, S.-I., Krebs, U., Goosse, H., 2005. ENSO suppression due to weakening of the North Atlantic Thermohaline Circulation. Journal of Climate 18, 3122-3139.

Wan, X., Chang, P., Schmidt, M.W., 2010. Causes of tropical Atlantic paleo−salinity variation during periods of reduced AMOC. Geophysical Research Letters 37, L04603, doi:10.1029/2009GL042013.

Yu, J., Elderfield, H., 2007. Benthic foraminiferal B/Ca ratios reflect deep water carbonate saturation state. Earth and Planetary Science Letters 258, 73-86.

Yu, J., Elderfield, H., 2008. Mg/Ca in the benthic foraminifera *Cibicidoides wuellerstorfi* and *Cibicidoides mundulus*: Temperature versus carbonate ion saturation. Earth and Planetary Science Letters 276, 129-139.

Zhang, R., 2007. Anticorrelated multidecadal variations between surface and subsurface tropical North Atlantic. Geophysical Research Letters 34, L12713, doi:10.1029/2007GL030225.

2.11 Auxiliary material

2.11.1 An assessment to estimate the carbonate-ion effect on the benthic Mg/Ca

We assume that the core-top *P. ariminensis* Mg/Ca ratios from the Gulf of California, the Florida Straits and the northeastern tropical Atlantic are a function of both bottom-water temperature and $\Delta[CO_3^{2-}]$:

$$Mg/Ca = A*Temperature + B*\Delta[CO_3^{2-}] + C, \quad (1)$$

where A and B are coefficients, C is a constant.

We can further obtain

$$\Delta(Mg/Ca) = \Delta(Mg/Ca)_{Temperature} + \Delta(Mg/Ca)_{\Delta[CO_3^{2-}]}, \quad (2)$$

where $\Delta(Mg/Ca)_{Temperature}$ and $\Delta(Mg/Ca)_{\Delta[CO_3^{2-}]}$ are the contributions of changes in temperature and $\Delta[CO_3^{2-}]$ to $\Delta(Mg/Ca)$, respectively (Elderfield et al., 2006). The global core-top *P. ariminensis* Mg/Ca data is linearly correlated with temperature, showing a slope of 0.15 mmol/mol per ºC (Figure 2.S1). We therefore arbitrarily adopted this value as the Mg/Ca-temperature sensitivity of *P. ariminensis*. One core-top sample with the highest

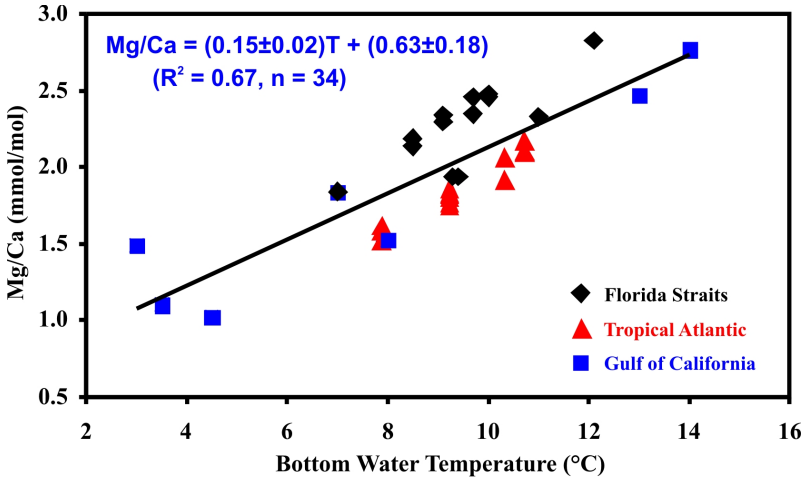

Figure 2.S1 Mg/Ca-bottom water temperature calibration of *P. ariminensis*, based on core-top data from the northeastern tropical Atlantic (this study), the Gulf of California (Lear et al., 2002) and the Florida Straits (Bryan and Marchitto, 2008). *P. ariminensis* Mg/Ca of the Gulf of California and the Florida Straits were corrected by +0.1 mmol/mol.

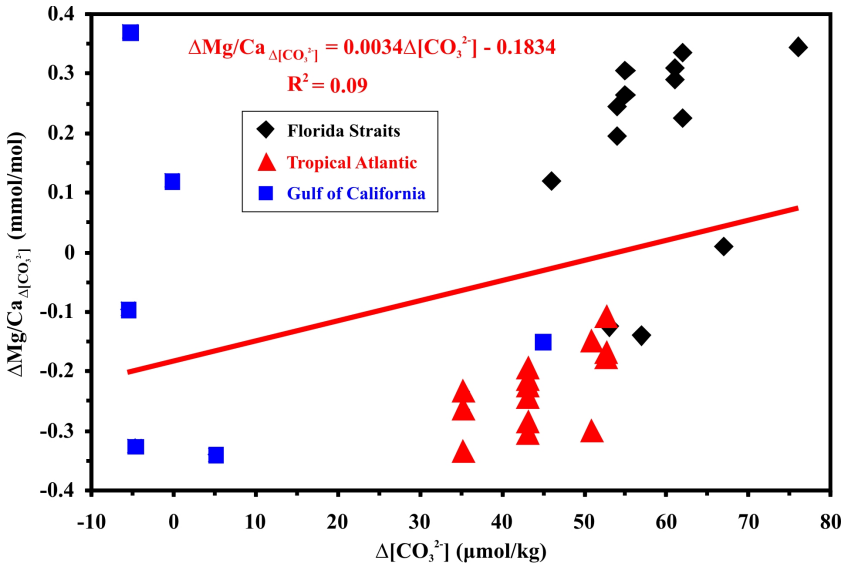

Figure 2.S2 The correlation between $\Delta(Mg/Ca)_{\Delta[CO_3^{2-}]}$ and bottom-water $\Delta[CO_3^{2-}]$. Data is from a global compilation showing in Figure 2.S1.

bottom-water temperature was selected as a baseline. With temperature differences between the baseline and other samples, we could calculate $\Delta(Mg/Ca)_{Temperature}$. The residual Mg/Ca ($\Delta(Mg/Ca)$ - $\Delta(Mg/Ca)_{Temperature}$), which is presumed to be equal to $\Delta(Mg/Ca)_{\Delta[CO_3^{2-}]}$ here, however does not show any correlation with $\Delta[CO_3^{2-}]$ (Figure 2.S2).

2.11.2 References

Bryan, S.P., Marchitto, T.M., 2008. Mg/Ca-temperature proxy in benthic foraminifera: New calibrations from the Florida Straits and a hypothesis regarding Mg/Li. Paleoceanography 23, PA2220, doi:10.1029/2007PA001553.

Elderfield, H., Yu, J., Anand, P., Kiefer, T., Nyland, B., 2006. Calibrations for benthic foraminiferal Mg/Ca paleothermometry and the carbonate ion hypothesis. Earth and Planetary Science Letters 250, 633-649.

Lear, C.H., Rosenthal, Y., Slowey, N., 2002. Benthic foraminiferal Mg/Ca paleothermometry: A revised core-top calibration. Geochimica et Cosmochimica Acta 66(19), 3375-3387.

Chapter 3

Radiocarbon distribution and radiocarbon-based circulation age of the Atlantic Ocean during the Last Glacial Maximum

Enqing Huang[1], Luke C. Skinner[2], Stefan Mulitza[1], André Paul[1], Michael Schulz[1]

1. MARUM - Center for Marine Environmental Sciences and Faculty of Geosciences, University of Bremen, Bremen, Germany
2. Godwin Laboratory for Palaeoclimate Research, Department of Earth Sciences, University of Cambridge, Cambridge, UK

(In preparation for *Quaternary Science Reviews*)

3.1 Abstract

A leading hypothesis in explaining the glacial low atmospheric CO_2 level is that CO_2 had been sequestrated in deep oceans partly because of the poor ventilation of glacial deep waters. However, the glacial deep ocean ventilation age has not been reconstructed by any robust methods. In this study, new paired planktonic-benthic foraminiferal ^{14}C results from 28 sediment cores combined with existing data are employed to investigate the ^{14}C distribution and to estimate the ^{14}C-based circulation age of the LGM (Last Glacial Maximum) Atlantic. We find that the glacial vertical distribution of B-P ages (^{14}C age difference between the paired benthic-planktonic foraminifera) and seawater $\Delta^{14}C$ values shows a strong gradient between the upper (< 1500 m) and the lower (> 1500 m) Atlantic. The glacial mean B-P age and the mean seawater $\Delta^{14}C$ value of the lower Atlantic are 700 years larger and 105‰ less than those of the upper Atlantic, respectively. We further attempt to identify $\Delta^{14}C$ end-member values of water masses from different sources and take seawater $\delta^{13}C$ as a conservative tracer to estimate the mixing ratio of different water masses at our core locations. By doing this, we are able to calculate the mixing $\Delta^{14}C$ signals at a given location. The

difference between the reconstructed $\Delta^{14}C$ value and the mixing $\Delta^{14}C$ value is further used to indicate the glacial circulation age. Our results suggest that the LGM circulations ages at the vast majority of our core locations from the lower Atlantic are less than 400 years, which are comparable to or less than pre-bomb values. Therefore, in contrast to the previous hypothesis, a fast glacial deep-ocean circulation rate might not have favored in sequestrating CO_2 in the ocean interior.

3.2 Introduction

Atmospheric CO_2 rose in two stages over the last deglaciation: a first 50 ppm rise during Heinrich Stadial 1 (HS1, 17.5-14.5 ka BP) and a later 25 ppm rise during the Younger Dryas interval (12.7-11.6 ka BP) (Monnin et al., 2001; Lemieux-Dudon et al., 2010). Although multiple processes might have contributed to the full CO_2 rise during the deglaciation (e.g., Sigman and Boyle, 2000; Köhler et al., 2005; Sigman et al., 2010), it is hypothesized that the initial CO_2 rise during HS1 originated from a stratified glacial deep ocean (e.g., Sarnthein et al., 1994; Toggweiler, 1999; Toggweiler et al., 2006; Tschumi et al., 2011). This deep-sea carbon reservoir is presumed to have been isolated from the atmosphere for a long time, allowing it to accumulate enough respired CO_2 and become depleted in both ^{13}C and ^{14}C. During the early deglaciation, the break down of the stratification in the Southern Ocean (Skinner et al., 2010; Burke and Robinson, 2012) as well as the enhanced upwelling there (Anderson et al., 2009) might have facilitated the release of the sequestrated CO_2. The ^{13}C-depleted signature of deep waters is inferred to have been transmitted to the atmosphere via CO_2 outgassing (Smith et al., 1999; Schmitt et al., 2012) and to low-latitude thermocline via the export of Subantarctic Mode Water and Antarctic Intermediate Water (AAIW) (Spero and Lea, 2002).

Besides lines of evidence listed above, a 190‰ drop in atmospheric $\Delta^{14}C$ during HS1 (Broecker and Barker, 2007; Southon et al., 2012) seemingly also supports the hypothesis of a CO_2 transfer from the deep ocean to the atmosphere. Because changes in the ^{14}C production rate could at most explain a 40‰ drop in atmospheric $\Delta^{14}C$ during HS1, the rest of the 150‰ drop is most likely induced by a dilution of ^{14}C-depleted CO_2 from the deep ocean (Broecker and Barker, 2007). Intermediate waters of the northeastern Pacific (Marchitto et al., 2007), the northern Arabian Sea (Bryan et al., 2010) as well as the northern North Atlantic (Thornalley et al., 2011) are 300-500‰ more depleted in $\Delta^{14}C$ than the contemporary atmosphere during HS1. In the eastern equatorial Pacific, the intermediate water-atmosphere $\Delta^{14}C$ difference is even larger during HS1, reaching by as much as 800-900‰ (Stott et al., 2009). These radiocarbon anomalies were also considered deep-ocean origin, which might have reached

intermediate-water depths through northward transport of Subantarctic Mode Water and AAIW (e.g., Marchitto et al., 2007).

Recently, a growing number of intermediate-water $\Delta^{14}C$ reconstructions from the south Atlantic and the south Pacific (De Pol-Holz et al., 2010; Mangini et al., 2010; Rose et al., 2010; Cléroux et al., 2011; Sortor and Lund, 2011; Burke and Robinson, 2012), however, do not reproduce these ^{14}C-depleted signals. As sediment core locations in the Southern Hemisphere are more approximate to formation areas of southern-sourced intermediate waters, this suggests that ^{14}C-depleted signals at northern intermediate-water depths were not acquired via the incursion of AAIW but by other processes (e.g., De Pol-Holz et al., 2010; Rose et al., 2010; Sortor and Lund, 2011). Nevertheless, the significant difference between northern and southern intermediate-water $\Delta^{14}C$ values does not necessarily preclude the presence of a ^{14}C-depleted deep ocean during full glacial time.

Taken together, it seems that the majority of reconstructions support that the deglacial atmospheric CO_2 rise sourced from a pre-existence of a carbon-enriched deep ocean during the glacial period. In a previous box-model study, the glacial deep ocean was considered to be able to sequestrate more CO_2 than that of the interglacial period due to the poor ventilation of deep waters (Toggweiler, 1999) (The ventilation age of water mass refers to "the ratio of reservoir volume to the injection rate of new deep water" (Broecker et al., 2004)). However, the ventilation age of glacial deep oceans has not been reconstructed by any robust methods. Although the volume and the distribution of water masses in the glacial Atlantic has been well established by benthic foraminiferal $\delta^{13}C$ (e.g., Duplessy et al., 1988; Sarnthein et al., 1994; Curry and Oppo, 2005) and Cd/Ca (e.g., Marchitto and Broecker, 2006), these paleonutrient proxies provide no direct information on the circulation rate (Legrand and Wunsch, 1995). The glacial intensity of the Atlantic Meridional Overturning Circulation is also contradictory in different proxy records (e.g., Yu et al., 1996; Lynch-Stieglitz et al., 1999) and climate model outputs (Otto-Bliesner et al., 2007).

^{14}C age of water mass has been suggested a promising proxy for the deep ocean circulation rate. The preformed ^{14}C of deep waters would decay at a known rate once they are isolated from the atmosphere and being transferred into the ocean interior. In practice, however, the application of B-P age (^{14}C age difference between paired planktonic and benthic foraminifera) or deepwater $\Delta^{14}C$ for reconstructing past ocean circulation age has long been hindered for several reasons. First, surface reservoir ages at core locations could differ from those at deepwater formation areas, and both kinds of reservoir ages are temporally variable (Adkins and Boyle, 1997; Franke et al., 2008a). Second, deep water at a given location and depth in

the Atlantic is usually a mixture of water masses from several sources with different end-member values, and this mixing ratio is also temporally variable (Adkins and Boyle, 1997; Wunsch, 2003; Franke et al., 2008a). Only when water-mass sources and their end-member values can be recognized, and the mixing ratio of different water masses at a give location and water depth can be calculated through using an independent conservative water-mass tracer, the ocean circulation age could then be estimated (Broecker, 1991; Matsumoto, 2007).

In this study, we combine existing results with newly measured ^{14}C ages of paired benthic and planktonic foraminifera from 28 sediment cores (Table 3.1) to map the seawater $\Delta^{14}C$ distribution in the LGM (Last Glacial Maximum, 24-18 ka BP) Atlantic. We find that the mean water mass below 1500 m is much more depleted in $\Delta^{14}C$ than that of above 1500 m by as much as 105‰. Based on the inferred water-mass end member values and the estimated water-mass mixing ratio at a given location and depth, we further attempt to calculate the circulation age of the glacial Atlantic. Our results suggest that the glacial deep ocean (> 1500 m) circulation rate is comparable to or even stronger than that of the pre-bomb era. Therefore, a well ventilated deep ocean in the glacial Atlantic might not have favored in sequestrating CO_2 in the ocean interior as suggested previously.

3.3 Material and Methods

3.3.1 Sampling strategy

In order to find out the LGM depth interval in each core, sediment cores from MARUM core repository with existing ^{14}C-constrianed age models were preferentially selected. Most of these cores are located at ocean margins (Figure 3.1) with relatively high glacial sedimentation rates (> 5 cm/ka) (Table 3.1). Therefore, the potential effect of bioturbation on ^{14}C results could be reduced. However, in order to improve the spatial coverage, especially for the deep Atlantic Ocean below 3000 m depth, several cores with lower sedimentation rates and without existing ^{14}C-constrained age models were also included (Table 3.1). These cores together with published results cover three different types of water masses in the modern Atlantic: AAIW, North Atlantic Deep Water (NADW) and Antarctic Bottom Water (AABW) (Figure 3.2).

In each core, two samples from the estimated LGM depth interval were taken using syringes or scoops. Each sample consists of core material from a 1.5-centimeter slice, in which enough planktonic and benthic foraminifera specimens were found for radiocarbon analyses. We did not combine foraminiferal samples from several depth intervals as many other studies did. This could further minimize the potential influence of bioturbation.

Table 3.1 A compilation of the Atlantic sediment cores with the LGM deepwater radiocarbon reconstructions (both published and new cores).

Core	Latitude (ºN)	Longitude (ºE)	Water Depth (m)	Pre-bomb Surface Reservoir Age (yr)	Pre-bomb Bottom-water $\Delta^{14}C$ (‰)	Pre-bomb Bottom-Surface ^{14}C age (yr)	Glacial Sedimentation Rate (cm/ka)	References
RAPiD-17-5P	61.48	-19.54	2303		-68	165	12	Thornalley et al., 2011
HU72-021-3	42.97	-59.92	2470	460	-82	224	122	Robinson et al., 2005
MD99-2334K	37.80	-10.17	3146		-98	389	17	Skinner and Shackleton, 2004
KNR140-37JPC	31.69	-75.43	2972	410	-88	334	31	Keigwin and Schlegal, 2002
KNR140-39GGC	31.67	-75.42	2975	410	-88	334	83	Keigwin and Schlegal, 2002
KNR140-12JPC	29.07	-72.90	4250	370	-97	453	25	Keigwin, 2004
KNR140-22JPC	28.25	-74.41	4712	370	-101	489	-	Keigwin, 2004
KNR140-26GGC	29.70	-73.40	3845	370	-95	429	25	Keigwin, 2004
KNR140-43GGC	32.02	-76.07	2590	410	-85	301	-	Keigwin, 2004
RC24-08 [c]	-1.33	-11.90	3885	570	-93	214	8	Cléroux et al., 2011
TNO57-21	-41.10	7.80	4981	600	-178	972	19	Barker et al., 2010
KNR159-5-36GGC	-27.50	-46.50	1268	400	-117	596	9	Sorter and Lund, 2011
MD07-3076	-44.15	-14.23	3770		-155	761	8	Skinner et al., 2010
NBP0805-DR23	-60.18	-57.83	819		-140	250	-	Burke and Robinson, 2012
NBP0805-DR27	-60.55	-65.95	1134		-139	277	-	Burke and Robinson, 2012
GeoB4242-5	29.68	-17.89	4286	400	-114	574	2	This study
GeoB4241-11	29.17	-15.45	3609	400	-109	528	3	This study
GeoB4240-2	28.89	-13.23	1358	400	-83	293	12	This study
GeoB4223-2	29.02	-12.47	775	400	-77	245	15	This study
GeoB9506-1	15.61	-18.35	2956	460	-102	407	13	This study
GeoB9508-5	15.50	-17.95	2384	460	-96	348	18	This study
GeoB9510-1	15.42	-17.65	1566	460	-88	282	19	This study
GeoB9512-5	15.34	-17.37	793	460	-89	292	18	This study
GeoB9513-3	15.32	-17.29	494	460	-82	229	7	This study
GeoB9526-5	12.44	-18.06	3223	500	-103	369	14	This study
GeoB9534-5	8.90	-14.94	492	540	-88	200	10	This study
GeoB4905-4	2.50	9.39	1328	530	-95	275	35	This study
GeoB8483-2	-23.00	12.84	803	440	-107	471	3	This study
GeoB3722-2	-25.25	12.02	3506	410	-127	680	2	This study
GeoB1023-5	-17.16	11.01	1978	430	-103	441	51	This study
GeoB1711-4	-23.32	12.38	1967	420	-107	488	21	This study
GeoB1515-1	4.24	-43.67	3129	560	-102	307	5	This study
GeoB3104-1	-3.67	-37.72	767	530	-101	327	9	This study
GeoB3202-1	-21.62	-39.98	1090	400	-112	556	4	This study
GeoB2204-2	-8.53	-34.02	2072	500	-89	247	3	This study
GeoB2109-1	-27.91	-45.88	2504	400	-101	454	6	This study
GeoB6201-5	-26.67	-46.44	475	400	-78	255	-	This study
GeoB2107-3	-27.18	-46.45	1048	400	-109	530	5	This study
GeoB6421-2	-36.45	-22.45	4220	450	-155	887	4	This study
GeoB1105-4	-1.67	-12.43	3225	570	-110	372	6	This study
GeoB1503-1	2.31	-30.65	2306	550	-96	265	1-2	This study
GeoB1905-3	-17.14	-13.99	2974	450	-114	529	-	This study
GeoB6412-2	-44.25	-17.65	3475	600	-159	793	-	This study

a. The pre-bomb surface reservoir age, bottom-water $\Delta^{14}C$ and bottom-surface ^{14}C age at each core location are derived from Key et al. (2004).

b. The glacial sedimentation rate of each core is estimated based on the ^{14}C-constrained age model.

c. At core RC24-08, ^{14}C ages of subsurface-water dwelling planktonic foramonifera (*Globorotalia crassaformis*) were used to reconstruct thermocline-water $\Delta^{14}C$. This species calcified between 500-600 m depth (Cléroux et al., 2011). Therefore, seawater $\Delta^{14}C$ at 550 m and the ^{14}C age difference between the 550 m and the 0 m depth at this core location are shown in Table 3.1. Water depth of core RC24-08 is also shown as 550 m in Figure 3.1.

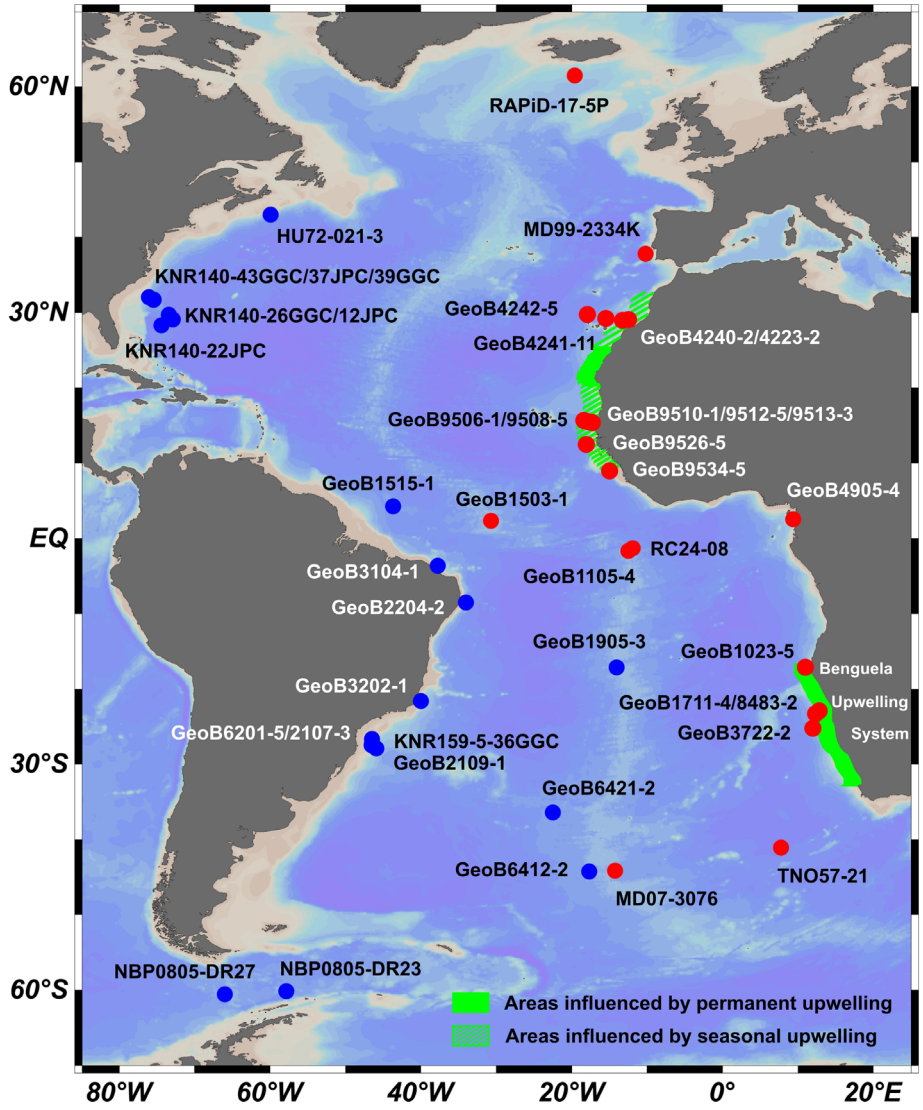

Figure 3.1 Geographic locations of the Atlantic sediment cores with the LGM seawater radiocarbon reconstructions. Blue and red dots denote cores from the western and the eastern Atlantic, respectively. The distribution of upwelling areas off Africa was adopted from Voituriez and Herbland (1982) and Chen et al. (2012). Figures 3.1-3.5 in this study were made by Ocean Data View 4 (R. Schlitzer, available at http://odv.awi.de).

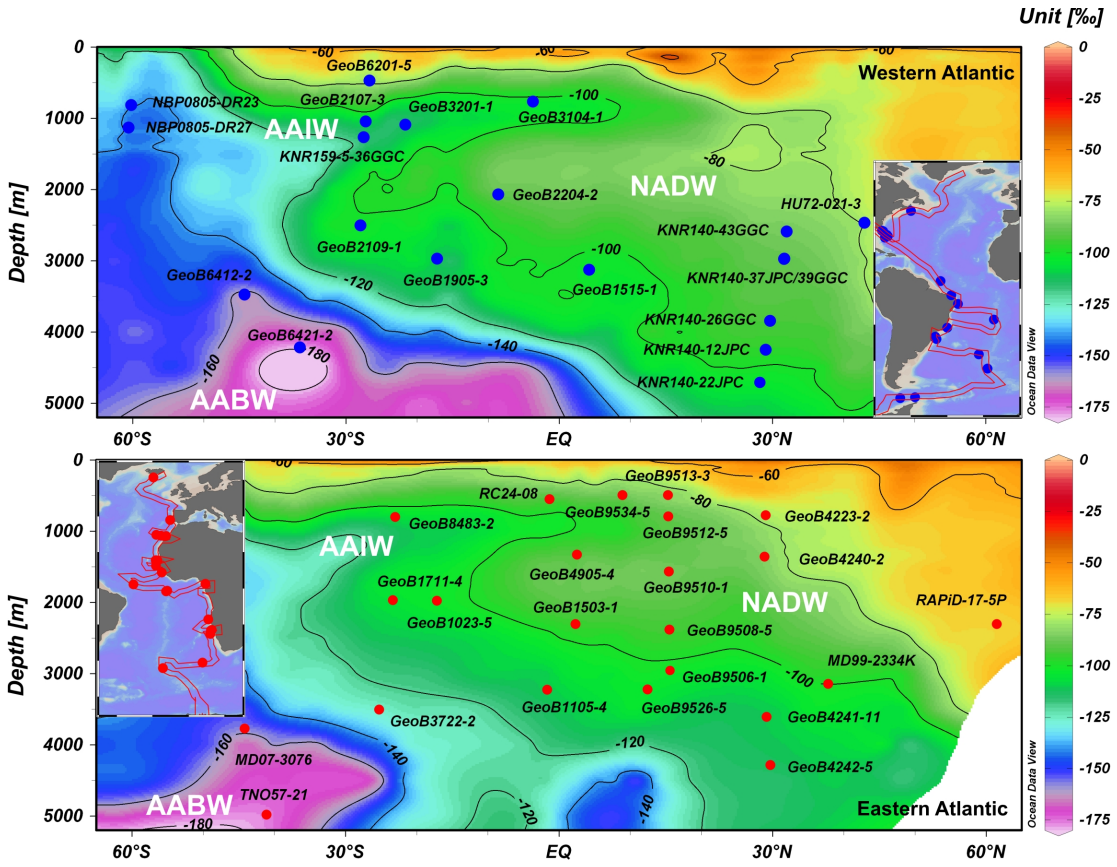

Figure 3.2 Vertical distribution of the Atlantic sediment cores with the LGM seawater radiocarbon reconstructions. Meridional sections of seawater $\Delta^{14}C$ (after correction of the bomb effect) along the western and the eastern Atlantic are derived from the gridded GLODAP dataset (Key et al., 2004). The position of the two sections is indicated in enclosed panels.

3.3.2 Radiocarbon dating

Mono-specific planktonic (in some cases a mixture of surface-water dwelling species) (Table 3.2) and mixed benthic foraminifera (excluded deep-infaunal species) (Table 3.3) were picked from the > 125 μm fraction for ^{14}C analyses. For samples with existing planktonic ^{14}C dates, only benthic foraminifera were analyzed in order to reduce the total number and the expense of ^{14}C measurements. Foraminiferal tests were crushed to open the test chambers, which were further transferred to vials and rinsed with deionized water and methanol for several times. Between each rinse, samples were ultrasonicated for one minute. Small-mass samples were rinsed only with water in order to avoid excess dissolution. The cleaning procedure could help to remove adhering material (such as clay, cocolith) other than primary carbonate.

Table 3.2 Planktonic foraminiferal radiocarbon dates of GeoB sediment cores.

Core	Core Depth (cm)	Dating Species	Lab Code	^{14}C Age (±1σ, yr)	Calendar Age (±1σ, yr BP)	References	Remarks
GeoB4242-5	23	*G. ruber*		16070 ± 140	18810 ± 200	Henderiks et al., 2002	
GeoB4242-5	98	*G. ruber*	S-ANU25917	28165 ± 140	31838 ± 340	This study	pre-LGM
GeoB4241-11	53	*G. ruber*	S-ANU25911	16295 ± 55	19094 ± 216	This study	
GeoB4241-11	58	*G. ruber*	S-ANU28732	19940 ± 90	23328 ± 366	This study	
GeoB4240-2	188	*G. bulloides*	S-ANU25909	17825 ± 75	20745 ± 332	This study	
GeoB4223-2	233	Planktonic mixture	S-ANU30221	18590 ± 100	21760 ± 291	This study	
GeoB4223-2	243	Planktonic mixture	S-ANU30223	19210 ± 100	22413 ± 301	This study	
GeoB9506-1	172	*G. ruber*	S-ANU25807	16835 ± 55	19594 ± 257	This study	
GeoB9506-1	180	*G. ruber*	S-ANU25810	17820 ± 55	20674 ± 329	This study	
GeoB9508-5	308	Planktonic mixture	KIA 31770	16650 ± 90	19339 ± 162	Mulitza et al., 2008	
GeoB9508-5	343	Planktonic mixture	KIA 31769	19590 ± 120	22790 ± 340	Mulitza et al., 2008	
GeoB9510-1	200	*G. ruber*	S-ANU28736	18260 ± 70	21211 ± 303	This study	
GeoB9510-1	255	*G. ruber*	S-ANU25817	20270 ± 70	23661 ± 275	This study	
GeoB9512-5	393	Planktonic mixture	S-ANU25820	15070 ± 50	17731 ± 301	This study	HS1
GeoB9512-5	423	Planktonic mixture	S-ANU25824	16360 ± 50	19096 ± 214	This study	
GeoB9513-3	178	Planktonic mixture	S-ANU25826	21385 ± 75	24860 ± 316	This study	Reversed age
GeoB9513-3	198	Planktonic mixture	KIA 31284	19820 ± 120	23030 ± 361	This study	
GeoB9526-5	227	*G. ruber*	S-ANU30217	18810 ± 100	21840 ± 283	This study	
GeoB9526-5	237	*G. ruber*	S-ANU30219	19700 ± 110	22873 ± 340	This study	
GeoB9534-5	105	Planktonic mixture	Poz-32136	16070 ± 100	18733 ± 190	This study	
GeoB9534-5	125	Planktonic mixture	Poz-32137	17550 ± 120	20160 ± 328	This study	
GeoB4905-4	433	Planktonic mixture	KIA 13716	16170 ± 110	18795 ± 208	Adegbie et al., 2003	
GeoB4905-4	523	Planktonic mixture	KIA 13715	18440 ± 150	21386 ± 421	Adegbie et al., 2003	
GeoB8483-2	99	*G. bulloides*	Poz-38023	16150 ± 100	18726 ± 190	A. Kloss, unpublished	
GeoB8483-2	103	*G. bulloides*	S-ANU26037	16845 ± 60	19348 ± 167	This study	
GeoB3722-2	60	*G. inflata*	S-ANU26032	13570 ± 55	15616 ± 494	This study	HS1
GeoB3722-2	73	*N. pachyderma*		18420 ± 160	21205 ± 328	G. Mollenhauer, unpublished	
GeoB1023-5	880	*G. inflata*	S-ANU26024	17865 ± 65	20390 ± 195	This study	
GeoB1023-5	913	*G. inflata*	KIA 2594	17890 ± 80	20413 ± 183	Kim et al., 2002	
GeoB1711-4	183	*G. inflata*	KIA 556	17140 ± 130	19685 ± 265	Little et al., 1997	
GeoB1711-4	203	*G. inflata*	S-ANU25829	17245 ± 70	19755 ± 246	This study	
GeoB1515-1	48	*G. sacculifer*	KIA1837	16920 ± 110	19582 ± 291	Vidal et al., 1999	
GeoB1515-1	70	*G. sacculifer*	KIA1313	20810 ± 280	24135 ± 423	Vidal et al., 1999	
GeoB3104-1	172	*G. sacculifer*	GrA 3720	16120 ± 160	18778 ± 227	Arz et al., 1998	
GeoB3104-1	192	*G. sacculifer*	S-ANU25936	19075 ± 65	22085 ± 290	This Study	
GeoB3202-1	93	*G. sacculifer*	S-ANU26020	16210 ± 60	19028 ± 231	This Study	
GeoB3202-1	99	*G. sacculifer*	KIA 1847	18090 ± 100	21142 ± 265	Arz et al., 1999	
GeoB2204-2	33	*G. sacculifer*	S-ANU25930	17970 ± 70	20793 ± 330	This Study	
GeoB2204-2	38	*G. sacculifer*	S-ANU25932	19955 ± 70	23211 ± 323	This Study	
GeoB2109-1	58	*G. ruber*	KIA 2618	17580 ± 90	20362 ± 246	This Study	
GeoB2109-1	73	*G. ruber*	S-ANU28816	19440 ± 90	22694 ± 325	This Study	
GeoB6201-5	145	*G. ruber*	Poz-32142	18860 ± 110	21981 ± 299	R. Portilho-Ramos, unpublished	
GeoB6201-5	180	*G. ruber*	Poz-32143	19180 ± 110	22366 ± 303	R. Portilho-Ramos, unpublished	
GeoB2107-3	138	*G. sacculifer*	S-ANU26012	13715 ± 50	16300 ± 455	This Study	HS1
GeoB2107-3	148	*G. sacculifer*	KIA 22409	19100 ± 130	22249 ± 350	Hendry et al., 2012	
GeoB6421-2	28	*G. bulloides*	S-ANU28727	16200 ± 60	18862 ± 163	This Study	
GeoB6421-2	38	*G. bulloides*	S-ANU28730	17060 ± 70	19744 ± 245	This Study	

Table 3.2 *Continued*.

Core	Core Depth (cm)	Dating Species	Lab Code	^{14}C Age (±1σ, yr)	Calendar Age (±1σ, yr BP)	References	Remarks
GeoB1105-4	83		KIA 4100	17670 ± 110	20234 ± 325	Bickert and Mackensen, 2004	
GeoB1105-4	103		KIA 4101	19570 ± 140	22670 ± 346	Bickert and Mackensen, 2004	
GeoB1503-1	23	*G. sacculifer*	S-ANU25921	16355 ± 55	19022 ± 231	This Study	
GeoB1503-1	28	*G. sacculifer*	S-ANU25924	21590 ± 75	25146 ± 345	This Study	pre-LGM
GeoB1905-3	23	*G. ruber*	S-ANU26007	20515 ± 80	23994 ± 282	This Study	Reversed age
GeoB1905-3	28	*G. ruber*	S-ANU26010	17775 ± 60	20643 ± 332	This Study	
GeoB6412-2	68	*G. bulloides*	S-ANU28724	9070 ± 40	9635 ± 265	This Study	Not LGM, reversed age
GeoB6412-2	78	*G. bulloides*	S-ANU28739	5850 ± 35	6091 ± 218	This Study	

Carbonate hydrolysis and CO_2 reduction were conducted at the department of Earth Sciences, University of Cambridge. The graphitized ^{14}C samples were measured at Research School of Earth Sciences, Australian National University (Lab code, S-ANU) using a Single Stage Accelerator Mass Spectrometer. Sample preparation backgrounds were subtracted during measurement. Existing planktonic ^{14}C dates were measured previously in other labs: the Leibniz-Laboratory for Radiometric Dating and Stable Isotope Research in Kiel (Lab code: KIA), or the Poznan Radiocarbon Laboratory (Lab code: Poz), or the Center for Isotope Research, Groningen (Lab code: GrA) (Table 3.2).

Except for two samples (one planktonic ^{14}C date at 203 cm depth of core GeoB1711-4, 0.35 mg of carbon; and the other planktonic ^{14}C date at 78 cm depth of core GeoB6412-2, 0.36 mg of carbon; Table 3.2), all other 93 samples measured at Australian National University have a mass > 0.40 mg of carbon, which are considered not to be subject to the size-dependent isotopic fractionation (Fallon et al., 2010). Therefore, no correction for size-dependent fractionation was applied. Nine samples of benthic foraminifera from different cores were divided into two aliquots, which were separately cleaned, graphitized and measured. Except samples from 255 cm depth of core GeoB9510-1, all other eight pairs of duplicate samples show very consistent results of ^{14}C ages (Table 3.3).

3.3.3 Estimates of the LGM surface reservoir ages

Past variations of marine surface ^{14}C reservoir ages have not yet been resolved. A simulation study, which is forced by the changing atmospheric Δ^{14}C, suggests that the LGM surface reservoir ages of the mid-to-low latitude Atlantic has a mean value closed to that of the pre-bomb era, but it also shows a temporal variability of ≤ 200 years within the LGM time interval (Franke et al., 2008b). Changes in the ocean circulation strength could also alter

Table 3.3 Benthic foraminiferal radiocarbon dates, estimates of B-P age, deepwater $\Delta^{14}C$ and $\Delta\Delta^{14}C$ of GeoB sediment cores. Uncertainties associated with B-P age, deepwater $\Delta^{14}C$ and $\Delta\Delta^{14}C$ are ±1 sigma standard error.

Core	Core Depth (cm)	Calendar Age (±1σ, yr BP)	Lab Code	Benthic ^{14}C Age (±1σ, yr)	Deepwater $\Delta^{14}C$ (±1σ, ‰)	B-P Age (±1σ, yr)	$\Delta\Delta^{14}C$ (±1σ, ‰)	Remarks
GeoB4242-5	23	18810 ± 200	S-ANU25916	17690 ± 65	76 ± 27	1620 ± 154	-306 ± 31	
GeoB4242-5	98	31838 ± 340	S-ANU25913	30240 ± 240	91 ± 55	2075 ± 278	-383 ± 56	pre-LGM
GeoB4241-11	53	19094 ± 216	S-ANU25912	20670 ± 80	-231 ± 21	4375 ± 97	-615 ± 27	
GeoB4241-11	58	23328 ± 366	S-ANU25914	22285 ± 80	49 ± 47	2345 ± 120	-437 ± 49	
GeoB4240-2	188	20745 ± 332	S-ANU25910	18280 ± 70	264 ± 52	455 ± 103	-136 ± 58	
GeoB4223-2	233	21760 ± 291	S-ANU28733	18500 ± 70	390 ± 50	-90 ± 122	-43 ± 54	Reject, negative B-P
GeoB4223-2	243	22413 ± 301	S-ANU25907	19475 ± 75	333 ± 50	265 ± 125	-110 ± 52	
GeoB9506-1	172	19594 ± 257	S-ANU25809	19010 ± 60	4 ± 32	2175 ± 81	-374 ± 38	
GeoB9506-1	180	20674 ± 329	S-ANU25811	21395 ± 70	-150 ± 35	3575 ± 89	-545 ± 42	
GeoB9506-1	180	20674 ± 329	S-ANU25812	21635 ± 70	-175 ± 34	3815 ± 89	-570 ± 41	Duplicated measurement
GeoB9508-5	308	19339 ± 162	S-ANU25813	17575 ± 55	164 ± 24	925 ± 105	-232 ± 29	
GeoB9508-5	343	22790 ± 340	S-ANU25814	20735 ± 70	192 ± 50	1145 ± 139	-256 ± 54	
GeoB9510-1	200	21211 ± 303	S-ANU25816	19075 ± 65	211 ± 45	815 ± 96	-224 ± 46	
GeoB9510-1	255	23661 ± 275	S-ANU25818	21240 ± 70	244 ± 43	970 ± 99	-245 ± 43	
GeoB9510-1	255	23661 ± 275	S-ANU25819	22280 ± 75	93 ± 38	2010 ± 103	-396 ± 38	Duplicated measurement; Reject, inconsistent with the other result
GeoB9513-3	178	24860 ± 316	S-ANU30214	18640 ± 100	988 ± 80	-2745 ± 125	518 ± 83	Reject, negative B-P
GeoB9513-3	198	23030 ± 361	S-ANU30216	19050 ± 100	514 ± 68	-770 ± 156	5 ± 70	Reject, negative B-P
GeoB9512-5	393	17731 ± 301	S-ANU25821	15285 ± 50	274 ± 47	215 ± 71	-120 ± 47	HS1
GeoB9512-5	393	17731 ± 301	S-ANU25823	15280 ± 50	275 ± 47	210 ± 71	-120 ± 47	Duplicated measurement; HS1
GeoB9512-5	423	19096 ± 214	S-ANU25825	17605 ± 60	126 ± 30	1245 ± 78	-258 ± 35	
GeoB9526-5	227	21840 ± 283	S-ANU30218	20260 ± 120	128 ± 17	1450 ± 156	-311 ± 27	
GeoB9526-5	237	22873 ± 340	S-ANU30220	21130 ± 130	146 ± 19	1430 ± 170	-309 ± 31	
GeoB9534-5	105	18733 ± 190	Poz-39035	16120 ± 90	296 ± 33	50 ± 210	-95 ± 36	
GeoB9534-5	125	20160 ± 328	Poz-39036	17840 ± 100	244 ± 51	290 ± 342	-143 ± 52	
GeoB4905-4	433	18795 ± 208	S-ANU26030	16605 ± 60	230 ± 32	435 ± 125	-154 ± 35	
GeoB4905-4	523	21386 ± 421	S-ANU26031	18800 ± 65	280 ± 66	360 ± 163	-150 ± 67	
GeoB8483-2	99	18726 ± 190	S-ANU26036	18945 ± 65	-89 ± 22	2795 ± 119	-483 ± 27	Reject, reversed benthic ^{14}C age
GeoB8483-2	103	19348 ± 167	S-ANU26038	17165 ± 60	226 ± 26	320 ± 85	-168 ± 31	
GeoB3722-2	60	15616 ± 494	S-ANU26033	15445 ± 55	-33 ± 58	1875 ± 78	-340 ± 66	HS1
GeoB3722-2	73	21205 ± 328	S-ANU26035	19620 ± 70	131 ± 46	1200 ± 175	-303 ± 47	
GeoB1023-5	880	20390 ± 195	S-ANU26025	18740 ± 65	143 ± 28	875 ± 92	-237 ± 30	
GeoB1023-5	913	20413 ± 183	S-ANU26026	19410 ± 70	55 ± 25	1520 ± 106	-325 ± 27	
GeoB1023-5	913	20413 ± 183	S-ANU26027	19275 ± 70	72 ± 25	1385 ± 106	-307 ± 27	Duplicated measurement
GeoB1711-4	183	19685 ± 265	S-ANU26039	18085 ± 65	139 ± 38	945 ± 145	-234 ± 40	
GeoB1711-4	203	19755 ± 246	S-ANU25830	18895 ± 60	38 ± 32	1650 ± 92	-336 ± 35	
GeoB1711-4	203	19755 ± 246	S-ANU25831	19085 ± 60	14 ± 31	1840 ± 92	-360 ± 35	Duplicated measurement
GeoB1515-1	48	19582 ± 291	S-ANU25926	17300 ± 65	240 ± 45	380 ± 128	-139 ± 49	
GeoB1515-1	70	24135 ± 423	S-ANU25927	21240 ± 70	317 ± 68	430 ± 289	-179 ± 69	
GeoB3104-1	172	18778 ± 227	S-ANU25935	16520 ± 55	240 ± 35	400 ± 169	-146 ± 39	
GeoB3104-1	192	22085 ± 290	S-ANU25937	20060 ± 65	191 ± 43	985 ± 92	-263 ± 44	

Table 3.3 *Continued*.

Core	Core Depth (cm)	Calendar Age (±1σ, yr BP)	Lab Code	Benthic ^{14}C Age (±1σ, yr)	Deepwater $\Delta^{14}C$ (±1σ, ‰)	B-P Age (±1σ, yr)	$\Delta\Delta^{14}C$ (±1σ, ‰)	Remarks
GeoB3202-1	93	19028 ± 231	S-ANU26021	17130 ± 65	185 ± 34	920 ± 88	-197 ± 38	
GeoB3202-1	98	20790 ± 259	S-ANU26023	17970 ± 65	321 ± 43	88 ± 93	-83 ± 50	Interpolated calendar age; Reject, the interpolated calendar age might be inaccurate due to the low sedimentation rate
GeoB3202-1	99	21142 ± 265						
GeoB2204-2	33	20793 ± 330	S-ANU25931	17585 ± 70	386 ± 57	-385 ± 99	-20 ± 63	Reject, Negative B-P
GeoB2204-2	38	23211 ± 323	S-ANU25933	20850 ± 70	237 ± 49	895 ± 99	-247 ± 51	
GeoB2109-1	58	20362 ± 246	S-ANU28813	19000 ± 80	103 ± 35	1420 ± 120	-278 ± 39	
GeoB2109-1	73	22694 ± 325	S-ANU28817	20700 ± 90	184 ± 48	1260 ± 127	-241 ± 53	
GeoB6201-5 [a]	145	21981 ± 299	S-ANU26018	20920 ± 75	56 ± 39	2060 ± 133	-393 ± 42	Reject, possible influence of dissociated methane
GeoB6201-5 [a]	145	21981 ± 299	S-ANU26019	20725 ± 75	82 ± 40	1865 ± 133	-367 ± 43	Duplicated measurement; Reject, possible influence of dissociated methane
GeoB6201-5 [a]	180	22366 ± 303	S-ANU26017	21755 ± 80	-2 ± 38	2575 ± 136	-447 ± 40	Reject, possible influence of dissociated methane
GeoB2107-3	138	16300 ± 455	S-ANU26013	17905 ± 60	-227 ± 43	4190 ± 78	-608 ± 50	HS1
GeoB2107-3	148	22249 ± 350	S-ANU26014	19070 ± 70	374 ± 59	-30 ± 148	-76 ± 61	Reject, Negative B-P
GeoB2107-3	148	22249 ± 350	S-ANU26016	19090 ± 65	371 ± 59	-10 ± 145	-79 ± 60	Duplicated measurement; Reject, Negative B-P
GeoB6421-2	28	18862 ± 163	S-ANU28729	14115 ± 50	690 ± 33	-2085 ± 78	313 ± 35	Reject, Negative B-P
GeoB6421-2	38	19744 ± 245	S-ANU28731	17820 ± 70	186 ± 35	760 ± 99	-188 ± 38	
GeoB1105-4	83	20234 ± 325	S-ANU25918	18340 ± 65	179 ± 47	670 ± 128	-206 ± 48	
GeoB1105-4	83	20234 ± 325	S-ANU28735	18460 ± 70	162 ± 47	790 ± 130	-224 ± 48	Duplicated measurement
GeoB1105-4	103	22670 ± 346	S-ANU25919	20555 ± 75	202 ± 51	985 ± 159	-242 ± 54	
GeoB1105-4	103	22670 ± 346	S-ANU25920	20715 ± 75	178 ± 50	1145 ± 159	-265 ± 53	Duplicated measurement
GeoB1503-1	23	19022 ± 231	S-ANU25923	15175 ± 55	510 ± 43	-1180 ± 78	128 ± 46	Reject, Negative B-P
GeoB1503-1	28	25146 ± 345	S-ANU25925	21690 ± 75	408 ± 60	100 ± 106	-111 ± 61	Not LGM
GeoB1905-3 [b]	23	23994 ± 282	S-ANU26009	21075 ± 75	322 ± 45	560 ± 110	-71 ± 50	Reject
GeoB1905-3 [b]	28	20643 ± 332	S-ANU26011	22060 ± 80	-220 ± 31	4285 ± 100	-715 ± 32	Reject
GeoB6412-2 [c]	68	9635 ± 265	S-ANU28725	17560 ± 70	-640 ± 12	8490 ± 81	-734 ± 14	Reject
GeoB6412-2 [c]	78	6091 ± 218	S-ANU28726	17870 ± 70	-774 ± 6	12020 ± 78	-854 ± 9	Reject

a. Very negative $\delta^{13}C$ (Table 3.S3) and $\Delta^{14}C$ values of benthic foraminiferal samples of core GeoB6201-5 are possibly contaminated by old carbon from dissociated methane, as this core locates in cold-seep areas off Brazil.

b. The age model of core GeoB1905-3 is constrained by only two planktonic ^{14}C dates that are reversed. Since we cannot determine which planktonic ^{14}C date is reliable, all estimates of deepwater $\Delta^{14}C$, $\Delta\Delta^{14}C$ and B-P ages of this core are rejected.

c. Based on the depth-sequence of *G. bulloides* $\delta^{18}O$, sediment of core GeoB6412-2 is severely disturbed.

marine surface reservoir ages (e.g., Franke et al., 2008b; Butzin et al., 2005, 2012). However, the LGM ocean state is still a matter under debate. Currently it is impractical to quantify the influence of a glacial ocean circulation on surface reservoir ages. The majority of our sediment cores are located in the tropical-subtropical areas. They are far away from the deepwater formation area in the high-latitude North Atlantic or the deepwater upwelling area in the high-latitude Southern Ocean, where surface reservoir ages were considered to have experienced significant changes since the last glacial (e.g., Skinner et al., 2010; Thornalley et al., 2011). Therefore, it seems reasonable to assume that the LGM surface reservoir ages at most of our cores were equal to pre-bomb values with an uncertainty of ±200 years (Table 3.1).

Nevertheless, half of our cores are also located at ocean margins off Africa, where past changes in the coastal upwelling might also have an effect on surface reservoir ages (Figure 3.1). Along the NW African margin, the LGM upwelling intensity in areas near several of our core locations (GeoB4223-2, GeoB4240-2, GeoB9526-5) is estimated to be comparable to that of the late Holocene (Holzwarth et al., 2010; Zarriess and Mackensen, 2010). This suggests that the LGM upwelling might not have resulted in a significant increase in surface reservoir ages with respect to the late Holocene. There is another line of evidence also supported this argument. Two cores GeoB9526-5 and GeoB9508-5 off NW Africa (Figure 3.1) and a core MD95-2042 off Iberian margin (Shackleton et al., 2000) were bathed in similar bottom water masses since the last glacial. High-resolution benthic foraminiferal $\delta^{18}O$ records derived from these three cores show very similar patterns (Mulitza et al., 2008; Zarriess et al., 2011). Since core MD95-2042 has a well established age model (Shackleton et al., 2000), age models of core GeoB9526-5 and GeoB9508-5 could also be reconstructed by tuning their benthic $\delta^{18}O$ records to that of MD95-2042. The tuned age models do not show any significant offset from the ^{14}C-constrained age models of these two cores. Therefore, we assume that the LGM surface reservoir ages at our core locations off NW Africa were still close to those of the late Holocene.

Along the SW African margin, the Benguela upwelling intensity is considered much stronger at the LGM compared to the late Holocene (e.g., Mollenhauer et al., 2002; Volbers et al., 2003). For core locations (GeoB1023-5, GeoB1711-4, GeoB8483-2, GeoB3722-2, Figure 3.1) influenced by this upwelling system, we assume that the LGM surface reservoir ages were 200 years greater than pre-bomb values based on estimates of climate model studies (Butzin et al., 2005; Franke et al., 2008b). We noticed that the location of core GeoB6412-2 is close to that of MD07-3076, whose surface reservoir age was estimated to be around 1300 years older during the LGM than the pre-bomb value (Skinner et al., 2010). However, both

planktonic and benthic ^{14}C results of core GeoB6412-2 are rejected in this study due to strong signs of bioturbation (Table 3.2 and 3.3). Therefore, corrections for glacial surface reservoir ages at this core location are not necessary.

Taken together, we assume that the LGM surface reservoir ages at core locations influenced the Benguela upwelling system were 200 years older than pre-bomb values, while at other core locations were equal to pre-bomb values. The uncertainty of the LGM surface reservoir age estimates is assumed to be around ±200 years based on the model output (Franke et al., 2008b). We further converted planktonic ^{14}C ages into calendar ages using the Marine09 calibration curve (Reimer et al., 2009) and the Calib6.02 program (Stuiver and Reimer, 1993) (Table 3.2). For published results without independent estimates of age models (core HU72-021-3, KNR140-37JPC, KNR140-39GGC, KNR140-12JPC, KNR140-22JPC, KNR140-26GGC, KNR140-43GGC, RC24-08, TNO57-21, KNR159-5-36GGC) (Table 3.1), the LGM planktonic ^{14}C ages were also recalibrated into calendar ages using the Marine09 curve (Reimer et al., 2009) and pre-bomb surface reservoir ages derived from the Key et al. (2004) dataset (Table 3.S1).

3.3.4 Estimates of seawater $\Delta^{14}C$, $\Delta\Delta^{14}C$ and B-P age

Seawater $\Delta^{14}C$ was calculated as follows (Adkins and Boyle, 1997):

$$\Delta^{14}C = (e^{-\text{Benthic radiocarbon age / 8033 yr}} / e^{-\text{Calendar age / 8266 yr}} - 1)*1000\ ‰.$$

The uncertainty of the seawater $\Delta^{14}C$ estimate is therefore determined by propagated errors from the calendar age estimate and the benthic ^{14}C age measurement (Table 3.2 and 3.3).

In each core we would combine results of several LGM samples to calculate the mean value. These samples might correspond to different atmospheric $\Delta^{14}C$ levels. In order to correct for this variable atmospheric $\Delta^{14}C$ background, the $\Delta^{14}C$ difference between the seawater and the contemporary atmosphere ($\Delta\Delta^{14}C$) was also calculated (Table 3.3 and 3.S2). The uncertainty of the $\Delta\Delta^{14}C$ estimate is therefore determined by propagated errors from the seawater $\Delta^{14}C$ estimate (Table 3.3 and 3.S2) and the atmospheric $\Delta^{14}C$ reconstruction (Reimer et al., 2009).

Although the interpretation of B-P age could be complicated by many other influences (e.g., Adkins and Boyle, 1997; Franke et al., 2008a), it is often used as a measure of the apparent ventilation age of deep waters in previous studies (e.g., Broecker et al., 2004). The advantage of the proxy B-P age is that it is calculated only using the paired planktonic and benthic ^{14}C

ages, which thus retains the raw information of measurements. Moreover, the estimate of B-P age does not incorporate into the uncertainty of the calendar age estimate as opposed to the estimate of $\Delta\Delta^{14}C$. Therefore, results of B-P ages were also shown in this study (Table 3.3 and 3.S2).

3.3.5 Stable oxygen and carbon isotope of epibenthic foraminifera

For sediment cores without existing epibenthic $\delta^{18}O$ and $\delta^{13}C$ records, epifaunal species (*Cibicidoides wuellerstorfi*, *Planulina ariminensis* or other *Cibicidoides* species, shell size > 400 μm) were picked for stable oxygen and carbon isotope measurement using a Finnigan MAT 252 mass spectrometer and an automatic carbonate preparation device at MARUM, University of Bremen (Table 3.S3). The final results were converted to Vienna Pee Dee Belemnite (VPDB) using NBS 18, 19 and 20. The precision for $\delta^{18}O$ and $\delta^{13}C$ analysis is better than ±0.07‰ and ±0.05‰, respectively.

3.3.6 A new compilation of the LGM epibenthic $\delta^{13}C$ data from the Atlantic Ocean

Since epibenthic $\delta^{13}C$ has the best spatial coverage than any other water-mass tracer, a revisit of $\delta^{13}C$ results in this study would facilitate the interpretation of ^{14}C results. A recent dataset of the LGM sediment core $\delta^{13}C$ was compiled by Hesse et al. (2011). Here we expanded the Hesse et al. (2011) dataset by combining a $\delta^{13}C$ data collection in Curry and Oppo (2005), newly published results from Thornalley et al. (2010), Waelbroeck et al. (2011) and Hoffman and Lund (2012), as well as our new data from 20 sediment cores (Table S3). The new compilation includes $\delta^{13}C$ data of 165 sediment cores from the eastern Atlantic and 115 cores from the western Atlantic, which in total has 76 more cores than the Hesse et al. (2011) dataset. The general pattern of the LGM $\delta^{13}C$ distribution based on our new compilation (Figure 3.3) is not different from that of Hesse et al. (2011) but with considerably improved details.

3.4 Results

3.4.1 The distribution of seawater $\delta^{13}C$ in the LGM Atlantic

The new compilation of seawater $\delta^{13}C$ (Figure 3.3) confirms the presence of three distinct water masses in the LGM Atlantic as conjectured and described in previous studies (e.g., Duplessy et al., 1988; Sarnthein et al., 1994; Curry and Oppo, 2005). Water mass in the upper 2000 m of the North Atlantic is dominantly ventilated by the glacial NADW (GNADW, in some literatures it is also referred to as glacial North Atlantic Intermediate Water; e.g.,

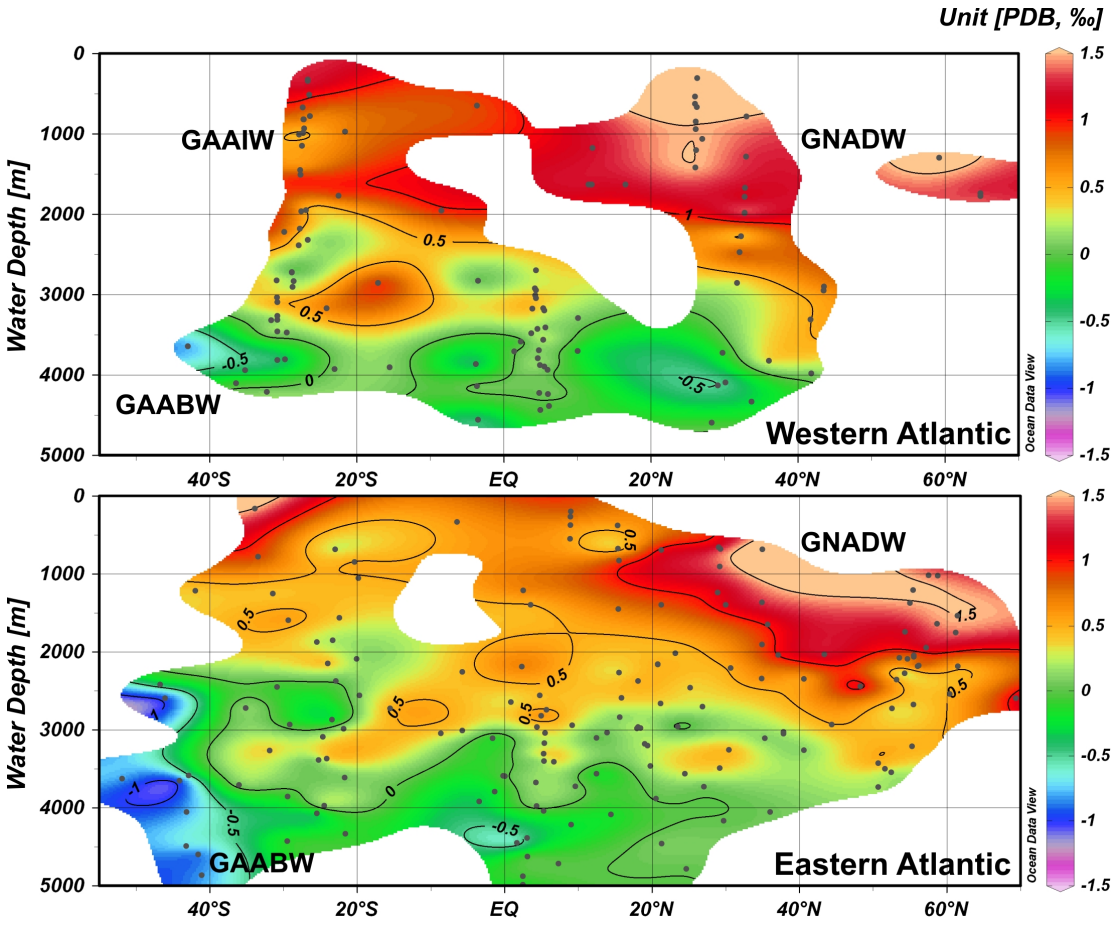

Figure 3.3 The distribution of seawater $\delta^{13}C$ in the LGM western and eastern Atlantic. Water depths of all sediment cores are corrected by -120 m due to the sea-level lowering at the LGM with respect to the present time (Peltier and Fairbanks, 2006).

Duplessy et al., 1988) with an end-member value of 1.5‰. The glacial counterpart of AAIW (GAAIW) with a possible end-member value of 0.3-0.5‰ could also be found at around 900-1100 m in the southwestern Atlantic (Curry and Oppo, 2005). However, the presence and the extent of GAAIW in the southeastern Atlantic are not clear due to the relatively poor coverage of $\delta^{13}C$ data at the intermediate water depth.

The abyssal Atlantic below 3500 m is mainly influenced by glacial AABW (GAABW) with an end-member value of -0.9±0.1‰. Along its pathway to the north, GAABW progressively mixes with GNADW, resulting in the $\delta^{13}C$ signature of water mass increases from -0.9‰ to 0.0‰. Water mass between 3500 and 2000 m has a $\delta^{13}C$ value ranging between 0.0-0.5‰, suggesting that the GNADW and GAABW mix even stronger within this depth interval. The whole interpretation of the LGM $\delta^{13}C$ distribution is also corroborated by other proxy records

such as benthic foraminiferal Cd/Ca (e.g., Marchitto and Broecker, 2006) and neodymium isotopes (e.g., Piotrowski et al., 2004, 2005). In this study, this conjecture of the water mass distribution in the LGM Atlantic would form the base on which we will interpret our reconstructions of B-P ages and $\Delta\Delta^{14}C$.

3.4.2 The distribution of B-P ages in the LGM Atlantic

Before we merge our reconstructions of B-P ages and seawater $\Delta\Delta^{14}C$ (Table 3.3) with published data (Table 3.S2), some results are apparently noisy signals and removed for the following reasons: negative B-P ages, reversed planktonic and/or benthic ^{14}C dates, inconsistent with duplicated results, disturbed sediments and possible contamination of old carbon on benthic $\Delta^{14}C$ and $\delta^{13}C$ signals due to dissociated methane (Table 3.3). We notice that in a few cases, the two LGM samples from the same core show different estimates of B-P ages and $\Delta\Delta^{14}C$. This could reflect either the variability within the LGM time interval, or one of them is simply the outlier. However, as there is no good reason to accept one measurement while reject the other, both measurements are accepted and their mean values (Figure 3.4 and 3.5) are discussed in this study.

When putting all results together, we find that some LGM B-P ages and seawater $\Delta\Delta^{14}C$ estimates are significantly larger or smaller than reconstructions from nearby coring sites (Figure 3.4 and 3.5). e.g., the LGM B-P age of core GeoB9512-5 off NW Africa is 1245 years, nearly 1000 years larger than results of other cores from similar water depths (Figure 3.4d). However, the mean HS1 B-P age of this core is only 212 years (Table 3.3), better in agreement with the LGM results of other cores. Small B-P age estimates are also more coherent with a better ventilated thermocline under glacial climate conditions (e.g., Jaccard and Galbraith, 2012). Therefore, there is a high possibility that the reconstruction of the large LGM B-P age at core GeoB9512-5 is only an outlier. Another example is that the LGM B-P age at two deep cores off NW Africa (GeoB9506-1 and GeoB4241-11) reaches up to 2935 and 3360 years, respectively, which is much higher than B-P age of a shallower core GeoB9508-5, a deeper core GeoB4242-5, and another core GeoB9526-5 from the similar water depth (Figure 3.4d). If we accepted all these reconstructions, it seems that a parcel of aged deep water mass was embedded between the abyssal water depth and the shallower water depth off the LGM NW Africa. This scenario is physically unlikely, as the aged water mass, if it ever existed, should have been dissipated through advection and diffusion over the duration of the LGM time interval. In addition, we could not track the source of this aged water mass based on our current data compilation (Figure 3.4d).

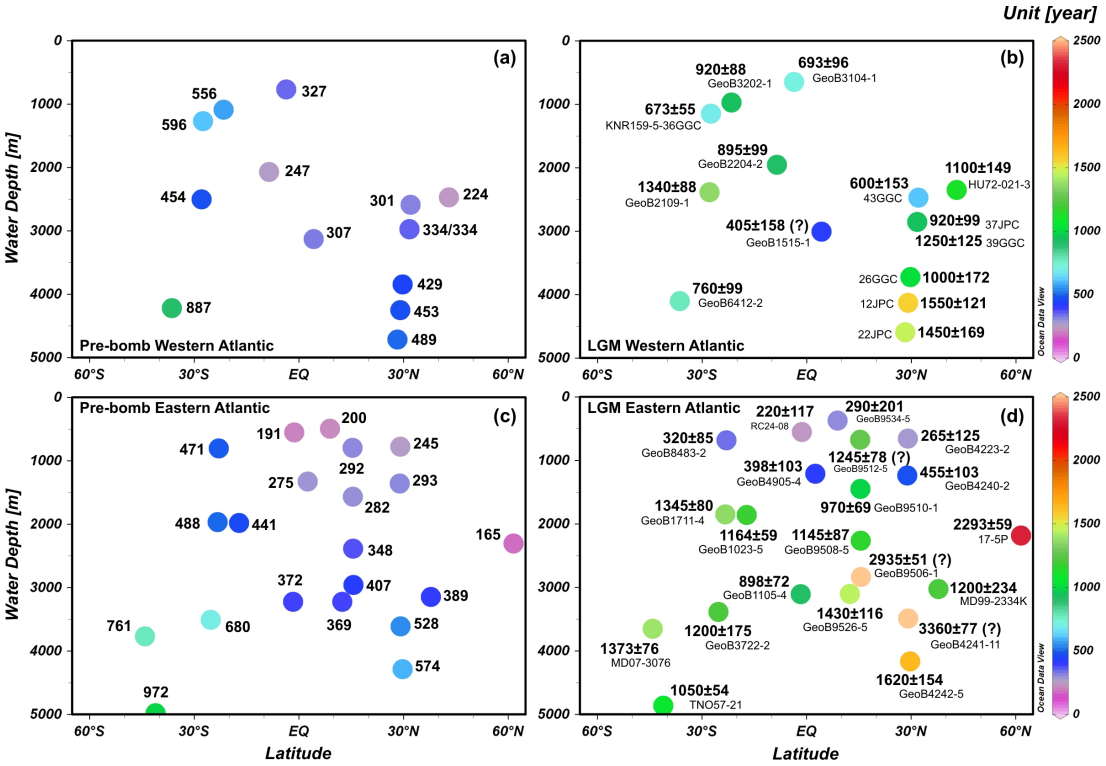

Figure 3.4 Comparison of the pre-bomb B-P ages (a and c) with the LGM reconstructions (b and d) at a set of Atlantic core locations. The LGM B-P age at each core is the mean result of several samples, and the associated uncertainty represents ±1 sigma standard error. Question marks indicate data excluded from the final analyses. The LGM water depths of all sediment cores are adjusted by -120 m.

The LGM B-P age of 405 years at core GeoB1515-1 is relatively smaller than other reconstructions from similar water depths (Figure 3.4b and 3.4d). Previously, small LGM B-P ages were also reconstructed for the deep western equatorial Atlantic (Breocker et al., 1988, 1990). Both old and new reconstructions are suspected to have been subject to the relatively severe influence of bioturbation due to low sedimentation rates of these cores, leading to underestimates of true B-P ages (Broecker et al., 1999; Keigwin and Schlegel, 2002). Taken together, reconstructions of LGM B-P ages and the relevant seawater $\Delta\Delta^{14}C$ estimates of core GeoB9512-5, GeoB9506-1, GeoB4241-11 and GeoB1515-1 are all questionable, and need to be considered with caution. Here they are excluded from the following discussion.

After removing noisy and questionable results, the remaining data show a relatively coherent distribution pattern. In the western Atlantic, two out of three LGM B-P ages from the upper 1500 m are approximately doubled relative to their pre-bomb values, while the one at the

southern limit is equal to its pre-bomb value (Figure 3.4b). Nearly all LGM B-P ages from the upper 1500 m of the eastern Atlantic are comparable to their pre-bomb values within uncertainties (Figure 3.4d). In the upper 1500 m, the LGM B-P ages in the southwestern Atlantic appears to be 300-400 years greater than those in the southeastern Atlantic.

Below 1500 m, the majority of the LGM B-P ages from either the western or the eastern Atlantic are doubled, tripled or even more in contrast to their pre-bomb values. A great expansion of the benthic ^{14}C database gives a more accurate and robust estimate of the mean B-P age for the LGM Atlantic below 1500 m, which reaches up to 1200 years, around 750 years larger than the pre-bomb mean value. When taken as a whole, the LGM B-P ages above 1500 m and below 1500 m show a much stronger gradient relative to that of the pre-bomb era. This strong glacial gradient between the shallow and the deep Atlantic is also observed in the vertical distribution of benthic $\delta^{13}C$ (Figure 3.3; Curry and Oppo, 2005) and Cd/Ca data (e.g., Marchitto and Broecker, 2006). We note that the depth of this gradient indicated by B-P ages seems to be shallower than that of 2000-2500 m suggested by benthic $\delta^{13}C$ and Cd/Ca. This difference is very likely caused by the spatial variability of the depth of this gradient, which could easily bias our estimate when the B-P data coverage is very sparse for the 1500-2000 m water depth (Figure 3.4).

3.4.3 The distribution of seawater $\Delta\Delta^{14}C$ in the LGM Atlantic

Generally, the spatial distribution of the LGM seawater $\Delta\Delta^{14}C$ shares a common feature with that of the LGM B-P ages (Figure 3.5). In the upper 1500 m the mean $\Delta\Delta^{14}C$ value of all LGM reconstructions is -170‰, which is 65‰ less than the pre-bomb mean value. The $\Delta\Delta^{14}C$ distribution in the upper 1500 m shows an evident increasing trend from the South Atlantic to the north. This is because intermediate waters in the south should have been influenced by the ^{14}C-depleted GAAIW to a greater extent. Based on the two reconstructions at 60ºS derived from deepwater corals (Burke and Robinson, 2012), the GAAIW is estimated to have a $\Delta\Delta^{14}C$ end-member value of about -220±30‰.

Below 1500 m, the majority of the LGM $\Delta\Delta^{14}C$ reconstructions range between -220‰ and -310‰. The mean value of all LGM $\Delta\Delta^{14}C$ reconstructions below 1500 m is -275‰, nearly 190‰ less than the pre-bomb value. As what the distribution of B-P ages shows, the LGM $\Delta\Delta^{14}C$ gradient for reconstructions above 1500 m and below 1500 m is also much larger relative to that of the pre-bomb era, reaching by as much as 105‰. Very negative $\Delta\Delta^{14}C$

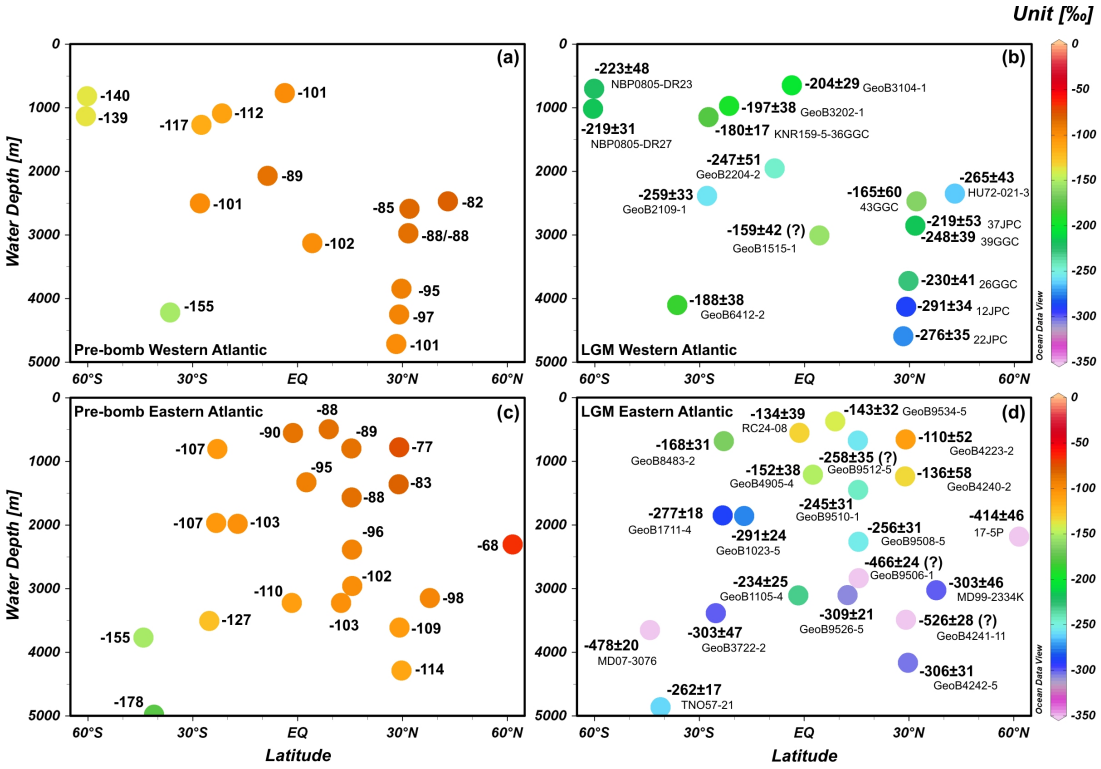

Figure 3.5 Comparison of the pre-bomb $\Delta\Delta^{14}C$ values (a and c) with the LGM reconstructions (b and d) at a set of Atlantic core locations. The LGM $\Delta\Delta^{14}C$ value at each other is the mean result of several samples, and the associated uncertainty represents ±1 sigma standard error. Question marks indicate data excluded from the final analyses. The LGM water depths of all sediment cores are adjusted by -120 m.

values down to -478‰ and -414‰ are found at core MD07-3076 and RAPiD-17-5P, respectively. In the abyssal South Atlantic, the LGM bottom waters at core MD07-3076 and TNO57-21 should have been dominantly influenced by GAABW as indicated by their $\delta^{13}C$ signals (Figure 3.3). However, the LGM bottom-water $\Delta\Delta^{14}C$ estimates at these two core locations show an offset as much as 210‰ (Figure 3.5). Reasons for this significant offset are currently unknown. Although surface reservoir ages at these two core locations were estimated to be 500-1500 years difference over the LGM time interval, the reconstructed sea-surface temperature records of these two cores still show a good agreement, and both temperature records are also well correlated with ice-core records with reliable age models (Barker et al., 2009; Skinner et al., 2010). Therefore, bottom-water $\Delta\Delta^{14}C$ reconstructions at these two locations seem both reliable based on robust methods they used (Barker et al., 2009; Skinner et al., 2010). Without any other available data from the abyssal South Atlantic, we

thus take the mean value -370±15‰ of these two cores (the uncertainty is the standard error of all LGM samples of these two cores) as the $\Delta\Delta^{14}C$ end-member value of GAABW.

It is noteworthy that extremely ^{14}C-depleted signals observed at core RAPiD-17-5P during the HS1 were interpreted to be caused by the northward incursion of glacial AAIW (Thornalley et al., 2011). However, very large B-P ages and depleted $\Delta\Delta^{14}C$ signals are also observed for the LGM interval at this core location (Figure 3.5; Thornalley et al., 2011). Based on the distribution of the LGM $\delta^{13}C$ and $\Delta\Delta^{14}C$ (Figure 3.3 and 3.5), the influence of the GAAIW is hard to track north to the equator and to a water depth of 2000 m. Therefore, the LGM bottom waters at core RAPiD-17-5P should have originated from another source rather than glacial AAIW. Since properties of HS1 bottom waters (at least between 17.5 and 16.0 ka BP) are similar to those of the LGM at core RAPiD-17-5P in terms of seawater $\delta^{13}C$ and B-P age changes (Thornalley et al., 2010, 2011), this would also cast doubt on the glacial AAIW-incursion hypothesis for the HS1 time interval. Indeed, a recent box-model study also suggests that if the extremely ^{14}C-depleted southern-sourced intermediate waters did exist during the HS1, it would be rapidly dispersed and mixed into the rest the ocean during its route to the north (Hain et al., 2011).

3.5 Circulation ages of the glacial Atlantic Ocean

In the following we attempt to estimate circulation ages of the Atlantic Ocean during the LGM period based on three assumptions. First, the majority of the LGM Atlantic was filled with waters from three sources, i.e. GNADW, GAAIW and GAABW. This assumption has been relatively well proved by benthic $\delta^{13}C$ (Figure 3.3; e.g., Curry and Oppo, 2005) and Cd/Ca data (e.g., Marchitto and Broecker, 2006). Therefore, bottom waters at the majority of sediment cores listed in Table 1 were influenced by mixtures of GNADW and GAAIW, or GNADW and GAABW. Some shallow cores (GeoB3104-1, GeoB8483-2, RC24-08, GeoB9534-5, GeoB9512-5 and GeoB4223-2) are located at ventilated thermocline depths, where bottom waters might also have been influenced by subducted surface waters from other sources.

Second, $\delta^{13}C$ and $\Delta\Delta^{14}C$ end-member values of GNADW, GAAIW and GAABW were constant or showed limited changes over a few thousand years prior to the LGM and within the LGM. $\delta^{13}C$ values of all three end members as well as $\Delta\Delta^{14}C$ values of GAAIW and GAABW have already been determined using our data compilations (Figure 3.3 and 3.5), but we still lack the $\Delta\Delta^{14}C$ end-member value of GNADW. In LGM modeling experiments with different geometry and intensity of the Atlantic Meridional Overturning Circulation, the water

mass at the intermediate water depth of the North Atlantic is always simulated to have a mean ^{14}C age that is 600±200 years older than the contemporary atmosphere (Butzin et al., 2005; Franke et al., 2008b). This agrees with the estimate of the mean LGM surface reservoir age in the high-latitude North Atlantic (Thornalley et al., 2011), and also coincides with a previous inference that the LGM air-sea exchange rate in the North Atlantic is stronger than or comparable to that of the Holocene (Marchitto and Broecker, 2006). Therefore, we estimate that GNADW had a $\Delta\Delta^{14}C$ end-member value of -100±30‰, when considering a mean LGM atmospheric $\Delta^{14}C$ value of 420‰ (Reimer et al., 2009).

Third, we assume that seawater $\delta^{13}C$ acted a largely conservative tracer in the Atlantic during the LGM. In that case, the fractional contribution of GNADW and GAAIW, or GNADW and GAABW at a given location and water depth could be determined based on the reconstructed bottom-water $\delta^{13}C$ value. This assumption is only justified when the replenishment of deep waters was accomplished relatively rapidly, so the remineralization of sinking organic particles would not significantly alter the seawater $\delta^{13}C$ signature. Indeed, a recent estimate of the tracer budget suggests that at least in the southwest Atlantic, seawater $\delta^{13}C$ behaves like the conservative tracer $\delta^{18}O$ both for the Holocene and the LGM time intervals (Hoffman and Lund, 2012). With these three assumptions, the mixing $\Delta\Delta^{14}C$ signal at a given location and depth can be calculated based on the estimated mixing ratio and end-member values of different sources. Further, the difference between the reconstructed $\Delta\Delta^{14}C$ signal and the mixing $\Delta\Delta^{14}C$ signal could be used to indicate the ^{14}C-based circulation age (Matsumoto, 2007).

When plotting all results in a $\delta^{13}C$-$\Delta\Delta^{14}C$ diagram (Figure 3.6), we find that the GAAIW end-member values happen to lie on the mixing line between GNADW and GAABW. This phenomenon is also observed in a previous study, that in a $\delta^{13}C$-$Cd_{seawater}$ diagram, waters in the upper South Atlantic could be equally represented by mixing between GNADW and GAABW (Marchitto and Broecker, 2006). Therefore, we could use the same mixing line to represent any mixing between GNADW and GAAIW, or between GNADW and GAABW. Except for one outlier (RAPiD-17-5P) and two questionable data points (core GeoB9506-1 and GeoB4242-11), the vast majority of reconstructions distribute along the mixing line within uncertainties. This strongly implies that the reconstructed $\Delta\Delta^{14}C$ signals comprise major information of mixing signals but only minor information of circulation ages. The result is not surprising, given that the fundamental distribution pattern of B-P ages and $\Delta\Delta^{14}C$ values (Figure 3.4 and 3.5) is in good agreement with that of paleonutrient data (Figure 3.3; Marchitto and Broecker, 2006). When taking a closer inspection, data points closed to the GNADW end member distribute equally on both sides of the mixing line (after excluding data

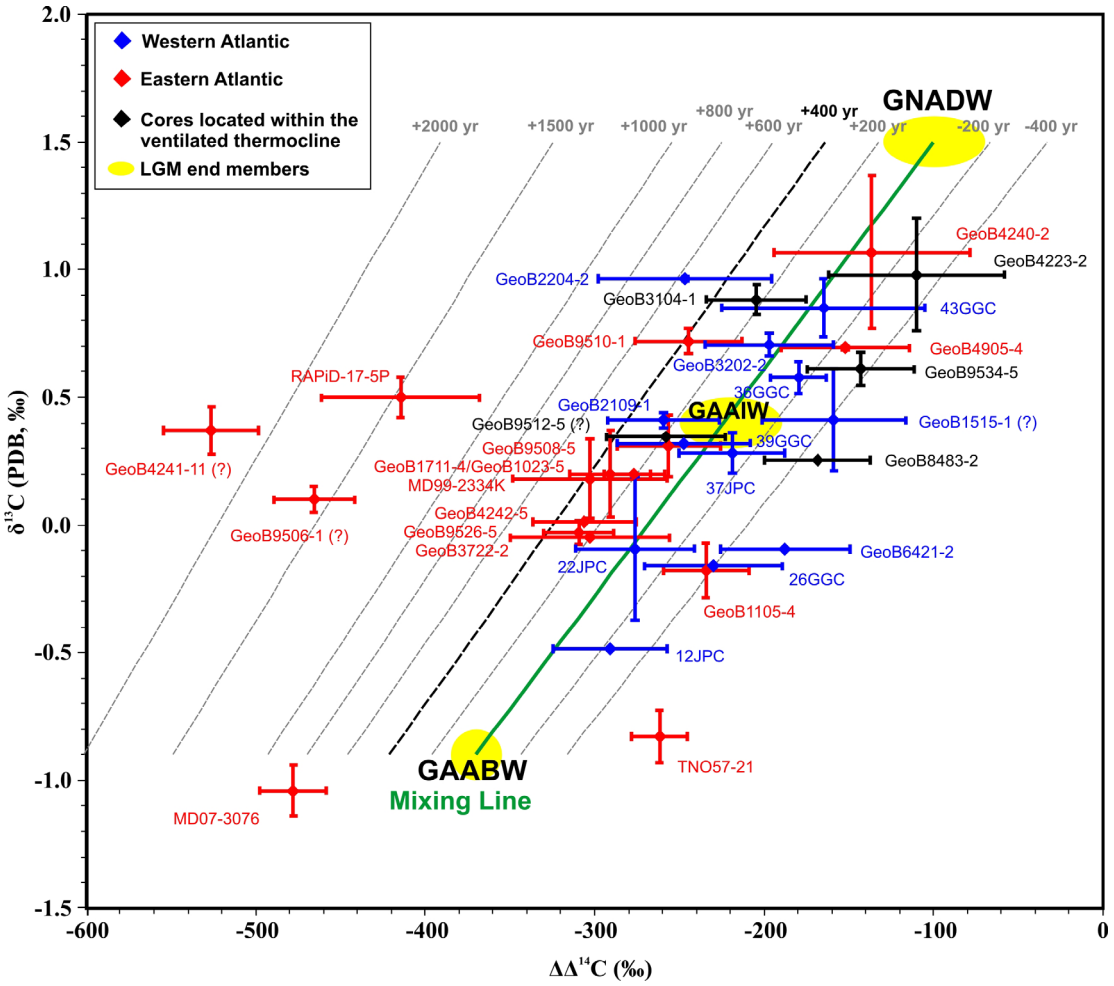

Figure 3.6 The $\delta^{13}C$-$\Delta\Delta^{14}C$ diagram of the LGM bottom waters at a set of Atlantic sediment cores and water masses from three end members. Blue and red diamonds are data from the western and the eastern Atlantic, respectively. Black diamonds denote sediment cores located within the ventilated thermocline, where bottom waters are possibly influenced by subducted waters from other sources besides the GNADW and GAAIW. The $\delta^{13}C$ value of core GeoB1023-5 is adopted from that of the adjacent core GeoB1711-4. Error bars represent ±1 sigma standard deviation for $\delta^{13}C$ and ±1 sigma standard error for $\Delta\Delta^{14}C$. The green line is the mixing line between the GNADW and GAABW. Dash lines represent contours with the constant radiocarbon age offset from the mixing line when assuming that $\delta^{13}C$ is a conservative tracer. From the left to the right, they are 2000, 1500, 1000, 800, 600, 400, 200, -200 and -400 years older than the mixing line, respectively. $\Delta\Delta^{14}C$ values on dashed lines were calculated using the formula $\Delta^{14}C$ = (exp(-t/8033 yr)-1)*1000 ‰ (Stuiver and Polach, 1977).

from the ventilated thermocline and questionable results), while data points located nearly at the middle part between the GAABW and the GNADW end members tend to cluster to the left of the mixing line (Figure 3.6). This can be simply explained by that circulation ages of data points from the upper Atlantic (< 1500 m) might be too small to be observed using our method, while those from deep basins (> 1500 m) might have relatively large and recognizable circulation ages. However, due to large uncertainties of $\Delta\Delta^{14}C$ reconstructions and the chosen $\Delta\Delta^{14}C$ end-member values, these trends can only be fully justified when more precise end-member values and more $\delta^{13}C$-$\Delta\Delta^{14}C$ data are available.

The current dataset suggest that circulation ages at the vast majority of core locations from the deep Atlantic (> 1500 m) are less than 400 years during the LGM (Figure 3.6), which are comparable to or less than pre-bomb values of 200-400 years (Matsumoto, 2007). It should be noted that the LGM circulation age of the deep Atlantic could be much less than 400 years, however, which cannot be resolved by the ^{14}C method due to its uncertainty. Nevertheless, our results at least provide an upper limit for the estimate of the glacial Atlantic circulation age. The fast glacial deepwater circulation rate is consistent with our assumption of taking $\delta^{13}C$ as a conservative tracer.

A strong ocean circulation during the LGM could actually explain a large number of observations. The chemical gradient between the upper and the lower Atlantic, shown by the vertical distribution of seawater $\delta^{13}C$, Cd/Ca and $\Delta\Delta^{14}C$ data, is the most robust characteristic of the glacial Atlantic. To sustain such a strong gradient, besides that end-member values of GAABW and GNADW are significantly different, either a strong export of GAABW and GNADW or a very limited mixing across the GNADW/GAABW boundary or a combination of both is also required. Indeed, the transport to vertical diffusivity ratio of GAABW in the southwestern Atlantic is estimated to be an order of magnitude larger during the LGM than the Holocene (Hoffman and Lund, 2012). Given that the vertical mixing in the LGM ocean interior is probably strengthened due to the generally enhanced wind field and the greater tidal mixing in deep basins (Wunsch, 2003), a strengthening of the water mass export is a more likely explanation for the presence of the chemical gradient (Curry and Oppo, 2005). In addition, our result is also consistent with a recent compilation of $^{231}Pa/^{230}Th$ data from the Atlantic, which indicates a vigorous circulation of GNADW but does not give good constraints on the circulation rate of GAABW (Lippold et al., 2012).

One question remains is how to interpret the presence of very negative deepwater $\delta^{13}C$ and $\Delta^{14}C$ values under fast deepwater circulation conditions during the LGM? Previously, at least depleted $\delta^{13}C$ signals were considered as implications for the existence of a poorly ventilated

deep ocean (e.g., Toggweiler, 1999). Recently, Mackensen (2012) found that the carbon isotopic fractionation effect during the air-sea exchange could cause modern bottom waters and epibenthic foraminifera in the Atlantic sector of the Southern Ocean to enrich in $\delta^{13}C$ by as much as 0.4-1.0‰. During the LGM, this effect should have been significantly reduced as deepwater formation occurred mostly below sea ice. The author further inferred that the depleted $\delta^{13}C$ signature observed in the glacial deep Southern Ocean is not necessarily caused by a reduced ventilation of deep waters but by a reduced isotopic fractionation at sea surface. If the air-sea exchange had been strongly suppressed due to the extensive sea-ice coverage and upper-ocean stratification during the LGM, the southern-sourced intermediate and bottom waters should also have very low performed $\Delta^{14}C$ values with respect to the contemporary atmosphere. Therefore, negative deep ocean $\Delta\Delta^{14}C$ reconstructions (Figure 3.5) are not induced by slow down of deepwater circulation but signals originated from source areas. To summarize, our results and inferences apparently do not support the hypothesis of trapping CO_2 in the deepest part of the ocean through a sluggish ocean circulation (e.g., Toggweiler, 1999; Tschumi et al., 2011). This indicates a necessity to reevaluate the role of marine physical processes in carbon cycle models.

3.6 Conclusion

An expansion of benthic foraminiferal ^{14}C database shows that the chemical gradient between the upper and the lower Atlantic during the LGM, previously indicated by the vertical distribution of benthic foraminiferal $\delta^{13}C$ and Cd/Ca data, is also well documented by the seawater $\Delta^{14}C$ distribution. The majority of B-P ages from the LGM upper Atlantic (< 1500 m) are comparable to or only slightly larger than pre-bomb values, while those from the LGM lower Atlantic (> 1500 m) are larger than pre-bomb values by around 750 years. The mean seawater $\Delta^{14}C$ value from the LGM upper and lower Atlantic is more depleted in $\Delta^{14}C$ by 170‰ and 275‰ than the contemporary atmosphere, respectively. We further give a first estimate of the ^{14}C-based circulation age for the LGM lower Atlantic, which is less than 400 years. A fast deep ocean circulation rate during the LGM seems to be consistent with the presence of the strong chemical gradient. Our estimates do not support a previous hypothesis, which suggests that the glacial deep ocean could sequestrate more CO_2 than that of the interglacial through a slowdown of deepwater circulation.

3.7 Acknowledgements

We are grateful to Stewart Fallon for radiocarbon measurements and Monika Segl and her team for stable isotope analyses. A. Kloss, G. Mollenhauer, R. Portilho-Ramos are thanked

for the generous sharing of their unpublished planktonic foraminiferal radiocarbon dates. Thanks also go to the MARUM GeoB core repository for providing sediment material. This work was funded through the DFG Research Center/Excellence Cluster "The Ocean in the Earth System" and by the Helmholtz Climate Initiative "REKLIM." EH is supported by the China Scholarship Council (CSC No. 2009626073) and the Bremen International Graduate School for Marine Sciences (GLOMAR).

3.8 References

Adegbie, A.T., Schneider, R.R., Röhl, U., Wefer, G., 2003. Glacial millennial-scale fluctuations in central African precipitation recorded in terrigenous sediment supply and freshwater signals offshore Cameroon. Palaeogeography, Palaeoclimatology, Palaeoecology 197, 323-333.

Adkins, J.F., Boyle, E.A., 1997. Changing atmospheric $\Delta^{14}C$ and the record of deep water paleoventilation ages. Paleoceanography 12(3), 337-344, doi:10.1029/97PA00379.

Anderson, R.F., Ali, S., Bradtmiller, L.I., Nielsen, S.H.H., Fleisher, M.Q., Anderson, B.E., Burckle, L.H., 2009. Wind driven upwelling in the Southern Ocean and the deglacial rise in atmospheric CO_2. Science 323, 1443-1446.

Arz, H.W., Pätzold, J., Wefer, G., 1998. Correlated millennial-scale changes in surface hydrography and terrigenous sediment yield inferred from last-glacial marine deposits off northeastern Brazil. Quaternary Research 50, 157-166.

Arz, H.W., Pätzold, J., Wefer, G., 1999. The deglacial history of the western tropical Atlantic as inferred from high resolution stable isotope records off northeastern Brazil. Earth and Planetary Science Letters 167, 105-117.

Barker, S., Diz, P., Vautravers, M.J., Pike, J., Knorr, G., Hall, I.R., Broecker, W.S., 2009. Interhemispheric Atlantic seesaw response during the last deglaciation. Nature 457, 1097-1102.

Barker, S., Knorr, G., Vautravers, M.J., Diz, P., Skinner, L.C., 2010. Extreme deepening of the Atlantic overturning circulation during deglaciation. Nature Geosciences 3, 567-571.

Bickert, T., Mackensen, A., 2004. Last Glacial to Holocene changes in South Atlantic deep water circulation. In: Wefer, G., Mulitza, S., Ratmeyer, V. (Eds.), The South Atlantic in the Late Quaternary: Reconstruction of Material Budgets and Current Systems. Springer-Verlag Berlin Heidelberg New York Tokyo, pp. 671-695.

Broecker, W., Clark, E., Hajdas, I., Bonani, G., 2004. Glacial ventilation rates for the deep Pacific Ocean. Paleoceanography 19, PA2002, doi:10.1029/2003PA000974.

Broecker, W., Matsumoto, K., Clark, E., Hajdas, T., Bonani, G., 1999. Radiocarbon age differences between coexisting foraminiferal species. Paleoceanography 14(4), 431-436.

Broecker, W.S., 1991. The great ocean conveyor. Oceanography 4(2), 79-89.

Broecker, W.S., Andree, M., Bonani, G., Wolfli, W., Oeschger, H., Klas, M., Mix, A., Curry, W., 1988. Preliminary estimates for the radiocarbon age of deep water in the glacial ocean. Paleoceanography 3(6), 659-669.

Broecker, W.S., Barker, S., 2007. A 190‰ drop in atmosphere's $\Delta^{14}C$ during the "Mystery Interval" (17.5-14.5 kyr). Earth and Planetary Science Letters 256, 90-99.

Broecker, W.S., Peng, T.-H., Trumbore, S., Bonani, G., Wolfli, W., 1990. The distribution of radiocarbon in the glacial ocean. Global Biogeochemical Cycles 4(1), 103-117.

Bryan, S.P., Marchitto, T.M., Lehman, S.J., 2010. The release of ^{14}C-depleted carbon from the deep ocean during the last deglaciation: evidence from the Arabian Sea. Earth and Planetary Science Letters 298, 244-254.

Burke, A., Robinson, L.F., 2012. The Southern Ocean's role in carbon exchange during the last deglaciation. Science 335, 557-561.

Butzin, M., Prange, M., Lohmann, G., 2005. Radiocarbon simulations for the glacial ocean: The effects of wind stress, Southern Ocean sea ice and Heinrich events. Earth and Planetary Science Letters 235, 45-61.

Butzin, M., Prange, M., Lohmann, G., 2012. Readjustment of glacial radiocarbon chronologies by self-consistent three-dimensional ocean circulation modeling. Earth and Planetary Science Letters 317-318, 177-184.

Chen, Z., Yan, X.-H., Jo, Y.-H., Jiang, L., Jiang, Y., 2012. A study of Benguela upwelling system using different upwelling indices derived from remotely sensed data. Continental Shelf Research 45, 27-33.

Cléroux, C., deMenocal, P., Guilderson, T., 2011. Deglacial radiocarbon history of tropical Atlantic thermocline waters: absence of CO_2 reservoir purging signal. Quaternary Science Reviews 30, 1875-1882.

Cléroux, C., deMenocal, P., Guilderson, T., 2011. Deglacial radiocarbon history of tropical Atlantic thermocline waters: absence of CO_2 reservoir purging signal. Quaternary Science Reviews 30, 1875-1882.

Curry, W.B., Oppo, D.W., 2005. Glacial water mass geometry and the distribution of $\delta^{13}C$ of ΣCO_2 in the western Atlantic Ocean. Paleoceanography 20, PA1017, doi:10.1029/2004PA001021.

De Pol-Holz, R., Keigwin, L.D., Southon, J., Hebbeln, D., Mohtadi, M., 2010. No signature of abyssal carbon in intermediate waters off Chile during deglaciation. Nature Geoscience 3, 192-195.

Duplessy, J.C., Shackleton, N.J., Fairbanks, R.G., Labeyrie, L., Oppo, D., Kallel, N., 1988. Deepwater source variations during the last climatic cycle and their impact on the global deepwater circulation. Paleoceanography 3, 343-60, doi:10.1029/PA003i003p00343.

Fallon, S.J., Fifield, L.K., Chappell, J.M., 2010. The next chapter in radiocarbon dating at the Australian National University: Status report on the single stage AMS. Nuclear Instruments and Methods in Physics Research B 268, 898-901.

Franke, J., Paul, A., Schulz, M., 2008b. Modeling variations of marine reservoir ages during the last 45000 years. Climate of the Past 4, 125-136.

Franke, J., Schulz, M., Paul, A., Adkins, J.F., 2008a. Assessing the ability of the ^{14}C projection-age method to constrain the circulation of the past in a 3-D ocean model. Geochemistry, Geophysics, Geosystems 9, Q08003, doi:10.1029/2008GC001943.

Hain, M.P., Sigman, D.M., Haug, G.H., 2011. Shortcomings of the isolated abyssal reservoir model for deglacial radiocarbon changes in the mid-depth Indo-Pacific Ocean. Geophysical Research Letters 38, L04604, doi10.1029/2010GL046158.

Henderiks, J., Freudenthal, T., Meggers, H., Nave, S., Abrantes, F., Bollmann, J., Thierstein, H.R., 2002. Glacial-interglacial variability of particle accumulation in the Canary Basin: a time-slice approach. Deep-Sea Research II 49, 3675-3705.

Hendry, K.R., Robinson, L.F., Meredith, M.P., Mulitza, S., Chiessi, C.M., Arz, H., 2012. Abrupt changes in high-latitude nutrient supply to the Atlantic during the last glacial cycle. Geology 40(2), 123-126.

Hesse, T., Butzin, M., Bickert, T., Lohmann, G., 2011. A model-data comparison of $\delta^{13}C$ in the glacial Atlantic Ocean. Paleoceanography 26, PA3220, doi:10.1029/2010PA002085.

Hoffman, J.L., Lund, D.C., 2012. Refining the stable isotope budget for Antarctic Bottom Water: New foraminiferal data from the abyssal southwest Atlantic. Paleoceanography 27, PA1213, doi:10.1029/2011PA002216.

Holzwarth, U., Meggers, H., Esper, O., Kuhlmann, H., Freudenthal, T., Hensen, C., Zonneveld, K.A.F., 2010. NW African climate variations during the last 47,000 years: Evidence from organic-walled dinoflagellate cysts. Palaeogeography, Palaeoclimatology, Palaeoecology 291, 443-455.

Jaccard, S.L., Galbraith, E.D., 2012. Large climate-driven changes of oceanic oxygen concentrations during the last deglaciation. Nature Geoscience 5, 151-156.

Keigwin, L.D., 2004. Radiocarbon and stable isotope constraints on last glacial maximum and younger Dryas ventilation in the western north Atlantic. Paleoceanography 19, PA4012, doi:10.1029/2004PA001029.

Keigwin, L.D., Schlegel, M.A., 2002. Ocean ventilation and sedimentation since the glacial maximum at 3 km in the western North Atlantic, Geochemistry Geophysics Geosystems 3(6), 10.1029/2001GC000283.

Key, R.M., Kozyr, A., Sabine, C.L., Lee, K., Wanninkhof, R., Bullister, J.L., Feely, R.A., Millero, F.J., Mordy, C., Peng, T.-H., 2004. A global ocean carbon climatology: Results

from Global Data Analysis Project (GLODAP). Global Biogeochemical Cycles 18, GB4031, doi:10.1029/2004GB002247.

Kim, J.-H., Schneider, R.R., Müller, P.J., Wefer, G., 2002. Interhemispheric comparison of deglacial sea-surface temperature patterns in Atlantic eastern boundary currents. Earth and Planetary Science Letters 194, 383-393.

Köhler, P., Fischer, H., Munhoven, G., Zeebe, R.E., 2005. Quantitative interpretation of atmospheric carbon records over the last glacial termination. Global Biogeochemical Cycles 19, GB4020. doi:10.1029/2004GB002345.

LeGrand, P., Wunsch, C., 1995. Constraints from paleo-tracer data on the North Atlantic circulation during the last glacial maximum. Paleoceanography 10(6), 1011-1045.

Lemieux-Dudon, B., Blayo, E., Petit, J.-R., Waelbroeck, C., Svensson, A., Ritz, C., Barnola, J.-M., Narcisi, B.M., Parrenin, F., 2010. Consistent dating for Antarctic and Greenland ice cores. Quaternary Science Reviews 29, 8-20.

Lippold, J., Luo, Y., Francois, R., Allen, S.E., Gherardi, J., Pichat, S., Hickey, B., Schulz , H., 2012. Strength and geometry of the glacial Atlantic Meridional Overturning Circulation. Nature Geosciences 5, 813-816.

Little, M.G., Schneider, R.R., Kroon, D., Price, B., Summerhayes, C.P., Segl, M., 1997. Trade wind forcing of upwelling, seasonality, and Heinrich events as a response to sub-Milankovitch climate variability. Paleoceanography 12(4), 568-576.

Lynch-Stieglitz, J., Curry, W.B., Slowey, N., 1999. Weaker Gulf Stream in the Florida Straits during the Last Glacial Maximum. Nature 402, 644-648.

Mackensen, A., 2012. Strong thermodynamic imprint on Recent bottom-water and epibenthic $\delta^{13}C$ in the Weddell Sea revealed: Implications for glacial Southern Ocean ventilation. Earth and Planetary Science Letters 317-318, 20-26.

Mangini, A., Godoy, J.M., Godoy, M.L., Kowsmann, R., Santos, G.M., Ruckelshausen, M., Schroeder-Ritzrau, A., Wacker, L., 2010. Deep sea corals off Brazil verify a poorly ventilated Southern Pacific Ocean during H2, H1 and the younger Dryas. Earth and Planetary Science Letters 293, 269-276.

Marchitto, T.M., Broecker, W.S., 2006. Deep water mass geometry in the glacial Atlantic Ocean: A review of constraints from the paleonutrient proxy Cd/Ca. Geochemistry Geophysics Geosystems 7, Q12003, doi:10.1029/2006GC001323.

Marchitto, T.M., Lehman, S.J., Ortiz, J.D., Fluckiger, J., van Geen, A., 2007. Marine radiocarbon evidence for the mechanism of deglacial atmospheric CO_2 rise. Science 316, 1456-1440.

Matsumoto, K., 2007. Radiocarbon-based circulation age of the world oceans. Journal of Geophysical Research 112, C09004, doi:10.1029/2007JC004095.

Mollenhauer, G., Schneider, R.R., Müller, P.J., Spieß, V., Wefer, G., 2002. Glacial/interglacial variablity in the Benguela upwelling system: Spatial distribution and budgets of organic carbon accumulation. Global Biogeochemical Cycles 16(4), 1134, doi:10.1029/2001GB001488, 2002.

Monnin, E., Indermuhle, A., Dallenbach, A., Fluckiger, J., Stauffer, B., Stocker, T.F., Raynaud, D., Barnola, J.M., 2001. Atmospheric CO_2 concentrations over the last glacial termination. Science 291, 112-114.

Mulitza, S., Prange, M., Stuut, J.-B., Zabel,M., von Dobeneck, T., Itambi, A.C., Nizou, J., Schulz, M., Wefer, G., 2008. Sahel megadroughts triggered by glacial slowdowns of Atlantic meridional overturning. Paleoceanography 23, PA4206, doi:10.1029/2008PA001637.

Otto-Bliesner, B.L., Hewitt, C.D., Marchitto, T.M., Brady, E., Abe-Ouchi, A., Crucifix, M., Murakami, S., Weber, S.L., 2007. Last Glacial Maximum ocean thermohaline circulation: PMIP2 model intercomparisons and data constraints. Geophysical Research Letters 34, L12706, doi:10.1029/2007GL029475.

Peltier, W.R., Fairbanks, R.G., 2006. Global glacial ice volume and Last Glacial Maximum duration from an extended Barbados sea level record. Quaternary Science Reviews 25, 3322-3337.

Piotrowski, A.M., Goldstein, S.L., Hemming, S.R., Fairbanks, R.G., 2004. Intensification and variability of ocean thermohaline circulation through the last deglaciation. Earth and Planetary Science Letters 225, 205-220.

Piotrowski, A.M., Goldstein, S.L., Hemming, S.R., Fairbanks, R.G., 2005. Temporal relationships of carbon cycling and ocean circulation at glacial boundaries. Science 307, 1933-1938.

Reimer, P.J., Baillie, M.G.L., Bard, E., Bayliss, A., Beck, J.W., Blackwell, P.G., Bronk Ramsey, C., Buck, C.E., Burr, G.S., Edwards, R.L., Friedrich, M., Grootes, P.M., Guilderson, T.P., Hajdas, I., Heaton, T.J., Hogg, A.G., Hughen, K.A., Kaiser, K.F., Kromer, B., McCormac, F.G., Manning, S.W., Reimer, R.W., Richards, D.A., Southon, J.R., Talamo, S., Turney, C.S.M., van der Plicht, J., Weyhenmeyer, C.E., 2009. IntCal09 and Marine09 radiocarbon age calibration curves, 0-50,000 years cal BP. Radiocarbon 51(4), 1111-1150.

Robinson, L.F., Adkins, J.F., Keigwin, L.D., Southon, J., Fernandez, D.P., Wang, S.-L., Scheirer, D.S., 2005. Radiocarbon variability in the western North Atlantic during the last deglaciation. Science 310, 1469-1473.

Rose, K.A., Sikes, E.L., Guilderson, T.P., Shane, P., Hill, T.M., Zahn, R., Spero, H.J., 2010. Upper-ocean-to-atmosphere radiocarbon offsets imply fast deglacial carbon dioxide release. Nature 466, 1093-1097.

Sarnthein, M., Winn, K., Jung, S.J.A., Duplessy, J.-C., Labeyrie, L., Erlenkeuser, H., Ganssen, G., 1994. Changes in east Atlantic deep-water circulation over the last 30,000 years: Eight time slice reconstructions. Paleoceanography 9, 209-267, doi:10.1029/93PA03301.

Schmitt, J., Schneider, R., Elsig, J., Leuenberger, D., Lourantou, A., Chappellaz, J., Köhler, P., Joos, F., Stocker, T.F., Leuenberger, M., Fischer, H., 2012. Carbon isotope constraints on the deglacial CO_2 rise from ice cores. Science 336, 711-714.

Shackleton, N.J., Hall, M.A., Vincent, E., 2000. Phase relationships between millennial-scale events 64,000-24,000 years ago. Paleoceanography 15, 565-569.

Sigman, D., Hain, M.P., Haug, G.H., 2010. The polar ocean and glacial cycles in atmospheric CO2 concentration. Nature 446, 47-55.

Sigman, D.M., Boyle, E.A., 2000. Glacial/interglacial variations in atmospheric carbon dioxide. Nature 407, 859-869.

Skinner, L.C., Fallon, S., Waelbroeck, C., Michel, E., Barker, S., 2010. Ventilation of the deep southern ocean and deglacial CO_2 rise. Science 328, 1147-1151.

Skinner, L.C., Shackleton, N.J., 2004. Rapid transient changes in northeast Atlantic deep water ventilation age across Termination I. Paleoceanography 19, PA2005, doi:10.1029/2003PA000983.

Smith, H.J., Fischer, H., Whalen, M., Mastroianni, D., Deck, B., 1999. Dual modes of the carbon cycle since the Last Glacial Maximum. Nature 400, 248-250.

Sortor, R.N., Lund, D.C., 2011. No evidence for a deglacial intermediate water $\Delta^{14}C$ anomaly in the SW Atlantic. Earth and Planetary Science Letters 310, 65-72.

Southon, J., Noronha, A.L., Cheng, H., Edwards, R.L., Wang, Y., 2012. A high-resolution record of atmospheric ^{14}C based on Hulu Cave speleothem H82. Quaternary Science Reviews 33, 32-41.

Spero, H.J., Lea, D.W., 2002. The cause of carbon isotope minimum events on glacial terminations. Science 296, 522-525.

Stott, L., Southon, J., Timmermann, A., Koutavas, A., 2009. Radiocarbon age anomaly at intermediate water depth in the Pacific Ocean during the last deglaciation. Paleoceanography 24, PA2223, doi:10.1029/2008PA001690.

Stuiver, M., Polach, H.A., 1977. Discussion: reporting of ^{14}C data. Radiocarbon 19(3), 355-363.

Stuiver, M., Reimer, P.J., 1993. Extended ^{14}C data base and revised CALIB 3.0 ^{14}C age calibration program. Radiocarbon 35, 215-230.

Thornalley, D.J.R., Barker, S., Broecker, W., Elderfield, H., McCave, I.N., 2011. The deglacial evolution of north Atlantic deep convection. Science 331, 202-205.

Thornalley, D.J.R., Elderfield, H., McCave, I.N., 2010. Intermediate and deep water paleoceanography of the northern North Atlantic over the past 21,000 years. Paleoceanography 25, PA1211, doi:10.1029/2009PA001833.

Toggweiler, J.R., 1999. Variation of atmospheric CO_2 by ventilation of the ocean's deepest water. Paleoceanography 14(5), 571-588, doi:10.1029/1999PA900033.

Toggweiler, J.R., Russell, J.L., Carson, S.R., 2006. Midlatitude westerlies, atmospheric CO_2, and climate change during the ice ages. Paleoceanography 21, PA2005, doi:10.1029/2005PA001154.

Tschumi, T., Joos, F., Gehlen, M., Heinze, C., 2011. Deep ocean ventilation, carbon isotopes, marine sedimentation and the deglacial CO_2 rise. Climate of the Past 7, 771-800, doi:10.5194/cp-7-771-2011, 2011.

Vidal, L., Schneider, R.R., Marchal, O., Bickert, T., Stocker, T.F., Wefer, G., 1999. Link between the North and South Atlantic during the Heinrich events of the last glacial period. Climate Dynamics 15, 909-919.

Voituriez, B., Herbland, A., 1982. Comparaison des systèmes productifs de l'Atlantique Tropical Est: dômes thermiques, upwellings côtiers et upwelling équatorial. Rapp. P.-V. Réun., Cons. Int. Explor. Mer. 180, pp. pp. 107-123.

Volbers, A.N.A., Niebler, H.-S., Giraudeau, J., Schmidt, H., Heinrich, R., 2003. Paleoceanographic changes in the northern Benguela upwelling system over the past 245,000 years as derived from planktik foraminifera assemblage. In: Wefer, G., Mulitza, S., Ratmeyer, V. (Eds.), The South Atlantic in the Late Quaternary: Reconstruction of Material Budgets and Current Systems. Springer-Verlag Berlin Heidelberg New York Tokyo, pp. 601-622.

Waelbroeck, C., Skinner, L.C., Labeyrie, L., Duplessy, J.-C., Michel, E., Vazquez Riveiros, N., Gherardi, J.-M., Dewilde, F., 2011. The timing of deglacial circulation changes in the Atlantic. Paleoceanography 26, PA3213, doi:10.1029/2010PA002007.

Wunsch, C., 2003. Determining paleoceanographic circulations, with emphasis on the Last Glacial Maximum. Quaternary Science Reviews 22, 371-385.

Yu, E.-F., Francois, R., Bacon, M.P., 1996. Similar rates of modern and last-glacial ocean thermohaline circulation inferred from radiochemical data. Nature 379, 689-694.

Zarriess, M., Johnstone, H., Prange, M., Steph, S., Groeneveld, J., Mulitza, S., Mackensen, A., 2011. Bipolar seesaw in the northeastern tropical Atlantic during Heinrich stadials. Geophysical Research Letters 38, L04706, doi:10.1029/2010GL046070.

Zarriess, M., Mackensen, A., 2010. The tropical rainbelt and productivity changes off northwest Africa: A 31,000-year high-resolution record. Marine Micropaleontology 76, 76-91.

3.9 Auxiliary material

3.9.1 Foraminiferal radiocarbon and stable isotope data from selected Atlantic sediment cores

Table 3.S1 The LGM planktonic radiocarbon ages of the Atlantic sediment cores with existing deepwater radiocarbon reconstructions.

Core	Core Depth (cm)	Dating Species	Lab Code	^{14}C Age (±1σ, yr)	Recalibrated Calendar Age (±1σ, yr BP)	References
RAPiD-17-5P	1005-1007	*N. pachyderma* sinistral	OS-79061	16350 ± 65		Thornalley et al., 2011
	1033-1035	*N. pachyderma* sinistral	OS-79062	16750 ± 65		
	1048-1049	*N. pachyderma* sinistral	SUERC-14116	18321 ± 63		
HU72021-3	632.25	Planktonic Mixture	OS5217	16650 ± 100	19216 ± 259	Keigwin and Jones, 1995
MD99-2334K	314	*G. bulloides*		19170 ± 150		Skinner and Shackleton, 2004
KNR140-39GGC	426-432	*G. ruber*	NOSAMS26432	16900 ± 75	19653 ± 242	Keigwin and Schlegal, 2002
KNR140-37JPC	314-316	*G. inflata*	NOSAMS27342	15750 ± 80	18650 ± 166	Keigwin and Schlegal, 2002
	406-408	*G. inflata*	NOSAMS27343	18260 ± 95	21244 ± 338	
KNR140-12JPC	229.5-232.5	Planktonic Mixture	NOSAMS33892	15750 ± 75	18674 ± 182	Keigwin, 2004
KNR140-22JPC	168-171	*G. inflata*	NOSAMS25804	15700 ± 95	18643 ± 163	Keigwin, 2004
KNR140-26GGC	328-330	*G. ruber*	NOSAMS33012	16650 ± 100	19380 ± 208	Keigwin, 2004
KNR140-43GGC	177-180	*G. ruber*	NOSAMS32900	18350 ± 95	21444 ± 363	Keigwin, 2004
RC24-08	82-83	*G. ruber*	LLNL144073	16570 ± 100	19147 ± 217	Cléroux et al., 2011
TNO57-21	200-205	*G. bolloides*	OS-64633	15650 ± 80	18213 ± 167	Barker et al., 2009
	210-215	*G. bolloides*	OS-64634	16050 ± 65	18698 ± 180	
	230-235	*G. bolloides*	OS-64636	16900 ± 80	19421 ± 173	
	240-245	*G. bolloides*	OS-64524	17400 ± 70	20008 ± 204	
	250-255	*G. bolloides*	OS-64637	18000 ± 85	20723 ± 335	
	290-295	*G. bolloides*	OS-64521	19300 ± 90	22281 ± 309	
KNR159-5-36GGC	146.5	*G.ruber*	UCIAMS92906	15240 ± 90	18004 ± 176	Sorter and Lund, 2011
	150.5	*G.ruber*	UCIAMS64791	15500 ± 70	18208 ± 156	
	150.5	*G.ruber*	UCIAMS64791	15500 ± 70	18208 ± 156	
	180.5	*G.ruber*	UCIAMS77930	17510 ± 60	20248 ± 307	
	182.5	*G.ruber*	UCIAMS92910	17590 ± 80	20375 ± 236	
	185.5	*G.ruber*	UCIAMS77931	18780 ± 70	21905 ± 280	
	190.5	*G.ruber*	UCIAMS77932	19340 ± 60	22606 ± 308	
MD07-3076	121	*N. pachyderma* sinistral	S-ANU5209	17030 ± 200		Skinner et al., 2010
	125	*N. pachyderma* sinistral	S-ANU3816	17400 ± 120		
	133	*N. pachyderma* sinistral	S-ANU2424	18220 ± 100		
	137	*N. pachyderma* sinistral	S-ANU2425	18070 ± 130		
	145	*N. pachyderma* sinistral	S-ANU2426	19060 ± 130		
	161	*N. pachyderma* sinistral	S-ANU2427	20580 ± 130		

a. Planktonic radiocarbon ages are recalibrated into calendar ages using the Marine09 curve (Reimer et al., 2009) and the pre-bomb surface reservoir ages derived from the Key et al. (2004) dataset.

b. Planktonic radiocarbon ages from sediment cores with independent estimates of age models are not necessary to be converted into calendar ages.

Table 3.S2 A compilation of the published benthic ^{14}C ages and B-P ages for the LGM Atlantic Ocean. Deepwater $\Delta^{14}C$ and $\Delta\Delta^{14}C$ and their uncertainties of these cores are re-estimated. Uncertainties associated with B-P age, deepwater $\Delta^{14}C$ and $\Delta\Delta^{14}C$ are ±1 sigma standard error.

Core	Core Depth (cm)	Calendar Age (±1σ, yr BP)	Core Depth (cm)	Dating Species	Lab Code	Benthic ^{14}C Age (±1σ, yr)	Deepwater $\Delta^{14}C$ (±1σ, ‰)	B-P Ages (±1σ, yr)	$\Delta\Delta^{14}C$ (±1σ, ‰)	References
RAPiD-17-5P	1005-1007	18050 ± 401	1005-1007	Benthic Mixture	OS-79069	18750 ± 80	-140 ± 43	2400 ± 103	-542 ± 48	Thornalley et al., 2011
	1033-1035	20240 ± 701	1033-1035	Benthic Mixture	OS-79070	19450 ± 75	28 ± 88	2700 ± 99	-358 ± 90	
	1048-1049	21373 ± 701	1046-1051	Benthic Mixture	OS-79071	20100 ± 85	87 ± 93	1779 ± 106	-343 ± 95	
HU72021-3	632.25	19216 ± 259	631	Benthic Mixture		17750 ± 110	122 ± 38	1100 ± 149	-265 ± 43	Robinson et al., 2005
MD99-2334K		18511 ± 376	241	Benthic Mixture	S-ANU2514	17100 ± 120	117 ± 53		-313 ± 56	Skinner and Shackleton, 2004; Skinner et al., 2010
	314	22219 ± 446	313	Benthic Mixture	Gif102651	20370 ± 180	164 ± 68	1200 ± 234	-292 ± 71	
KNR140-39GGC	426-432	19653 ± 242	426-432	Benthic Mixture	NOSAMS11196	18150 ± 100	125 ± 36	1250 ± 125	-248 ± 39	Keigwin and Schlegal, 2002
KNR140-37JPC	314-316	18650 ± 166	313-317	*U. peregrina*	NOSAMS29280	16550 ± 95	217 ± 28	800 ± 124	-188 ± 34	Keigwin and Schlegal, 2002
	406-408	21244 ± 338	404-408	*U. peregrina*	NOSAMS29282	19300 ± 120	182 ± 51	1040 ± 153	-250 ± 53	
KNR140-12JPC	229.5-232.5	18674 ± 182	230.5-232.5	*N. umbonifera*	NOSAMS33891	17300 ± 95	111 ± 28	1550 ± 121	-291 ± 34	Keigwin, 2004
KNR140-22JPC	168-171	18643 ± 163	168-171	*N. umbonifera*	NOSAMS25805	17150 ± 140	128 ± 30	1450 ± 169	-276 ± 35	Keigwin, 2004
KNR140-26GGC	328-330	19380 ± 208	328-330	*N. umbonifera*	NOSAMS33011	17650 ± 140	159 ± 35	1000 ± 172	-230 ± 41	Keigwin, 2004
KNR140-43GGC	177-180	21444 ± 363	177-180	*U. peregrina*	NOSAMS32899	18950 ± 120	265 ± 59	600 ± 153	-165 ± 60	Keigwin, 2004
RC24-08	82-83	19147 ± 217	82-83	*G. crassaformis*	LLNL144072	16790 ± 60	254 ± 34	220 ± 117	-134 ± 39	Cléroux et al., 2011
TNO57-21	200-205	18213 ± 167	200-205	Benthic Mixture	OS-62541	16700 ± 90	133 ± 26	1050 ± 120	-266 ± 34	Barker et al., 2010
	210-215	18698 ± 180	210-215	Benthic Mixture	OS-62532	17050 ± 90	150 ± 28	1000 ± 111	-249 ± 33	
	230-235	19421 ± 173	230-235	Benthic Mixture	OS-62531	18100 ± 110	101 ± 27	1200 ± 136	-285 ± 35	
	240-245	20008 ± 204	240-245	Benthic Mixture	OS-62537	18250 ± 80	160 ± 31	850 ± 106	-229 ± 31	
	250-255	20723 ± 335	250-255	Benthic Mixture	OS-62529	18700 ± 130	196 ± 52	700 ± 155	-202 ± 58	
	290-295	22281 ± 309	290-295	Benthic Mixture	OS-62534	20800 ± 120	112 ± 45	1500 ± 150	-338 ± 47	
KNR159-5-36GGC	146.5	18004 ± 176	146.5	*Cibicidoides* and *Uvigerina*	UCIAMS94730	15890 ± 90	221 ± 29	650 ± 127	-169 ± 31	Sorter and Lund, 2011
	150.5	18208 ± 156	150.5	*Cibicidoides*	UCIAMS73541	16390 ± 55	176 ± 24	890 ± 89	-222 ± 32	
	150.5	18208 ± 156	150.5	*Uvigerina*	UCIAMS73542	16080 ± 290	223 ± 50	580 ± 298	-176 ± 54	
	180.5	20248 ± 307	180.5	*Cibicidoides* and *Uvigerina*	UCIAMS77918	18000 ± 40	232 ± 46	490 ± 72	-154 ± 47	
	182.5	20375 ± 236	182.5	*Cibicidoides* and *Uvigerina*	UCIAMS94732	18380 ± 100	193 ± 37	790 ± 128	-189 ± 39	
	185.5	21905 ± 280	185.5	*Cibicidoides* and *Uvigerina*	UCIAMS77919	19320 ± 60	278 ± 44	540 ± 92	-167 ± 48	
	190.5	22606 ± 308	190.5	*Cibicidoides* and *Uvigerina*	UCIAMS77920	20110 ± 60	260 ± 48	770 ± 85	-180 ± 50	
MD07-3076	121	18009 ± 324	121	Benthic Mixture	S-ANU3809	17640 ± 80	-17 ± 40	610 ± 215	-412 ± 41	Skinner et al., 2010
	125	18380 ± 278	125	Benthic Mixture	S-ANU3805	18490 ± 70	-75 ± 32	1090 ± 139	-489 ± 40	
	133	19028 ± 231	133	Benthic Mixture	S-ANU2512	19530 ± 120	-121 ± 28	1310 ± 156	-503 ± 32	
	137	19398 ± 255	137	Benthic Mixture	S-ANU2513	19870 ± 130	-119 ± 31	1800 ± 184	-503 ± 39	
	145	20509 ± 440	145	Benthic Mixture	S-ANU2514	20800 ± 130	-103 ± 50	1740 ± 184	-495 ± 53	
	161	22870 ± 532	161	Benthic Mixture	S-ANU2517	22270 ± 180	-6 ± 68	1690 ± 222	-466 ± 73	
NBP0805-DR23		20330 ± 173		deepwater coral	OS-79685	18550 ± 280	162 ± 47		-223 ± 48	Burke and Robinson, 2012
NBP0805-DR27		21524 ± 110		deepwater coral	OS-78131	19450 ± 330	201 ± 52		-219 ± 53	Burke and Robinson, 2012

Table 3.S3 Epibenthic stable carbon and oxygen isotope of GeoB sediment cores.

Core	Lat. (ºN)	Long. (ºE)	Water Depth (m)	Core Depth (cm)	Species	Benthic $\delta^{13}C$	Benthic $\delta^{18}O$	Time Interval	Stratigraphy	References for age models
GeoB1503-1	2.31	-30.65	2306	23	*C. wuellerstorfi*	0.68	4.38	LGM	^{14}C	This study
				28	*C. wuellerstorfi*	0.71	4.21	not LGM		
GeoB1905-3	-17.14	-13.99	2974	23	*C. wuellerstorfi*	1.03	3.79	?	^{14}C	This study
				28	*C. wuellerstorfi*	0.82	4.13	?		
GeoB2204-2	-8.53	-34.02	2072	33	*C. wuellerstorfi*	0.97	4.32	LGM	^{14}C	This study
				38	*C. wuellerstorfi*	0.96	4.36	LGM		
GeoB3202-1	-21.62	-39.98	1090	93	*C. mundulus*	0.68	4.06	LGM	^{14}C	Arz et al., 1999; This study
				98	*C. mundulus*	0.74	4.04	LGM		
GeoB3722-2	-25.25	12.02	3506	60	*C. wuellerstorfi*	-0.09	4.60	HS1	^{14}C	This study
				73	*C. wuellerstorfi*	-0.05	4.40	LGM		
GeoB4223-2	29.02	-12.47	775	233	*C. pachyderma*	0.82	3.59	LGM	^{14}C	This study
				243	*C. pachyderma*	1.14	3.48	LGM		
GeoB4241-11	29.17	-15.45	3609	53	*C. wuellerstorfi*	0.31	4.56	LGM	^{14}C	This study
				58	*C. wuellerstorfi*	0.32	4.25	LGM		
GeoB4242-5	29.68	-17.89	4286	23	*C. wuellerstorfi*	0.01	4.41	LGM	^{14}C	This study
				98	*C. wuellerstorfi*	0.37	3.80	not LGM		
GeoB4905-4	2.50	9.39	1328	433	*C. wuellerstorfi*	0.69	4.16	LGM	^{14}C	Adegbie et al. 2003
				523	*C. wuellerstorfi*	0.70	4.10	LGM		
GeoB6201-5 [a]	-26.67	-46.44	475	145	*C. pachyderma*	-0.74	2.99	LGM	^{14}C	R. Portilho-Ramos, unpublished
				180	*C. pachyderma*	0.00	3.16	LGM		
GeoB6412-2	-44.25	-17.65	3475	68	*C. wuellerstorfi*	-0.55	4.75	not LGM	planktonic $\delta^{18}O$ stratigraphy and ^{14}C	This study
				78	*C. wuellerstorfi*	-0.14	3.96	not LGM		
GeoB6421-2	-36.45	-22.45	4220	28	*C. wuellerstorfi*	0.13	4.20	LGM	planktonic $\delta^{18}O$ stratigraphy and ^{14}C	This study
				38	*C. wuellerstorfi*	-0.09	4.59	LGM		
GeoB8483-2	-23.00	12.84	803	103	*Cibicidoides spp.*	0.25	3.05	LGM	^{14}C	This study
GeoB9506-1	15.61	-18.35	2956	172	*C. wuellerstorfi*	0.14	4.71	LGM	^{14}C	This study
				180	*C. wuellerstorfi*	0.07	4.67	LGM		
GeoB9510-1	15.42	-17.65	1566	200	*C. wuellerstorfi*	0.75	4.21	LGM	^{14}C	This study
				225	*C. wuellerstorfi*	0.68	4.21	LGM		
GeoB9512-5	15.34	-17.37	793	393	*C. pachyderma*	0.41	3.51	not LGM	^{14}C	This study
				423	*C. pachyderma*	0.34	3.67	LGM		
GeoB9513-3	15.32	-17.29	494	178	*C. pachyderma*	0.62	2.97	LGM	^{14}C	This study
				198	*C. pachyderma*	0.55	2.86	LGM		
GeoB9527-5	12.43	-18.22	3679	122	*C. wuellerstorfi*	0.01	4.77	LGM	carbonate stratigraphy and ^{14}C	Zarriess and Mackensen, 2010
				127	*C. wuellerstorfi*	-0.44	4.68	LGM		
GeoB9532-2 [b]	8.95	-14.89	317	110	*P.ariminensis*	0.74	2.74	LGM	benthic $\delta^{18}O$ stratigraphy and ^{14}C	Huang et al., 2012
				115	*P.ariminensis*	0.86	2.68	LGM		
				120	*P.ariminensis*	0.91	2.69	LGM		
				125	*P.ariminensis*	0.76	2.68	LGM		
				130	*P.ariminensis*	0.82	2.88	LGM		
				135	*P.ariminensis*	0.88	2.57	LGM		
				140	*P.ariminensis*	0.73	2.75	LGM		

Table 3.S3 *Continued*.

Core	Lat. (ºN)	Long. (ºE)	Water Depth (m)	Core Depth (cm)	Species	Benthic $\delta^{13}C$	Benthic $\delta^{18}O$	Time Interval	Stratigraphy	References for age models
GeoB9533-2 [b]	8.93	-14.91	384	145	*P.ariminensis*	0.65	3.01	LGM	benthic $\delta^{18}O$ stratigraphy and ^{14}C	Huang et al., 2012
				150	*P.ariminensis*	0.62	3.07	LGM		
				155	*P.ariminensis*	0.61	3.10	LGM		
				160	*P.ariminensis*	0.80	2.97	LGM		
				165	*P.ariminensis*	1.07	2.93	LGM		
				170	*P.ariminensis*	0.79	2.98	LGM		
GeoB9534-5 [b]	8.90	-14.94	492	105	*P.ariminensis*	0.67	3.28	LGM	benthic $\delta^{18}O$ stratigraphy and ^{14}C	Huang et al., 2012
				110	*P.ariminensis*	0.65	3.05	LGM		
				115	*P.ariminensis*	0.58	3.31	LGM		
				120	*P.ariminensis*	0.63	3.16	LGM		
				125	*P.ariminensis*	0.48	3.32	LGM		
				130	*P.ariminensis*	0.59	3.45	LGM		
				135	*P.ariminensis*	0.66	3.30	LGM		
GeoB9535-4 [b]	8.88	-14.96	669	84	*P.ariminensis*	0.50	3.04	LGM	benthic $\delta^{18}O$ stratigraphy and ^{14}C	Collins et al., 2011; Huang et al., 2012
				92	*P.ariminensis*	0.49	3.15	LGM		
				98	*P.ariminensis*	0.58	3.50	LGM		
				105	*P.ariminensis*	0.56	3.46	LGM		
				109	*P.ariminensis*	0.51	3.59	LGM		
				116	*P.ariminensis*	0.60	3.28	LGM		
				124	*P.ariminensis*	0.55	3.43	LGM		
				128	*P.ariminensis*	0.65	3.56	LGM		

a. Very negative benthic foraminiferal $\delta^{13}C$ values of core GeoB6201-5 are possibly contaminated by old carbon from dissociated methane, as this core locates in cold-seep areas off Brazil.

b. Benthic $\delta^{18}O$ of core GeoB9532-2, 9533-2, 9534-5, 9535-4 were published previously by Huang et al. (2012).

3.9.2 References

Adegbie, A.T., Schneider, R.R., Röhl, U., Wefer, G., 2003. Glacial millennial-scale fluctuations in central African precipitation recorded in terrigenous sediment supply and freshwater signals offshore Cameroon. Palaeogeography, Palaeoclimatology, Palaeoecology 197, 323-333.

Arz, H.W., Pätzold, J., Wefer, G., 1999. The deglacial history of the western tropical Atlantic as inferred from high resolution stable isotope records off northeastern Brazil. Earth and Planetary Science Letters 167, 105-117.

Barker, S., Diz, P., Vautravers, M.J., Pike, J., Knorr, G., Hall, I.R., Broecker, W.S., 2009. Interhemispheric Atlantic seesaw response during the last deglaciation. Nature 457, 1097-1102.

Barker, S., Knorr, G., Vautravers, M.J., Diz, P., Skinner, L.C., 2010. Extreme deepening of the Atlantic overturning circulation during deglaciation, Nature Geosciences 3, 567-571.

Burke, A., Robinson, L.F., 2012. The Southern Ocean's role in carbon exchange during the last deglaciation. Science 335, 557-561.

Cléroux, C., deMenocal, P., Guilderson, T., 2011. Deglacial radiocarbon history of tropical Atlantic thermocline waters: absence of CO_2 reservoir purging signal. Quaternary Science Reviews 30, 1875-1882.

Collins, J.A., Schefuß, E., Heslop, D., Mulitza, S., Prange, M., Zabel, M., Tjallingii, R., Dokken, T.M., Huang, E., Mackensen, A., Schulz, M., Tian, J., Zarriess, M., Wefer, G., 2011. Interhemispheric symmetry of the tropical African rainbelt over the past 23,000 years. Nature Geoscience 4, 42-45.

Huang, E., Mulitza, S., Paul, A., Groeneveld, J., Steinke, S., Schulz, M., 2012. Response of eastern tropical Atlantic central waters to Atlantic meridional overturning circulation changes during the Last Glacial Maximum and Heinrich Stadial 1. Paleoceanography 27, PA3229, doi:10.1029/2012PA002294.

Keigwin, L.D., 2004. Radiocarbon and stable isotope constraints on last glacial maximum and younger Dryas ventilation in the western north Atlantic. Paleoceanography 19, PA4012, doi:10.1029/2004PA001029.

Keigwin, L.D., Jones, G.A., 1995. The marine record of deglaciation from the continental margin off Nova Scotia. Paleoceanography 10(6), 973-985.

Keigwin, L.D., Schlegel, M.A., 2002. Ocean ventilation and sedimentation since the glacial maximum at 3 km in the western North Atlantic, Geochemistry Geophysics Geosystems 3(6), 10.1029/2001GC000283.

Key, R.M., Kozyr, A., Sabine, C.L., Lee, K., Wanninkhof, R., Bullister, J.L., Feely, R.A., Millero, F.J., Mordy, C., Peng, T.-H., 2004. A global ocean carbon climatology: Results from Global Data Analysis Project (GLODAP). Global Biogeochemical Cycles 18, GB4031, doi:10.1029/2004GB002247.

Reimer, P.J., Baillie, M.G.L., Bard, E., Bayliss, A., Beck, J.W., Blackwell, P.G., Bronk Ramsey, C., Buck, C.E., Burr, G.S., Edwards, R.L., Friedrich, M., Grootes, P.M., Guilderson, T.P., Hajdas, I., Heaton, T.J., Hogg, A.G., Hughen, K.A., Kaiser, K.F., Kromer, B., McCormac, F.G., Manning, S.W., Reimer, R.W., Richards, D.A., Southon, J.R., Talamo, S., Turney, C.S.M., van der Plicht, J., Weyhenmeyer, C.E., 2009. IntCal09 and Marine09 radiocarbon age calibration curves, 0-50,000 years cal BP. Radiocarbon 51(4), 1111-1150.

Robinson, L.F., Adkins, J.F., Keigwin, L.D., Southon, J., Fernandez, D.P., Wang, S.-L., Scheirer, D.S., 2005. Radiocarbon variability in the western North Atlantic during the last deglaciation. Science 310, 1469-1473.

Skinner, L.C., Fallon, S., Waelbroeck, C., Michel, E., Barker, S., 2010. Ventilation of the deep southern ocean and deglacial CO_2 rise. Science 328, 1147-1151.

Skinner, L.C., Shackleton, N.J., 2004. Rapid transient changes in northeast Atlantic deep water ventilation age across Termination I. Paleoceanography 19, PA2005, doi:10.1029/2003PA000983.

Sortor, R.N., Lund, D.C., 2011. No evidence for a deglacial intermediate water $\Delta^{14}C$ anomaly in the SW Atlantic. Earth and Planetary Science Letters 310, 65-72.

Thornalley, D.J.R., Barker, S., Broecker, W., Elderfield, H., McCave, I.N., 2011. The deglacial evolution of north Atlantic deep convection. Science 331, 202-205.

Zarriess, M., Mackensen, A., 2010. The tropical rainbelt and productivity changes off northwest Africa: A 31,000-year high-resolution record. Marine Micropaleontology 76, 76-91.

Chapter 4

A ^{14}C-depleted abyssal Atlantic Ocean prior to the Last Glacial Maximum and its potential influence on the atmospheric $\Delta^{14}C$

Enqing Huang[1], Luke C. Skinner[2], Stefan Mulitza[1], André Paul[1], Michael Schulz[1]

1. MARUM - Center for Marine Environmental Sciences and Faculty of Geosciences, University of Bremen, Bremen, Germany
2. Godwin Laboratory for Palaeoclimate Research, Department of Earth Sciences, University of Cambridge, Cambridge, UK

(Submitted to *Geophysical Research Letters*)

4.1 Abstract

The atmospheric radiocarbon activity ($\Delta^{14}C$) prior to the Last Glacial Maximum (LGM) was around 580‰ higher than during the preindustrial era. Current estimates of radiocarbon production changes due to geomagnetic field variability are unable to account for all of this increase in the atmospheric radiocarbon inventory, suggesting a significant change in the marine carbon cycle that would have also contributed to past atmospheric CO_2 changes. However, marine radiocarbon data that would confirm this expectation remain sparse. New paired planktonic and benthic foraminiferal ^{14}C ages, together with previously published data, confirm that the abyssal Atlantic Ocean was around 400‰ more depleted in $\Delta^{14}C$ with respect to the contemporary atmosphere between 36,000 and 25,000 yr BP. In the southwestern Atlantic, this ^{14}C-depleted water mass expanded upward to a depth of at least 2500 m during the LGM and the early deglaciation. Extreme ^{14}C-depleted signatures in the pre-LGM abyssal ocean were likely induced by a decrease in $\Delta^{14}C$ end-member values of southern-sourced waters due to the extensive sea ice coverage. Assumming that our reconstructions are representative of the ocean volume below 3000 m prior to the LGM, a simple ^{14}C mass-

balance calculation indicates that the glacial abyssal ocean might have been responsible for a 150‰ increase in the atmospheric $\Delta^{14}C$ level, thus accounting for much of the atmospheric $\Delta^{14}C$ change that cannot be accounted for by production changes.

4.2 Introduction

Reconstructions based on either marine sediment cores (e.g., Hughen et al., 2004, 2006; Shackleton et al., 2004) or fossil corals (e.g., Chiu et al., 2007) or stalagmites (Beck et al., 2001; Southon et al., 2012), all reveal that the atmospheric radiocarbon concentration has varied significantly over the past 50,000 years. Between 40,000 and 25,000 yr BP, the mean atmospheric $\Delta^{14}C$ was ~580‰; after this it decreased via a series of pulses and reversals toward the preindustrial value of 0‰ (Reimer et al., 2009) (Figure 4.1). Variations of atmospheric $\Delta^{14}C$ are controlled by changes in the ^{14}C production rate (induced by changes in cosmic ray flux, solar activity and geomagnetism) and the ^{14}C partitioning among different carbon reservoirs (e.g., Beck et al., 2001; Hughen et al., 2004). However, deciphering the relative contributions of these two controls on past atmospheric $\Delta^{14}C$ variations is difficult, not only because uncertainties in past atmospheric $\Delta^{14}C$ and past ^{14}C production rates increase further back in time, but also because precise knowledge of past carbon-cycle dynamics is lacking.

As might be expected, reconstructed atmospheric $\Delta^{14}C$ and geomagnetic field intensity share many features over the past 50,000 years, demonstrating a role for changing geomagnetic field intensity as an important driver of atmospheric $\Delta^{14}C$ fluctuations (e.g., Beck et al., 2001; Hughen et al., 2004). Thus, lowered geomagnetic field intensity during the later part of the last glaciation and the last deglaciation (Laj et al., 2004) allowed more cosmic rays to reach the Earth's atmosphere and produce more ^{14}C atoms. However, it would appear that the magnitude and pattern of reconstructed radiocarbon production changes, across the last deglaciation in particular (Broecker and Barker, 2007), are not able to account entirely for reconstructed atmospheric $\Delta^{14}C$ fluctuations, suggesting an additional influence from past carbon cycle changes.

This inference is supported by box-model studies that assume a constant preindustrial carbon cycle combined with reconstructed ^{14}C production rate changes (Figure 4.1, Hughen et al., 2004). Especially between 40,000 and 25,000 yr BP, the mean offset between the reconstructed and the modeled atmospheric $\Delta^{14}C$ in such a box model reaches up to 290‰ (Figure 4.1), indicating an important contribution from a changed carbon cycle. A similar inference has been drawn from general circulation model simulations (e.g., Franke et al.,

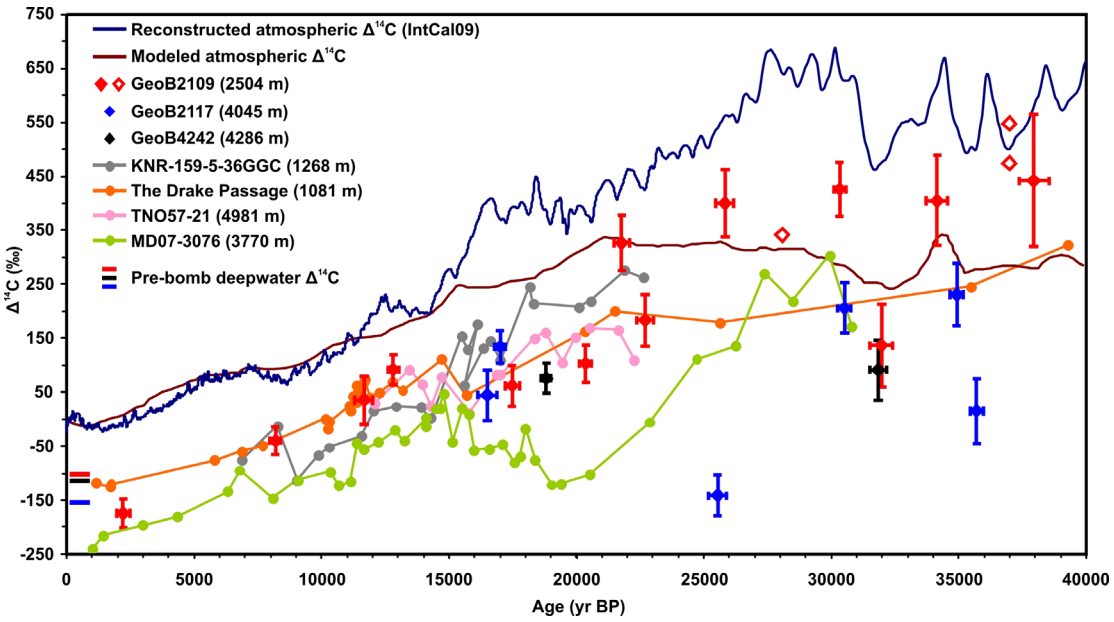

Figure 4.1 A comparison of the reconstructed atmospheric (Reimer et al., 2009) and deepwater $\Delta^{14}C$ records over the past 40,000 years. The modeled atmospheric $\Delta^{14}C$ is from Hughen et al., (2004). New data are shown as diamonds. Open diamonds are results of core GeoB2109-1 using interpolated calendar ages for calculation (Auxiliary Material). Error bars associated with each diamond represent $\pm 1\sigma$ standard errors. Pre-bomb deepwater $\Delta^{14}C$ values of core GeoB2109-1, GeoB2117-1 and GeoB4242-5 (Key et al., 2004) are denoted by solid lines on the lower left of the plot. Deepwater $\Delta^{14}C$ records from core KNR159-5-36GGC (Sorter and Lund, 2011), MD07-3076 (Skinner et al., 2010), TNO57-21 (Barker et al., 2010) and the Drake Passage (Burke and Robinson, 2012) are also shown. For simplification, error bars of these published $\Delta^{14}C$ results are not shown. Deep-sea corals of the Drake Passage are from several dredging sites, and here a mean water depth of these sites is given.

2008), while more complex box-model experiments suggest that carbon cycle changes could account for 60-100‰ of the atmospheric $\Delta^{14}C$ 'excess' between 40,000 and 25,000 yr BP (Köhler et al., 2006). Not surprisingly, the estimate of the carbon-cycle contribution to past atmospheric $\Delta^{14}C$ change is model-dependent, and depends crucially on assumed ^{14}C production rates (Muscheler et al., 2004). Currently, ^{10}Be-derived past ^{14}C production rates are generally higher than derived from the geomagnetic field intensity (Köhler et al., 2006). If the ^{10}Be-derived ^{14}C production rate is adopted, a smaller carbon-cycle contribution is implied.

One way to help resolve these ambiguities is to seek evidence for past changes in the ^{14}C inventory of other large carbon reservoirs that exchange carbon with the atmosphere. The

inorganic carbon reservoir in the deep ocean is a key target in this regard, as it currently contains more than 63 times more carbon than the preindustrial atmosphere (Sigman and Boyle, 2000). Due to its relatively rapid exchange of carbon with the atmosphere, the ocean is therefore the most important modulator of the atmospheric carbon reservoir on orbital and suborbital time scales. The ^{14}C transfer from the atmosphere to ocean interior is mainly accomplished through the 'ventilation' of the ocean interior (e.g. Khatiwala et al., 2009), via the formation of deep and intermediate waters. If the ventilation rate was reduced and/or the preformed deep waters obtained lower $\Delta^{14}C$ values during the last glacial period, there would be less ^{14}C storage in the ocean interior and an accumulation of ^{14}C in the atmosphere. Therefore, if marine carbon cycling contributed to elevated atmospheric $\Delta^{14}C$ during the last glacial period, a carbon reservoir significantly depleted in ^{14}C with respect to the contemporary atmosphere would have existed in the deep ocean between 40,000 and 25,000 yr BP.

Past deepwater $\Delta^{14}C$ values can be reconstructed by ^{14}C dating on benthic foraminifera and deep-sea corals. So far most reconstructions and discussion have concentrated on the deepwater $\Delta^{14}C$ variability during the Last Glacial Maximum (LGM) and the last deglaciation. Especially, the possible ^{14}C-depleted CO_2 transfer from the deep ocean to the atmosphere and its influence on the atmospheric $\Delta^{14}C$ during Heinrich Stadial 1 have been extensively discussed (e.g., Broecker and Barker, 2007; Marchitto et al., 2007; Skinner et al., 2010; Burke and Robinson, 2012). However, only a few records have been extended prior to the LGM when the contribution of a changed glacial carbon cycle to atmospheric $\Delta^{14}C$ seems relatively larger (Hughen et al., 2004) (Figure 4.1). In this study our new paired planktonic-benthic foraminiferal ^{14}C data together with previously published results (Skinner et al., 2010) confirms the presence of a ^{14}C-depleted abyssal Atlantic ocean prior to the LGM. We further use a simple mass-balance calculation to estimate the influence of this ^{14}C-depleted carbon reservoir on the pre-LGM atmospheric $\Delta^{14}C$ level.

4.3 Material and Methods

Paired samples of monospecific planktonic foraminifera and mixed benthic foraminifera from core GeoB2109-1 (2504 m, off southern Brazil), GeoB2117-1 (4045 m, off southern Brazil) and GeoB4242-5 (4286 m, off NW Africa) (Figure 4.2, Table 4.S1) were picked for ^{14}C analyses (Auxiliary Material, Table 4.S2 and 4.S3). Epibenthic species *Cibicidoides wuellerstorfi* from these three cores were selected for stable isotope measurement (Auxiliary Material, Table 4.S4). Modern bottom waters over core GeoB2109-1 and GeoB2117-1 are dominantly influenced by North Atlantic Deep Water and Antarctic Bottom Water,

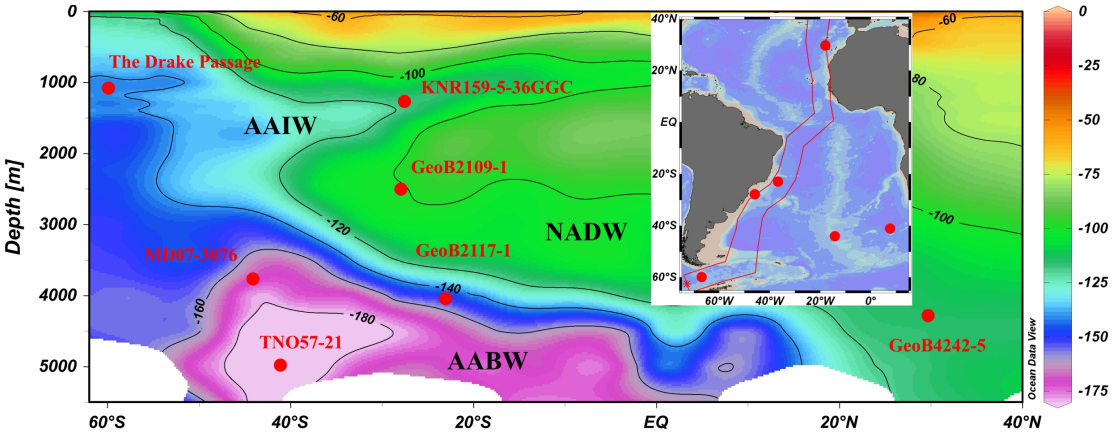

Figure 4.2 Meridional section of seawater $\Delta^{14}C$ (after correction of the bomb effect) of the Atlantic Ocean. The position of the section is indicated in the panel on the right. Data is from the gridded GLODAP dataset (Key et al., 2004) and the figure was made by Ocean Data View 4 (R. Schlitzer, available at http://odv.awi.de). Dots denote core locations: KNR159-5-36GGC -27.5ºN, -46.5ºE; MD07-3076, -44.1ºN, -14.2ºE; TNO57-21, -41.1ºN, 7.8ºE. Deep-sea corals of the Drake Passage are from several dredging sites, and here a mean location of these sites (-59.9ºN, -66.9ºE) is shown.

respectively. Bottom waters at core GeoB4242-5 are mainly influenced by North Atlantic Deep Water and to a lesser extent by Antarctic Bottom Water (Figure 4.2 and 4.S1, Auxiliary Material). Previous bottom-water $\Delta^{14}C$ reconstructions at core KNR159-5-36GGC (Sorter and Lund, 2011), TNO57-21 (Barker et al., 2010), several dredging sites in the Drake Passage (Burke and Robinson, 2012) and core MD07-3076 (Skinner et al., 2010) (Figure 4.1 and 4.2) are also presented for comparison. Modern bottom waters at these locations are ventilated by Antarctic Intermediate Water (36GGC), Antarctic Bottom Water (TNO57-21), Upper (dredging sites in the Drake Passage) and Lower (MD07-3076) Circumpolar Deep Water, respectively.

Our core locations are not currently influenced by coastal upwelling. Pre-bomb surface reservoir ages over these core locations are estimated to be close to 400 years ($\Delta R = 0$, ΔR is the deviation from the global mean of 400 years) (Table 4.S1, Key et al., 2004). Although simulations show that surface reservoir ages in the tropical-subtropical oceans vary temporally in response to changing atmospheric $\Delta^{14}C$, ocean circulation, etc. (e.g., Franke et al., 2008), they are poorly constrained for past time intervals. In a model study, either using preindustrial or LGM boundary conditions, changing atmospheric $\Delta^{14}C$ can cause surface reservoir ages near our core locations to deviate from pre-bomb values by < 200 years during

most time of the past 40,000 years (Franke et al., 2008). In order to account for these reservoir-age variations in the past, we took an uncertainty of $\Delta R = 0 \pm 200$ years when converting conventional planktonic ^{14}C ages into calendar ages using the Marine09 calibration curve (Reimer et al., 2009). We then calculated deepwater $\Delta^{14}C$ as follows (Adkins and Boyle, 1997):

$$\Delta^{14}C = (e^{-\text{Benthic radiocarbon age / 8033 yr}} / e^{-\text{Calendar age / 8266 yr}} - 1)*1000\ ‰.$$

The uncertainty of the $\Delta^{14}C$ estimate is determined by propagated errors from the calendar age estimate and the benthic ^{14}C measurement. In order to compare deepwater $\Delta^{14}C$ values of different time periods, $\Delta^{14}C$ differences between the contemporary atmosphere and bottom waters ($\Delta\Delta^{14}C$) were also calculated. The uncertainty of the $\Delta\Delta^{14}C$ estimate is determined by propagated errors from the atmospheric $\Delta^{14}C$ estimate (Reimer et al., 2009) and the deepwater $\Delta^{14}C$ estimate.

4.4 Results

Several reversed or abnormal planktonic ^{14}C ages from core GeoB2109-1 and GeoB2117-1 are either rejected or replaced by interpolated ages (Auxiliary Material, Table 4.S2). Two pairs of negative B-P ages (^{14}C age differences between paired benthic and planktonic foraminifera) from core GeoB2117-1 are also excluded from the following discussion (Auxiliary Material, Figure 4.S2 and Table 4.S3). We notice that the mean sedimentation rate of core GeoB2117-1 is only 2 cm per thousand years, which raises the concern that ^{14}C results of this core may be subject to the influence of bioturbation. However, the estimated bottom-water $\Delta^{14}C$ values of core GeoB2117-1 are consistent with those of GeoB4242-5 and MD07-3076 during the pre-LGM time interval, and they are in agreement with those of GeoB4242-5 and TNO57-21 during the LGM and the last deglaciation (Figure 4.1). Although these cores are located in different areas of the Atlantic, they were probably all bathed in the same southern-sourced water mass during the last glacial (e.g., Sarnthein et al., 1994; Marchitto and Broecker, 2006). Therefore, the general agreement between bottom-water $\Delta^{14}C$ reconstructions at core GeoB2117-1 and at other locations increases our confidence that the potential bioturbation influence on ^{14}C results should be minor. Our new results thus add to the existing dataset to give a better constraint on $\Delta^{14}C$ values and on the spatial distribution of ^{14}C-depleted water masses in glacial deep oceans.

Reconstructions of glacial $\Delta\Delta^{14}C$ values and B-P ages of core GeoB4242-5 were nearly identical to those of core GeoB2117-1 (Figure 4.3b and 4.3c). Prior to the LGM, except for

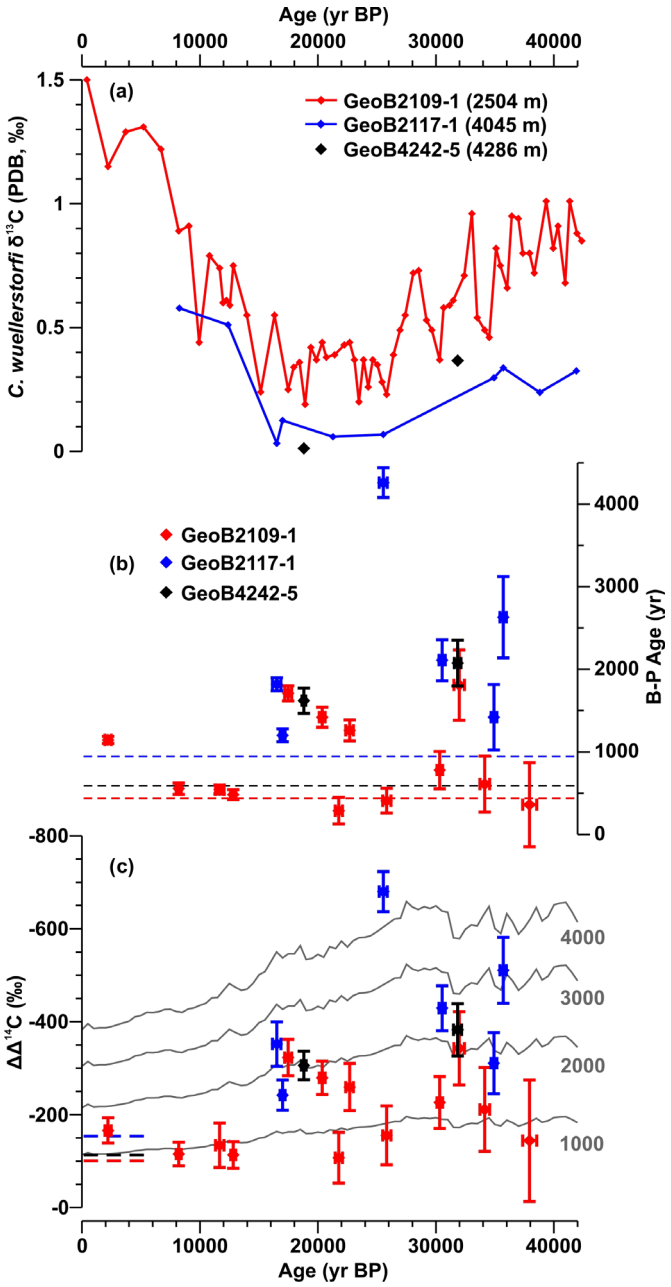

Figure 4.3 Reconstructions of *C. wuellerstorfi* $\delta^{13}C$ (a), B-P ages (b) and $\Delta\Delta^{14}C$ values (c) of core GeoB2109-1, GeoB2117-1 and GeoB4242-5 over the past 42,000 years. Age models of benthic $\delta^{13}C$ are derived from calendar ages of planktonic foraminifera. Error bars associated with each dot represent ±1σ standard errors. Dash lines in (b) and (c) represent pre-bomb values at each core location (Table S1, Key et al., 2004). Gray contours in (c) are lines of constant radiocarbon age offset (1000, 2000, 3000 and 4000 ^{14}C yr) from the atmosphere.

one outlier at 25,539 yr BP, the other four data points showed a mean $\Delta\Delta^{14}C$ value of -408‰ and a mean B-P age of 1848 years; while during the LGM and the early deglaciation, the

mean $\Delta\Delta^{14}C$ value and the mean B-P age derived from three samples was -300‰ and 1547 years, respectively. The outlier at 25,539 yr BP had an extremely low bottom-water $\Delta^{14}C$ value of -141‰. However, this low value was not reproduced by samples from core GeoB2117-1 or GeoB4242-5, nor by other published reconstructions (Figure 4.1, Skinner et al., 2010; Burke and Robinson, 2012), and should therefore be considered with caution. Within uncertainties all glacial and deglacial $\Delta\Delta^{14}C$ values of core GeoB2117-1 and GeoB4242-5 were significantly lower, while B-P ages were much higher than their pre-bomb values, respectively (Figure 4.3b and 4.3c). *C. wuellerstorfi* $\delta^{13}C$ values of both cores were around 0.31‰ prior to the LGM and decreased to 0.06‰ during the LGM and the early deglaciation (Figure 4.3a).

At core GeoB2109-1, except for one estimate at 31,972 yr BP, $\Delta\Delta^{14}C$ values were 30-120‰ lower than pre-bomb values between 38,000 and 25,000 yr BP; while B-P ages were close to or only slightly higher than pre-bomb values during the same time period (Figure 4.3b and 4.3c). Between 23,000 and 17,000 yr BP, three out of four data points showed that the mean $\Delta\Delta^{14}C$ value was 190‰ lower and the mean B-P age was 1020 years higher than pre-bomb values, respectively. The one exception at 21,765 yr BP is probably caused by the unreliable result of the benthic ^{14}C age (Figure 4.S2, Auxiliary Material). The late deglacial and the early Holocene $\Delta\Delta^{14}C$ values and B-P ages were approximately equal to pre-bomb values, respectively (Figure 4.3b and 4.3c). The mean *C. wuellerstorfi* $\delta^{13}C$ value of GeoB2109-1 was 0.80‰ between 42,000 and 33,200 yr BP, thereafter it showed a stepwise decrease to 0.40‰ at 26,400 yr BP. The mean $\delta^{13}C$ value was as low as 0.35‰ between 26,400 and 15,150 yr BP, and it continuously increased up to 1.5‰ over the deglaciation and the Holocene (Figure 4.3a).

4.5 Discussion

As illustrated in Figure 4.1, although uncertainties in bottom-water $\Delta^{14}C$ estimates are relatively large prior to the LGM, reconstructions from several core locations consistently show the presence of ^{14}C-depleted water masses in the abyssal Atlantic and at intermediate water depths of the high-latitude Southern Ocean. The mean bottom-water $\Delta^{14}C$ value of four core locations (GeoB2117-1, GeoB4242-5, MD07-3076 and the Drake Passage) was around 175±20‰ between 36,000 and 25,000 yr BP (the uncertainty represents the standard error of all available samples; two data points between 40,000-35,000 yr BP from the Drake Passage were not included in calculation due to their huge error bars, Burke and Robinson (2012)), which deviated from the contemporary atmosphere by as much as around 400‰. This equals to a ^{14}C age difference between the atmosphere and the abyssal ocean of 2380 years.

The reconstructions at core GeoB2109-1 indicate that the mean deepwater $\Delta^{14}C$ value at 2500 m was only 200‰ lower than that of the atmosphere between 38,000 and 25,000 yr BP (Figure 4.1). Therefore, there is a strong $\Delta^{14}C$ gradient between the abyssal and the deep water mass in the southwestern Atlantic prior to the LGM. This gradient seems to have decreased sharply during the LGM and the early deglaciation (Figure 4.3b and 4.3c). This phenomenon could also be found in benthic $\delta^{13}C$ results. Prior to the LGM, the benthic $\delta^{13}C$ offset between the abyssal and the deep water depth of the southwestern Atlantic was around 0.5‰, whereas it decreased to 0.3‰ during the LGM and the early deglaciation (Figure 4.3a). The weakened chemical gradient might indicate an upward expansion of the ^{13}C- and ^{14}C-depleted bottom water mass in the southwestern Atlantic. Taken together, abyssal water masses rather than deep or upper water masses were more isolated from the atmosphere prior to the LGM than during the present. Our reconstructions at core GeoB2109-1 provide a constraint on the upper boundary of the ^{14}C-depleted water mass prior to the LGM, which should have been below 2500 m.

Extreme ^{14}C-depleted signatures found in the pre-LGM Atlantic Ocean could be resulted from a poor ventilation of deep oceans and/or a decrease in ^{14}C values of preformed bottom waters. Previous studies suggest that the deepwater circulation might still be vigorous under glacial climate conditions (Wunsch, 2003; Curry and Oppo, 2005; Huang et al., in preparation). Therefore, it is more likely that the newly preformed bottom waters from the southern end member might have been assigned with very low initial ^{14}C values prior to the LGM. This inference is in agreement with the maximum extent of summer sea ice in the Southern Ocean between 30 and 22 ka (Allen et al., 2011). Sea ice coverage could have reduced the air-sea exchange, limiting the ^{14}C transfer from the atmosphere to the deep ocean.

If our reconstructions accurately document the chemistry/radiocarbon concentration of the ocean below 3000 m prior to the LGM, the sizable abyssal ocean carbon reservoir (around 30% of the whole ocean volume) should have contributed considerably to the elevated atmospheric $\Delta^{14}C$ level when it became less effective in sequestrating ^{14}C. Here we performed a simple ^{14}C mass-balance calculation to estimate this contribution. Previously, similar estimates have been carried out for the deglacial time. The ^{14}C budget among the deep ocean, the upper ocean and the atmosphere prior to and after Heinrich Stadial 1 was calculated based on changes in ^{14}C ages of different reservoirs (Broecker and Barker, 2007; Skinner et al., 2010; Burke and Robinson, 2012). Because the pre-LGM ^{14}C age offset between the upper ocean and the atmosphere is similar to the pre-bomb value (as shown by reconstructions at core GeoB2109-1, Figure 4.3b), in this study we only consider the ^{14}C budget between the atmosphere and the abyssal ocean reservoirs.

The pre-LGM atmosphere is estimated to have a carbon inventory of 426 PgC (10^{15} g of carbon) based on a mean CO_2 concentration of 200 ppm (parts per million) during that time (Petit et al., 1999; Ahn and Brook, 2008). Model simulations indicate 3-5% increase in the dissolve inorganic carbon concentration of glacial deep waters with respect to the late Holocene (e.g., Toggweiler et al., 2006). We thus assume that the pre-LGM abyssal ocean carbon reservoir had a size of 12060 PgC, according to that modern seawater below 3000 m has a mean dissolved inorganic carbon concentration of 2277 μmol/kg (Key et al., 2004). If the total radiocarbon inventory prior to the LGM was constant, and the amount of the ^{14}C transfer between the atmosphere and the abyssal ocean was given, changes in the ^{14}C activity of these two reservoirs can be calculated. We further assume that the pre-LGM abyssal ocean was as effective as its modern counterpart in sequestrating ^{14}C, and the pre-LGM ^{14}C age difference between the abyssal ocean and the atmosphere decreased from 2380 years to its preindustrial level of 1545 years (Key et al., 2004). This would raise the abyssal ocean $\Delta^{14}C$ value by only 5.3‰ but reduces the atmospheric $\Delta^{14}C$ value by around 150‰ (Auxiliary Material). Despite the obvious simplicity of the calculation, the result still clearly underlines the important contribution of a ^{14}C-depleted abyssal ocean carbon reservoir to the extra ^{14}C accumulation in the atmosphere prior to the LGM. Our reconstructions can be employed to calibrate the glacial carbon cycle in more complex climate models, which in turn would give more accurate estimates on the contribution of a changed carbon-cycle to the atmospheric $\Delta^{14}C$ level.

4.6 Conclusions

A compilation of new data and published results reveals that ^{14}C-depleted water masses, with a mean $\Delta^{14}C$ value 400‰ lower than that of the contemporary atmosphere, existed in the abyssal Atlantic Ocean and at intermediate water depths of the high-latitude Southern Ocean between 36,000-25,000 yr BP. The ^{14}C-depleted abyssal water mass expanded upward to 2500 m or probably even shallower depths in the southwestern Atlantic during the LGM and the early deglaciation. A simple mass-balance calculation suggests that if the pre-LGM ^{14}C age difference between the abyssal ocean and the atmosphere was reduced to its pre-industrial level, the abyssal ocean would be more effective in sequestrating ^{14}C atoms from the atmosphere and draw down the atmospheric $\Delta^{14}C$ level by as much as 150‰.

4.7 Acknowledgements

We are grateful to Stewart Fallon for radiocarbon measurements and Monika Segl and her team for stable isotope analyses. We thank Anke Dürkoop for allowing us to use her

unpublished stable isotope results of core GeoB2109-1. Thanks also go to the MARUM GeoB core repository for providing sediment material. This work was funded through the DFG Research Center/Excellence Cluster "The Ocean in the Earth System" and by the Helmholtz Climate Initiative "REKLIM." EH is supported by the China Scholarship Council (CSC No. 2009626073).

4.8 References

Adkins, J.F., Boyle, E.A., 1997. Changing atmospheric $\Delta^{14}C$ and the record of deep water paleoventilation ages. Paleoceanography 12(3), 337-344.

Ahn, J., Brook, E.J., 2008. Atmospheric CO_2 and climate on millennial time scales during the last glacial period. Science 322, 83-85.

Allen, C.S., Pike, J., Pudsey, C.J., 2011. Last glacial-interglacial sea-ice cover in the SW Atlantic and its potential role in global deglaciation. Quaternary Science Reviews 30, 2446-2458.

Barker, S., Knorr, G., Vautravers, M.J., Diz, P., Skinner, L.C., 2010. Extreme deepening of the Atlantic overturning circulation during deglaciation. Nature Geosciences 3, 567-571.

Beck, J.W., Richards, D.A., Edwards, R.L., Silverman, B.W., Smart, P.L., Donahue, D.J., Hererra-Osterheld, S., Burr, G.S., Calsoyas, L., Jull, A.J.T., Biddulph, D., 2001. Extremely large variations of atmospheric ^{14}C concentration during the last glacial period. Science 292, 2453-2458.

Broecker, W.S., Barker, S., 2007. A 190‰ drop in atmosphere's $\Delta^{14}C$ during the "Mystery Interval" (17.5-14.5 kyr). Earth and Planetary Science Letters 256, 90-99.

Burke, A., Robinson, L.F., 2012. The Southern Ocean's role in carbon exchange during the last deglaciation. Science 335, 557-561.

Chiu, T.-C., Fairbanks, R.G., Cao, L., Mortlock, R.A., 2007. Analysis of the atmospheric ^{14}C record spanning the past 50,000 years derived from high-precision $^{230}Th/^{234}U/^{238}U$, $^{231}Pa/^{235}U$ and ^{14}C dates on fossil corals. Quaternary Science Reviews 26, 18-36.

Curry, W.B., Oppo, D.W., 2005. Glacial water mass geometry and the distribution of $\delta^{13}C$ of ΣCO_2 in the western Atlantic Ocean. Paleoceanography 20, PA1017, doi:10.1029/2004PA001021.

Franke, J., Paul, A., Schulz, M., 2008. Modeling variations of marine reservoir ages during the last 45000 years. Climate of the Past 4, 125-136.

Huang, E., Skinner, L.C., Mulitza, S., Paul, A., Schulz, M. Radiocarbon distribution and radiocarbon-based circulation age of the Atlantic Ocean during the Last Glacial Maximum. In preparation.

Hughen, K., Lehman, S., Southon, J., Overpeck, J., Marchal, O., Herring, C., Turnbull, J., 2004. ^{14}C activity and global carbon cycle changes over the past 50,000 years. Science 303, 202-207.

Hughen, K., Southon, J., Lehman, S., Bertrand, C., Turnbull, J., 2006. Marine-derived ^{14}C calibration and activity record for the past 50,000 years updated from the Cariaco Basin. Quaternary Science Reviews 25, 3216-3227.

Key, R.M., Kozyr, A., Sabine, C.L., Lee, K., Wanninkhof, R., Bullister, J.L., Feely, R.A., Millero, F.J., Mordy, C., Peng, T.-H., 2004. A global ocean carbon climatology: Results from Global Data Analysis Project (GLODAP). Global Biogeochemical Cycles 18, GB4031, doi:10.1029/2004GB002247.

Khatiwala, S., Primeau, F., Hall, T., 2009. Reconstruction of the history of anthropogenic CO_2 concentrations in the ocean. Nature 462, 346-349.

Köhler, P., Muscheler, R., Fischer, H., 2006. A model-based interpretation of low-frequency changes in the carbon cycle during the last 120,000 years and its implications for the reconstruction of atmospheric $\Delta^{14}C$. Geochemistry, Geophysics, Geosystems 7, Q11N06, doi:10.1029/2005GC001228.

Laj, C., Kissel, C., Beer, J., 2004. High resolution global paleointenity stack since 75Ka (GLOPIS-75) calibrated to absolute values. In: Channell, J.E.T., Kent, D.V., Lowrie, W., Meert, J.G. (Eds.), Timescales of the Paleomagnetic Field. Geophysical Monograph Series, 145, AGU, Washington, D.C., pp. 255-265.

Marchitto, T.M., Broecker, W.S., 2006. Deep water mass geometry in the glacial Atlantic Ocean: A review of constraints from the paleonutrient proxy Cd/Ca. Geochemistry Geophysics Geosystems 7, Q12003, doi:10.1029/2006GC001323.

Marchitto, T.M., Lehman, S.J., Ortiz, J.D., Fluckiger, J., van Geen, A., 2007. Marine radiocarbon evidence for the mechanism of deglacial atmospheric CO_2 rise. Science 316, 1456-1440.

Muscheler, R., Beer, J., Wagner, G., Laj, C., Kissel, C., Raisbeck, G.M., Yiou, F., Kubik, P.W., 2004. Changes in the carbon cycle during the last deglaciation as indicated by the comparison of ^{10}Be and ^{14}C records. Earth and Planetary Science Letters 219, 325-340.

Petit, J.R., Jouzel, J., Raynaud, D., Barkov, N.I., Barnola, J.-M., Basile, I., Bender, M., Chappellaz, J., Davisk, M., Delaygue, G., Delmotte, M., Kotlyakov, V.M., Legrand, M., Lipenkov, V.Y., Lorius, C., Pépin, L., Ritz, C., Saltzmank, E., Stievenard, M., 1999. Climate and atmospheric history of the past 420,000 years from the Vostok ice core, Antarctica. Nature 399, 429-436.

Reimer, P.J., Baillie, M.G.L., Bard, E., Bayliss, A., Beck, J.W., Blackwell, P.G., Bronk Ramsey, C., Buck, C.E., Burr, G.S., Edwards, R.L., Friedrich, M., Grootes, P.M., Guilderson, T.P., Hajdas, I., Heaton, T.J., Hogg, A.G., Hughen, K.A., Kaiser, K.F.,

Kromer, B., McCormac, F.G., Manning, S.W., Reimer, R.W., Richards, D.A., Southon, J.R., Talamo, S., Turney, C.S.M., van der Plicht, J., Weyhenmeyer, C.E., 2009. IntCal09 and Marine09 radiocarbon age calibration curves, 0-50,000 years cal BP. Radiocarbon 51(4), 1111-1150.

Sarnthein, M., Winn, K., Jung, S.J.A., Duplessy, J.-C., Labeyrie, L., Erlenkeuser, H., Ganssen, G., 1994. Changes in east Atlantic deep-water circulation over the last 30,000 years: Eight time slice reconstructions. Paleoceanography 9, 209-267, doi:10.1029/93PA03301.

Shackleton, N.J., Fairbanks, R.G., Chiu, T.-c., Parrenin, F., 2004. Absolute calibration of the Greenland time scale: implications for Antarctic time scales and for $\Delta^{14}C$. Quaternary Science Reviews 23, 1513-1522.

Sigman, D.M., Boyle, E.A., 2000. Glacial/interglacial variations in atmospheric carbon dioxide. Nature 407, 859-869.

Skinner, L.C., Fallon, S., Waelbroeck, C., Michel, E., Barker, S., 2010. Ventilation of the deep southern ocean and deglacial CO_2 rise. Science 328, 1147-1151.

Sortor, R.N., Lund, D.C., 2011. No evidence for a deglacial intermediate water $\Delta^{14}C$ anomaly in the SW Atlantic. Earth and Planetary Science Letters 310, 65-72.

Southon, J., Noronha, A.L., Cheng, H., Edwards, R.L., Wang, Y., 2012. A high-resolution record of atmospheric ^{14}C based on Hulu Cave speleothem H82. Quaternary Science Reviews 33, 32-41.

Toggweiler, J. R., Russell, J.L., Carson, S.R., 2006. Midlatitude westerlies, atmospheric CO2, and climate change during the ice ages. Paleoceanography, 21, PA2005, doi:10.1029/2005PA001154.

Wunsch, C., 2003. Determining paleoceanographic circulations, with emphasis on the Last Glacial Maximum. Quaternary Science Reviews 22, 371-385.

4.9 Auxiliary Material

4.9.1 Oceanographic Setting

As illustrated in Figure 4.S1, temperature-salinity characteristics of modern bottom waters at core locations of GeoB2109-1 and GeoB2117-1 are consistent with those of typical North Atlantic Deep Water (NADW) and Antarctic Bottom Water (AABW), respectively (Emery, 2003) (Figure 4.S1). Bottom waters at core GeoB4242-5 are a mixture of NADW and AABW.

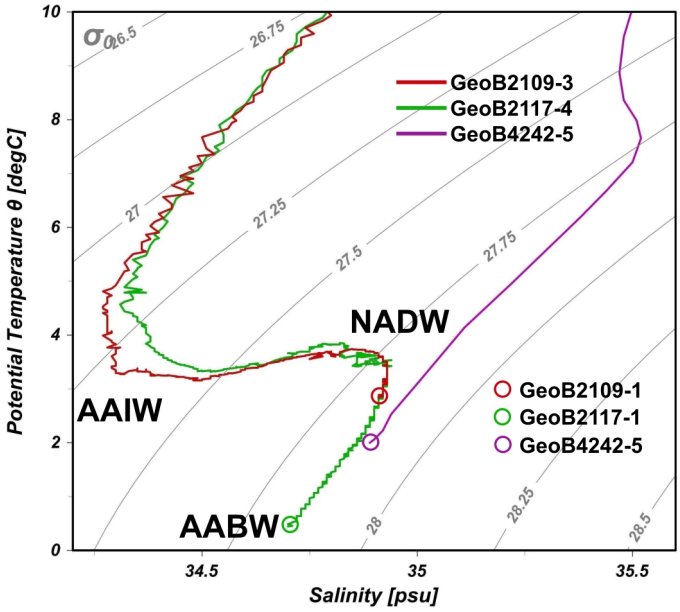

Figure 4.S1 Potential temperature-salinity diagram for water masses at locations of GeoB2109-3 (27.91ºS, 45.87ºW, 2513 m), GeoB2117-4 (23.04ºS, 36.65ºW, 4047 m) and GeoB4242-5 (29.68ºN, 17.89ºW, 4286 m). Temperature and salinity data at GeoB2109-3 and GeoB2117-4 are from in situ conductivity-temperature-depth (CTD) measurements (Bleil et al., 1993), and those at GeoB4242-5 are annual-mean data from World Ocean Atlas 2009 (Antonov et al., 2010; Locarnini et al., 2010). Temperature-salinity properties of bottom waters at core locations of GeoB2109-1, GeoB2117-1 and GeoB4242-5 are indicated by open dots. Contours of potential density (σ_0) are shown in gray curves.

4.9.2 Methods

4.9.2.1 Stable Isotope

The $\delta^{18}O$ and $\delta^{13}C$ composition of benthic foraminifera *Cibicidoides wuellerstorfi* (shell size >400 μm) was measured using a Finnigan MAT 252 mass spectrometer equipped with an

automatic carbonate preparation device at MARUM, University of Bremen (Table 4.S4). The working standard was calibrated against VPDB (Vienna Pee Dee Belemnite) by using the National Bureau of Standards (NBS) 18, 19 and 20 standards. Internal precision for $\delta^{18}O$ and $\delta^{13}C$ analysis, based on replicates of an internal limestone standard, was better than ±0.07% and ±0.05%, respectively. The oxygen isotope stratigraphy of core GeoB2109-1, GeoB2117-1 and GeoB4242-5 were shown in Figure 4.S2.

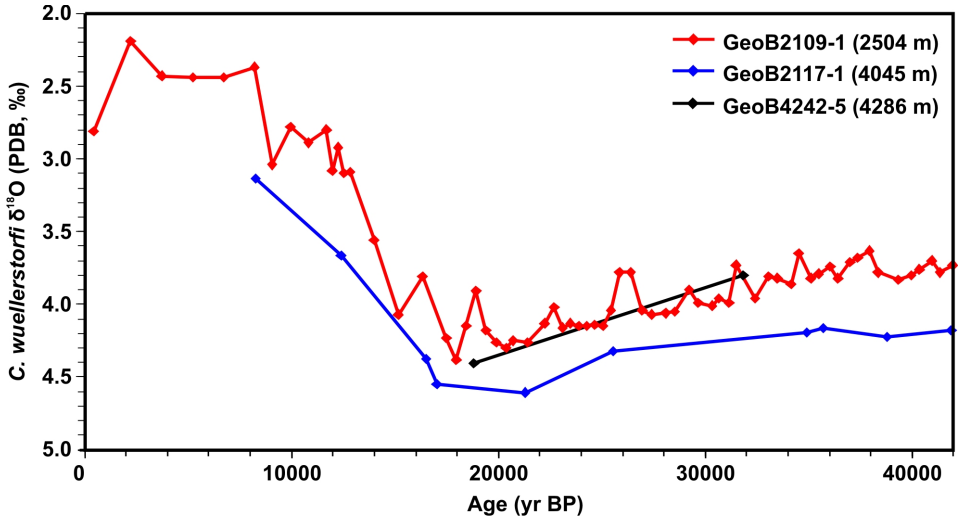

Figure 4.S2 The oxygen isotope stratigraphy of core GeoB2109-1, GeoB2117-1 and GeoB4242-5. Age models are based on the planktonic foraminiferal calendar ages.

4.9.2.2 Radiocarbon Dating

Mono-specific planktonic and mixed benthic foraminifera (deep-infaunal species were excluded) were picked from the > 125 μm fraction. Each sample typically weighed between 4 and 9 mg. After foraminiferal tests were gently crushed using two glass plates, fragments were rinsed with deionized water and methanol for a few times. Between each rinse, samples were ultrasonicated for one minute. Small-mass samples were rinsed only with water in order to avoid excess dissolution. The cleaning step favors to remove adhering substances such as small foraminifera, coccoliths or clays inside big foraminiferal shells.

The graphitization of ^{14}C samples were conducted at the department of Earth Sciences, University of Cambridge. Foraminiferal samples were hydrolyzed in phosphoric acid. The created CO_2 was purified using liquid nitrogen and was further reduced to graphite in catalytic (iron powder) reaction with hydrogen in a quartz tube at 600ºC. The graphitized samples were analyzed at Research School of Earth Sciences, Australian National University using a Single

Stage Accelerator Mass Spectrometer (Fallon et al., 2010) (Table 4.S2 and 4.S3). Sample preparation backgrounds were subtracted during measurement. On-line $\delta^{13}C$ values were used to correct ^{14}C ages.

Several planktonic ^{14}C samples of core GeoB2109-1 and GeoB4242-5 (Henderiks et al., 2002) were previously measured at the Leibniz-Laboratory for Radiometric Dating and Stable Isotope Research in Kiel (Table 4.S2). These data combined with newly measured benthic ^{14}C results were used to calculate deepwater $\Delta^{14}C$ values and benthic-plantonic ^{14}C age differences in this study.

4.9.2.3 Radiocarbon Data Quality Control

At core GeoB2109-1, the planktonic ^{14}C age at 83 cm is reversed (Figure 4.S3). The one at 103 cm seems abnormal, which does not follow the general linear relationship between the core depth and the ^{14}C age. Another one at 148 cm is older than its paired benthic foraminiferal ^{14}C age. Therefore, we used the interpolated calendar ages to calculate deepwater $\Delta^{14}C$ values at 103 and 148 cm (Table 4.S3). Benthic ^{14}C age at 68 cm is also reversed, but which could occur if there were changes in properties of preformed deep waters or in deepwater ventilation rates. Therefore, this doubtful result was kept in discussion. At core GeoB2117-1, planktonic ^{14}C age at 53 cm is reversed (Figure 4.S3). Negative B-P ages occur at 3 and 58 cm. These results were ignored in further discussion.

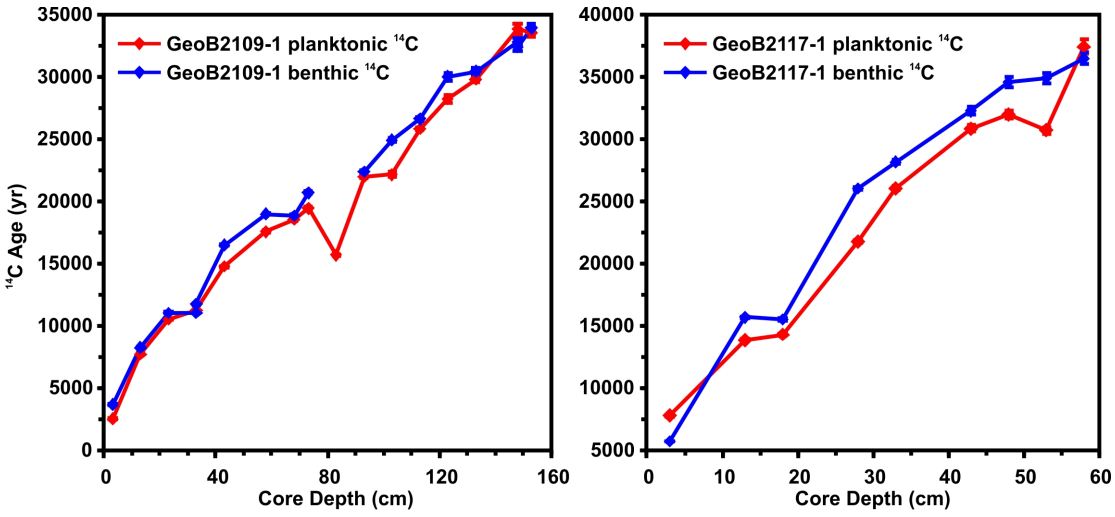

Figure 4.S3 Planktonic and benthic foraminiferal ^{14}C ages of core GeoB2109-1 and GeoB2117-1 plotted versus core depths.

4.9.2.4 The ^{14}C Mass-Balance Calculation

Given the radiocarbon activity ($\Delta^{14}C$, ‰) and the carbon inventory of a reservoir, the radiocarbon inventory of this reservoir can be calculated by:

^{14}C inventory = $(\Delta^{14}C/1000+1) * (^{14}C/^{12}C)_{standard}$ * carbon inventory,

where $(^{14}C/^{12}C)_{standard} = 1.176*10^{-12}$ (e.g., Keeling, 1981).

The ^{14}C difference between the atmosphere and the deep ocean can be calculated by (Stuiver and Polach, 1977):

^{14}C age difference = $8033 * (\ln(\Delta^{14}C_{ocean}/1000+1) - \ln(\Delta^{14}C_{atmosphere}/1000+1))$,

assuming that the preformed ^{14}C of deep waters are not replenished by other ^{14}C sources and decay at a constant rate after deep waters are isolated from the atmosphere.

Table 4.S1 Sediment cores used in this study.

Core	Latitude (°N)	Longitude (°E)	Water Depth (m)	Surface Reservoir Age (^{14}C yr) [a]	Bottom-water $\Delta^{14}C$ (‰) [a]	^{14}C age(bottom-surface) (yr) [a, b]
GeoB2109-1	-27.91	-45.88	2504	413	-101	440
GeoB2117-1	-23.04	-36.65	4045	397	-154	945
GeoB4242-5	29.68	-17.89	4286	376	-113	589

a. Surface and bottom water $\Delta^{14}C$ values and ^{14}C ages at each core location are from the gridded GLODAP dataset, which have been corrected for the bomb effect (Key et al., 2004).
b. ^{14}C age(bottom-surface) is the ^{14}C age difference between bottom and surface waters.

Table 4.S2 Planktonic foraminiferal radiocarbon results of core GeoB2109-1, GeoB2117-1 and GeoB4225-5.

Core	Sample Depth (cm)	Dating Species	Lad Code	^{14}C Age (yr)	^{14}C Age Error (±1σ, yr)	Calendar Age (yr BP)	Calendar Age Error (±1σ, yr)	Note
GeoB2109-1	3	*G. ruber*	S-ANU25832	2550	30	2220	267	
GeoB2109-1	13	*G. ruber*	KIA 3265	7740	60	8201	213	
GeoB2109-1	23	*G. ruber*	S-ANU25836	10525	35	11677	351	
GeoB2109-1	33	*G. ruber*	S-ANU25838	11265	40	12820	209	
GeoB2109-1	43	*G. ruber*	S-ANU28811	14790	60	17478	285	
GeoB2109-1	58	*G. ruber*	KIA 2618	17580	90	20362	246	Huang et al., in preparation
GeoB2109-1	68	*G. ruber*	KIA 2617	18590	140	21765	307	

Table 4.S2 *Continued*.

Core	Sample Depth (cm)	Dating Species	Lad Code	^{14}C Age (yr)	^{14}C Age Error (±1σ, yr)	Calendar Age (yr BP)	Calendar Age Error (±1σ, yr)	Note
GeoB2109-1	73	*G. ruber*	S-ANU28816	19440	90	22694	325	Huang et al., in preparation
GeoB2109-1	83	*G. ruber*	S-ANU28188	15690	60	18608	139	Reversed ^{14}C age
GeoB2109-1	93	*G. ruber*	S-ANU28820	21990	100	25833	354	
GeoB2109-1	103	*G. ruber*	KIA 2616	22150	220	26124	482	
GeoB2109-1	113	*G. ruber*	S-ANU28823	25840	150	30326	233	
GeoB2109-1	123	*G. ruber*	S-ANU30225	28230	270	31972	445	
GeoB2109-1	133	*G. ruber*	S-ANU28825	29840	230	34141	419	
GeoB2109-1	148	*G. ruber*	KIA 4112	33830	440	38121	641	
GeoB2109-1	153	*G. ruber*	S-ANU28830	33570	350	37939	594	
GeoB2117-1	3	*G. sacculifer*	S-ANU28832	7805	35	8260	213	
GeoB2117-1	13	*G. sacculifer*	S-ANU28835	13880	50	16515	362	
GeoB2117-1	18	*G. sacculifer*	S-ANU28837	14320	50	17011	214	
GeoB2117-1	28	*G. sacculifer*	S-ANU28709	21780	100	25539	336	
GeoB2117-1	33	*G. sacculifer*	S-ANU28711	26050	160	30525	257	
GeoB2117-1	43	*G. sacculifer*	S-ANU28713	30840	260	34914	246	
GeoB2117-1	48	*G. sacculifer*	S-ANU28716	31940	300	35698	273	
GeoB2117-1	53	*G. sacculifer*	S-ANU28718	30710	250	34856	208	Reversed ^{14}C age
GeoB2117-1	58	*G. sacculifer*	S-ANU28720	37450	550	41893	419	
GeoB4242-5	23	*G. ruber*		16070	140	18810	200	Henderiks et al., 2002
GeoB4242-5	98	*G. ruber*	S-ANU25917	28165	140	31838	340	Huang et al., in preparation

Table 4.S3 Benthic foraminiferal radiocarbon dates, estimates of deepwater $\Delta^{14}C$ and B-P ages of core GeoB2109-1, GeoB2117-1 and GeoB4225-5. Uncertainties associated with deepwater $\Delta^{14}C$ values and B-P ages are ±1σ standard errors.

Core	Sample Depth (cm)	Lab Code	Benthic ^{14}C Age (yr)	Benthic ^{14}C Age error (±1σ, yr)	Deepwater $\Delta^{14}C$ (‰)	Deepwater $\Delta^{14}C$ Error (±1σ, ‰)	B-P Age (yr)	B-P Error (±1σ, yr)	Note
GeoB2109-1	3	S-ANU25833	3695	30	-174	27	1145	42	
GeoB2109-1	13	S-ANU25835	8295	35	-40	25	555	69	
GeoB2109-1	23	S-ANU25837	11070	40	35	44	545	53	
GeoB2109-1	33	S-ANU28809	11045	40	192	31	-220	57	Negative B-P age
GeoB2109-1	33	S-ANU28810	11750	45	92	28	485	60	
GeoB2109-1	43	S-ANU28812	16500	70	62	38	1710	92	
GeoB2109-1	58	S-ANU28813	19000	80	103	35	1420	120	Huang et al., in preparation
GeoB2109-1	68	S-ANU28814	18880	80	327	51	290	161	Benthic ^{14}C age reversal
GeoB2109-1	73	S-ANU28817	20700	90	184	48	1260	127	Huang et al., in preparation
GeoB2109-1	93	S-ANU28821	22400	110	400	63	410	149	
GeoB2109-1	103	S-ANU28819	24930	140	341				a
GeoB2109-1	113	S-ANU28824	26620	170	426	50	780	227	
GeoB2109-1	123	S-ANU30226	30040	330	137	77	1810	426	
GeoB2109-1	133	S-ANU28826	30450	250	404	83	610	340	
GeoB2109-1	148	S-ANU28827	32830	320	474				a
GeoB2109-1	148	S-ANU28829	32440	310	547				a
GeoB2109-1	153	S-ANU28831	33930	370	442	123	360	509	
GeoB2117-1	3	S-ANU28833	5750	30	328	34	-2055	46	Negative B-P age
GeoB2117-1	13	S-ANU28836	15700	60	44	46	1820	78	
GeoB2117-1	18	S-ANU28838	15520	60	134	30	1200	78	
GeoB2117-1	28	S-ANU28710	26040	150	-141	38	4260	180	
GeoB2117-1	33	S-ANU28712	28160	190	206	47	2110	248	

Table 4.S3 *Continued*.

Core	Sample Depth (cm)	Lab Code	Benthic ^{14}C Age (yr)	Benthic ^{14}C Age error (±1σ, yr)	Deepwater $\Delta^{14}C$ (‰)	Deepwater $\Delta^{14}C$ Error (±1σ, ‰)	B-P Age (yr)	B-P Error (±1σ, yr)	Note
GeoB2117-1	43	S-ANU28714	32260	300	231	59	1420	397	
GeoB2117-1	48	S-ANU28717	34570	390	15	60	2630	492	
GeoB2117-1	53	S-ANU28719	34920	410	-122	50	4210	480	Planktonic ^{14}C age reversal
GeoB2117-1	58	S-ANU28721	36490	490	691	134	-960	737	Negative B-P age
GeoB4242-5	23	S-ANU25913	17690	65	76	27	1620	154	Huang et al., in preparation
GeoB4242-5	98	S-ANU25916	30240	240	91	55	2075	278	Huang et al., in preparation

a. Deepwater $\Delta^{14}C$ were calculated using interpolated calendar ages.

Table 4.S4 *Cibicidoides wuellerstorfi* $\delta^{13}C$ and $\delta^{18}O$ of core GeoB2109-1, GeoB2117-1 and GeoB4225-5.

Core	Sample Depth (cm)	*C. wuellerstorfi* $\delta^{13}C$ (‰, PDB)	*C. wuellerstorfi* $\delta^{18}O$ (‰, PDB)	Core	Sample Depth (cm)	*C. wuellerstorfi* $\delta^{13}C$ (‰, PDB)	*C. wuellerstorfi* $\delta^{18}O$ (‰, PDB)
GeoB2109-1	0.0	1.50	2.81	GeoB2109-1	43.0	0.25	4.23
GeoB2109-1	3.0	1.15	2.19	GeoB2109-1	45.5	0.34	4.38
GeoB2109-1	5.5	1.29	2.43	GeoB2109-1	48.0	0.36	4.15
GeoB2109-1	8.0	1.31	2.44	GeoB2109-1	50.5	0.19	3.91
GeoB2109-1	10.5	1.22	2.44	GeoB2109-1	53.0	0.42	4.18
GeoB2109-1	13.0	0.89	2.37	GeoB2109-1	55.5	0.37	4.26
GeoB2109-1	15.5	0.91	3.04	GeoB2109-1	58.0	0.44	4.30
GeoB2109-1	18.0	0.44	2.78	GeoB2109-1	60.5	0.38	4.25
GeoB2109-1	20.5	0.79	2.89	GeoB2109-1	65.5	0.39	4.26
GeoB2109-1	23.0	0.74	2.80	GeoB2109-1	70.5	0.43	4.13
GeoB2109-1	25.5	0.60	3.08	GeoB2109-1	73.0	0.44	4.02
GeoB2109-1	28.0	0.61	2.92	GeoB2109-1	75.5	0.37	4.16
GeoB2109-1	30.5	0.59	3.10	GeoB2109-1	78.0	0.20	4.13
GeoB2109-1	33.0	0.75	3.09	GeoB2109-1	80.5	0.37	4.15
GeoB2109-1	35.5	0.55	3.56	GeoB2109-1	83.0	0.26	4.15
GeoB2109-1	38.0	0.24	4.07	GeoB2109-1	85.5	0.37	4.14
GeoB2109-1	40.5	0.55	3.81	GeoB2109-1	88.0	0.35	4.15
GeoB2109-1	90.5	0.28	4.04	GeoB2109-1	150.0	0.80	3.68
GeoB2109-1	93.0	0.23	3.78	GeoB2109-1	153.0	0.80	3.63
GeoB2109-1	95.5	0.39	3.78	GeoB2109-1	155.0	0.72	3.78
GeoB2109-1	98.0	0.49	4.04	GeoB2109-1	160.0	1.01	3.83
GeoB2109-1	100.0	0.55	4.07	GeoB2109-1	163.0	0.82	3.80
GeoB2109-1	103.0	0.72	4.06	GeoB2109-1	165.0	0.91	3.76
GeoB2109-1	105.0	0.73	4.05	GeoB2109-1	168.0	0.68	3.70
GeoB2109-1	108.0	0.53	3.90	GeoB2109-1	170.0	1.01	3.78
GeoB2109-1	110.0	0.49	3.99	GeoB2109-1	173.0	0.88	3.73
GeoB2109-1	113.0	0.37	4.01	GeoB2109-1	175.0	0.85	3.73
GeoB2109-1	115.0	0.58	3.96	GeoB2117-1	3.0	0.58	3.14
GeoB2109-1	118.0	0.59	3.99	GeoB2117-1	8.0	0.51	3.66
GeoB2109-1	120.0	0.61	3.73	GeoB2117-1	13.0	0.03	4.38
GeoB2109-1	125.0	0.71	3.96	GeoB2117-1	18.0	0.12	4.55
GeoB2109-1	128.0	0.96	3.81	GeoB2117-1	23.0	0.06	4.61
GeoB2109-1	130.0	0.54	3.82	GeoB2117-1	28.0	0.07	4.32
GeoB2109-1	133.0	0.49	3.86	GeoB2117-1	43.0	0.30	4.19
GeoB2109-1	135.0	0.46	3.65	GeoB2117-1	48.0	0.34	4.16
GeoB2109-1	138.0	0.82	3.82	GeoB2117-1	53.0	0.24	4.23
GeoB2109-1	140.0	0.75	3.79	GeoB2117-1	58.0	0.33	4.18
GeoB2109-1	143.0	0.66	3.74	GeoB4242-5	23.0	0.01	4.41
GeoB2109-1	145.0	0.95	3.82	GeoB4242-5	98.0	0.37	3.80
GeoB2109-1	148.0	0.94	3.71				

4.9.3 Reference

Antonov, J.I., Seidov, D., Boyer, T.P., Locarnini, R.A., Mishonov, A.V., Garcia, H.E., Baranova, O.K., Zweng, M.M., Johnson, D.R., 2010. World Ocean Atlas 2009, Volume 2: Salinity. In: Levitus, S. (Ed), NOAA Atlas NESDIS 69. U.S. Government Printing Office, Washington, D.C., 184 pp.

Bleil, U., Ayres Neto, A., Beese, D., Breitzke, M., Dehning, K., Diekamp, V., Dobeneck, T.v., Figueiredo, A., Pimentel Esteves, M., Giese, M., Glud, R., Grigel, J., Gundersen, J., Haese, R., Hinrichs, S,. Kasten, S., Meinecke, G., Mulitza, S., Petermann, H., Petschick, R., Rapp, R., Richter, M., Rühlemann, C., Scholz, M., Wallmann, K., Zabel., M., 1993. Report and preliminary results of Meteor-Cruise M23/2. Berichte No. 43, Fachbereich Geowissenschaften, Universität Bremen, Bremen.

Emery, W.J., 2003. Ocean circulation: water types and water masses. In: Holton, J.R., Curry, J.A., Pyle, J.A. (Eds.), Encyclopedia of Atmospheric Sciences. Academic Press, Oxford, pp. 1556-1567.

Fallon, S.J., Fifield, L.K., Chappell, J.M., 2010. The next chapter in radiocarbon dating at the Australian National University: Status report on the single stage AMS. Nuclear Instruments and Methods in Physics Research B 268, 898-901.

Henderiks, J., Freudenthal, T., Meggers, H., Nave, S., Abrantes, F., Bollmann, J., Thierstein, H.R., 2002. Glacial-interglacial variability of particle accumulation in the Canary Basin: a time-slice approach. Deep-Sea Research II 49, 3675-3705.

Huang, E., Skinner, L.C., Mulitza, S., Paul, A., Schulz, M. Radiocarbon distribution and radiocarbon-based circulation age of the Atlantic Ocean during the Last Glacial Maximum. In preparation.

Keeling, C.D., 1981. The modeling of rare isotopic carbon with regard to notations. In: Bolin, B. (Ed.), SCOPE(16), Carbon Cycle Modeling. John Wiley and Sons, Chichester, pp. 89-94.

Key, R.M., Kozyr, A., Sabine, C.L., Lee, K., Wanninkhof, R., Bullister, J.L., Feely, R.A., Millero, F.J., Mordy, C., Peng, T.-H., 2004. A global ocean carbon climatology: Results from Global Data Analysis Project (GLODAP). Global Biogeochemical Cycles 18, GB4031, doi:10.1029/2004GB002247.

Locarnini, R.A., Mishonov, A.V., Antonov, J.I., Boyer, T.P., Garcia, H.E., Baranova, O.K., Zweng, M.M., Johnson, D.R., 2010. World Ocean Atlas 2009, Volume 1: Temperature. In: Levitus, S. (Ed), NOAA Atlas NESDIS 68. U.S. Government Printing Office, Washington, D.C., 184 pp.

Stuiver, M., Polach, H.A., 1977. Discussion: reporting of 14C data. Radiocarbon 19(3), 355-363.

Chapter 5

Summary and Perspectives

5.1 General conclusions

In this thesis, estimates of thermocline temperatures in the northeastern tropical Atlantic for the LGM (Last Glacial Maximum) and HS1 (Heinrich Stadial 1) time periods have been presented. The seawater $\Delta^{14}C$ distribution in the LGM Atlantic and seawater $\Delta^{14}C$ variations of the deep and the abyssal southwestern Atlantic over the past 40,000 years have also been shown. These reconstructions have been linked to past changes in the AMOC strength and the Atlantic deepwater circulation rate. Results and conclusions presented in chapters 2, 3 and 4 test the three working hypotheses proposed at the beginning of the thesis.

Working hypothesis 1: If thermocline temperatures in the eastern tropical Atlantic are sensitive to past changes in AMOC strength, then the significant reduction in AMOC strength from the LGM to Heinrich Stadial 1 would be recorded as a pronounced increase in thermocline temperatures.

The Mg/Ca ratio of epibenthic foraminifer *P. ariminensis* was confirmed to be a reliable proxy for thermocline temperature, with a sensitivity of 0.19 mmol/mol per ºC. The reconstructed LGM and HS1 thermocline temperatures of the northeastern tropical Atlantic were comparable to modern values between 200 and 400 m water depth, but were around 1.5ºC warmer at 550-570 m depth. The HS1 thermocline temperatures were indistinguishable from LGM reconstructions between 200-570 m. Therefore, thermocline temperatures at our core locations (~ 9ºN) were insensitive to changes in the AMOC strength during the glacial and deglacial time periods. We thus reject working hypothesis 1.

In contrast to tempearture, thermocline-water $\delta^{18}O$ and salinity between 200-550 m water depths were significantly increased during the LGM relative to the present. Temperature-

salinity properties of thermocline waters were similar to those of surface waters from the central North Atlantic during the LGM. It was concluded that the themocline waters at the core locations used in this study was ventilated by the glacial North Atlantic Central Water rather than the glacial South Atlantic Central Water during the LGM.

During HS1, temperature-salinity properties of upper themocline waters (between 200-400 m water depths) were similar to those of the LGM, while lower themocline waters (at 570 m water depth) became much fresher. This could indicate a northward incursion of the southern-sourced waters in the lower thermocline during HS1.

Working hypothesis 2: If the deep Atlantic Ocean was poorly ventilated during the LGM, then deepwater $\Delta^{14}C$ reconstructions from the glacial deep Atlantic should contain a large fraction of ventilation signals.

Paired benthic and planktonic foraminiferal ^{14}C ages from 36 core locations (from previously published and new data) provided the first mapping of seawater $\Delta^{14}C$ distribution in the LGM Atlantic. The calculated mean seawater $\Delta^{14}C$ and the mean B-P age (^{14}C age difference between paired benthic and planktonic foraminifera) of the lower Atlantic (> 1500 m) is 105‰ lower and 700 years larger than those of the upper Atlantic (< 1500 m), respectively. This strong gradient between the upper and the lower Atlantic was also found previously in the vertical distribution of seawater $\delta^{13}C$ and Cd/Ca values (e.g., Sarnthein et al., 1994; Curry and Oppo, 2005; Marchitto and Broecker, 2006).

We assumed that the seawater $\delta^{13}C$ behaved as a conservative water-mass tracer in the LGM Atlantic. The mixing ratio of the northern- and the southern-sourced waters at our core locations could thus be estimated based on the reconstructed bottom-water $\delta^{13}C$ signature. The ^{14}C-based circulation age was obtained by subtracting the mixing $\Delta^{14}C$ signal from the reconstructed $\Delta^{14}C$ value. The final result showed that the LGM circulation ages at the vast majority of the core locations from the lower Atlantic (> 1500 m) were less than 400 years, which were similar to, or less than, pre-bomb values. The LGM deep Atlantic Ocean was actually well ventilated. Strong circulation rates were also consistent with the presence of the strong chemical gradient in the LGM Atlantic. Accordingly, the working hypothesis 2 is rejected.

These conclusions also cast doubt on a previous hypothesis (Toggweiler, 1999), which suggested that the reduction in atmospheric CO_2 during glacial periods could be explained by increased sequestration of carbon in deep oceans through a slowdown of deepwater

ventilation. The role of this physical process in drawing down atmospheric CO_2 needs to be thorougly reevaluated in a set of carbon cycle models.

Working hypothesis 3: If the deep ocean prior to the LGM was significantly depleted in ^{14}C with respect to the contemporary atmosphere, then the glacial marine carbon cycle should have contributed to the elevated atmospheric $\Delta^{14}C$ level considerably.

New reconstructions combined with existing published results confirmed that the abyssal Atlantic Ocean prior to the LGM was significantly depleted, by 400‰, in $\Delta^{14}C$ with respect to the contemporary atmosphere. The ^{14}C-depleted water masses were found to reside below 2500 m in the Atlantic Ocean and at intermediate water depths in the high-latitude Southern Ocean. During the LGM and the early deglaciation, the ^{14}C-depleted water mass in the southwestern Atlantic expanded upward.

If our pre-LGM reconstructions are representative of the ocean volume below 3000 m depth, and if the pre-LGM ^{14}C age difference between the abyssal ocean and the atmosphere was reduced to its pre-industrial level, a simple mass-balance calculation indicates that the abyssal ocean could store more ^{14}C atoms from the atmosphere and draw down the atmospheric $\Delta^{14}C$ level by as much as 150‰. This calculation explicitly demonstrates the influence of a changed glacial carbon cycle on the atmospheric $\Delta^{14}C$ level. The working hypothesis 3 is therefore accepted. Since the deep ocean ventilation was inferred to be vigorous during the glacial period, the extremely ^{14}C-depleted signature of the abyssal ocean was most likely caused by a decrease in the preformed $\Delta^{14}C$ values in the southern source areas due to expanded sea ice coverage.

5.2 Future perspectives

Several of the conclusions reached in this study could be consolidated by more reconstructions using similar or different methods in further studies. Moreover, several interesting research topics can be proposed based on current conclusions.

(1) Although thermocline temperatures of the northeastern tropical Atlantic (around ~9ºN) appear to be insensitive to changes in the AMOC strength under glacial climate conditions, climate model studies using the LGM boundary conditions have indicated other promising locations. Thermocline temperatures of the southeastern Atlantic (5ºS-30ºS) (Brady and Otto-Bliesner, 2011) and the northwestern Atlantic (0-15ºN) (Schmidt et al., 2012) seem to be highly sensitive to variations of the AMOC strength in models. The benthic foraminiferal

Mg/Ca-based paleotemperature proxy could be applied to reconstruct thermocline temperature changes in these areas and to test model simulation results.

(2) In Chapter 2, reconstructed temperature-salinity properties of thermocline and surface waters indicated that the modern frontal zone between the North Atlantic and the South Atlantic central waters shifted to the south during the LGM and the HS1. This conclusion can be tested by using other conservative water-mass tracer in future studies, such as neodymium isotope of seawater.

(3) In order to calculate the ^{14}C-based circulation age, it is crucial to determine the $\Delta^{14}C$ end-member values of water masses from different sources. So far, the $\Delta^{14}C$ end-member value of the glacial North Atlantic Deep Water has not been reconstructed. In this study we took the estimate from model simulations for calculations. The $\Delta^{14}C$ end-member value of the glacial Antarctic Bottom Water was derived from reconstructions at two cores locations in the abyssal South Atlantic, MD07-3076 (Skinner et al., 2010) and TNO57-21 (Barker et al., 2010). However, LGM bottom-water $\Delta^{14}C$ estimates for the two cores show an offset of as much as 220‰. Therefore, a better constraint on the $\Delta^{14}C$ end-member values of glacial North Atlantic Deep Water and Antarctic Bottom Water is required in further studies. In addition, more benthic ^{14}C data from the deep Atlantic, especially those with independent estimates of calendar ages, are also needed in order to validate the estimate of the LGM circulation age presented in chapter 3.

(4) A simple mass-balance model was used to estimate the influence of a ^{14}C-depleted deep ocean carbon reservoir on the atmospheric $\Delta^{14}C$ level in chapter 4. The reconstructions presented of the pre-LGM deepwater $\Delta^{14}C$ values could be used to calibrate more complex box- or general circulation models. This would allow more accurate estimates of the contribution of a changed glacial carbon cycle to the elevated atmospheric $\Delta^{14}C$ value.

5.3 References

Barker, S., Knorr, G., Vautravers, M.J., Diz, P., Skinner, L.C., 2010. Extreme deepening of the Atlantic overturning circulation during deglaciation. Nature Geosciences 3, 567-571.

Brady, E.C., Otto-Bliesner, B.L., 2011. The role of meltwater-induced subsurface ocean warming in regulating the Atlantic meridional overturning in glacial climate simulations. Climate Dynamics 37, 1517-1532, doi:10.1007/s00382-010-0925-9.

Broecker, W.S., Barker, S., 2007. A 190‰ drop in atmosphere's $\Delta^{14}C$ during the "Mystery Interval" (17.5-14.5 kyr). Earth and Planetary Science Letters 256, 90-99.

Curry, W.B., Oppo, D.W., 2005. Glacial water mass geometry and the distribution of $\delta^{13}C$ of ΣCO_2 in the western Atlantic Ocean. Paleoceanography 20, PA1017, doi:10.1029/2004PA001021.

Marchitto, T.M., Broecker, W.S., 2006. Deep water mass geometry in the glacial Atlantic Ocean: A review of constraints from the paleonutrient proxy Cd/Ca. Geochemistry Geophysics Geosystems 7, Q12003, doi:10.1029/2006GC001323.

Sarnthein, M., Winn, K., Jung, S.J.A., Duplessy, J.-C., Labeyrie, L., Erlenkeuser, H., Ganssen, G., 1994. Changes in east Atlantic deep-water circulation over the last 30,000 years: Eight time slice reconstructions. Paleoceanography 9, 209-267, doi:10.1029/93PA03301.

Schmidt, M.W., Chang, P., Hertzberg, J.E., Them II, T.R., Link, J., Otto-Bliesner, B.L., 2012. Impact of abrupt deglacial climate change on tropical Atlantic subsurface temperatures. Proceedings of the National Academy of Sciences of the United States of America 109(36), 14348-14352.

Skinner, L.C., Fallon, S., Waelbroeck, C., Michel, E., Barker, S., 2010. Ventilation of the deep southern ocean and deglacial CO_2 rise. Science 328, 1147-1151.

Toggweiler, J.R., 1999. Variation of atmospheric CO_2 by ventilation of the ocean's deepest water. Paleoceanography 14(5), 571-588, doi:10.1029/1999PA900033.